Alma Mater Studiorum · Università di Bologna

FACOLTÀ DI SCIENZE MATEMATICHE, FISICHE E NATURALI

DOTTORATO DI RICERCA IN FISICA

CICLO XXIII

Settore Scientifico Disciplinare di Afferenza

FIS/03 - FISICA DELLA MATERIA

ORGANIC HETEROSTRUCTURE APPROACH FOR MULTIFUNCTIONAL LIGHT-EMITTING FIELD-EFFECT TRANSISTORS

Dottorando: Gianluca Generali

Coordinatore Dottorato:
Prof. Fabio Ortolani

Relatore :
Dott. Giorgio Matteucci

Supervisori :
Dott. Raffaella Capelli
Dott. Michele Muccini

Acknowledgements

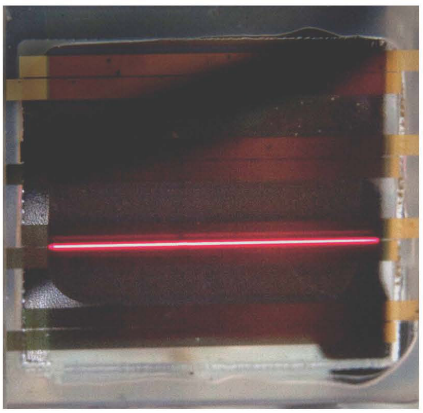

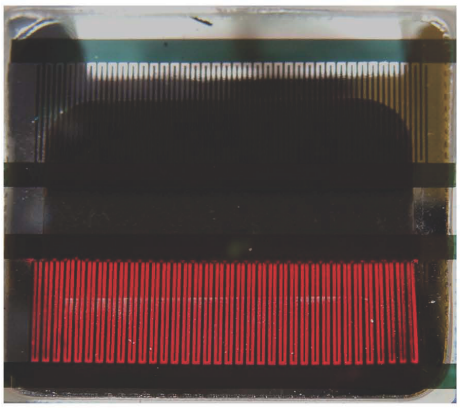

I would like to thank all the people who supported me during this PhD work and encouraged me to give always the best from myself.

In particular I would like to thank my University supervisor, Dr. Giorgio Matteucci and my CNR-ISMN supervisors Dr. Raffaella Capelli (Raffa) and Dr. Michele Muccini without whom I would not be here.

A warm thank also to all my colleagues from CNR of Bologna and Pisa, Stefano Toffanin (Toffi), Andrea Stefani (Il Basso), Riccardo d'Alpaos, Viviana Biondo, Wouter Koopman, Stefano Troisi, Guido Turatti, Giovanna Guidicelli, Mirko Seri, Valentina Benfenati and Franco Dinelli who accompanied me in this journey and showed me the importance of friendship and teamwork.

A very special thank to Guido Turatti (The Responsible of the "Electronic Department"!) who initiated me to the world of "Salama da Sugo".

A grateful thank to my "monday evenings" old friends. Someone says that a friend is like a treasure... I totally agree!

Thank you from the deep of my heart to all of my family (Marina, Dario and Lorenzo) that always supported me in an unimaginable way.

Finally, I would like to dedicate this thesis to my girlfriend, Eleonora, for having changed the colours of my life and for the patience she demonstrated in these years.

Contents

Publications List

- R. Capelli, S. Toffanin, G. Generali, H. Usta, A. Facchetti and M. Muccini . Organic light-emitting transistors with an efficiency that outperforms the equivalent light-emitting diodes - Nat. Mater. June 2010, 9, 496-503.

- G. Generali, R. Capelli, S. Toffanin, A. Facchetti and M. Muccini . Ambipolar field-effect transistor based on α,ω-dihexylquaterthiophene and α,ω-diperfluoroquaterthiophene vertical heterojunction - Microelectron. Reliab. September 2010, 50, 9-11, 1861-1865.

- P. Lutsyk, K. Janus, G. Generali, R. Capelli, M. Muccini and J. Sworakowski. "Photo-Switching of an N-Type Organic Field Effect Transistor by a Reversible Photochromic Reaction in the Dielectric Film" J. Phys. Chem. C . In press.

- G. Generali, F. Dinelli, R. Capelli, S. Toffanin and M. Muccini. "Influence of the Substrate Platform on the Opto-Electronic Properties of Multi-Layer Organic Light-Emitting Field-Effect Transistors" - J. Phys. D: Appl. Phys. - In press.

Chapter 1

Introduction

Organic compounds have been studied as multi-functional materials, since the first discovery of the photoelectric effect in anthracene by the Italian scientist Pochettino [1], thanks to their capability of showing a variety of properties such as charge transport, light absorption/emission, photoconductivity, electroluminescence and superconductivity.

The principal distinguishing property of this class of material arise from their chemical structure. Essentially, organics are composed by π-conjugated double bonds attached to a carbon backbone structure. The wave functions of these π-bonds are largely delocalized over the carbon atoms, thus creating a condition capable of semiconducting properties.

Moreover, organic materials offer the possibility of tailoring the chemical structure to change the chemical-physical properties thereby adapting the material functionality and improving key properties such as thermal and environmental stability.

On the basic research side, π-conjugated materials are fascinating systems whose functional properties are strictly connected to the interplay between their π-electronic structure and their molecular structure [2]. On the applied research side, they are expected to replace silicon-based technologies, organic semiconductors promise the

advent of fully flexible devices for applications including organic field-effect transistors (OFETs) [3], light-emitting diodes (OLEDs) [4], photovoltaic cells [5], sensors [6], and radio frequency identification (RF-ID) tags [7].

The semiconducting properties of organics have been studied in a number of conjugated molecules that can be grown in the form of reasonably large single crystals by vacuum sublimation techniques under controlled conditions. Well-defined structures with a limited number of impurities can be obtained through repeated sublimation steps [8]. Such crystals provide an ideal test bed to investigate the fundamental parameters affecting charge mobility. However, their slow growth and lack of processability prevent them from being integrated in industrial processes. For industrial applications, cost-effective approaches are sought after, based in particular on solution processing of (substituted) molecules or on the deposition of polycrystalline or amorphous films by vacuum sublimation.

In both cases, in organic field-effect transistors key figures of merit are the charge carriers mobility in the organic semiconductor layer, the efficiency of the charge injection mechanism from the metal to the organic and the interfacial compatibility between the organic/dielectric surfaces. For all classes of organic semiconductors the intrinsic carrier mobility depends critically on the degree of molecular ordering and on the extent of the $\pi - \pi$ stacking in the material [9]. Despite their different chemical structures, materials showing highest mobility values in OFET device structures have in common the unidimensionality of their elemental unit, which results in anisotropic charge transport and optical properties. An important consequence of this anisotropy is that the realization of efficient electronic or photonic devices requires a precise control of the material organization for guaranteeing the proper overlap between molecular orbitals.

In addition to the tight molecular packing and strong intermolecular interactions

needed to reach a high charge-carrier mobility, efficient control of the orientation of the conjugated chains on the substrate is crucial to obtain optimal charge transport in the desired direction. In order to enhance the performance of opto-electronic devices based on thin film, it is of high interest to understand which morphological features are detrimental for charge transport or energy transfer. Whereas it has been demonstrated that the molecular properties can be tuned by chemical tailoring, morphology and supramolecular arrangement are generally more difficult to control, and this appears to be one of the next challenges in the field of organic π-conjugated materials.

Photoluminescence spectroscopy has proven to be a powerful and highly sensitive technique to probe how the electronic structure and energy transport processes in conjugated molecules are modulated by aggregation in solid state thin-film [10, 11]. The transfer of the exciton energy within the electronic manifold, which occurs upon charge recombination in opto-electronic devices, is highly sensitive to the local molecular environment [12]. Therefore, luminescence eventually depends on how the molecules pack in the solid into aggregates, rather than being exclusively an intrinsic property of the molecule [2]. So correlating PL spectroscopy with morphological probing tools allows to gain fundamental information on the thin-film supra-molecular organization, and provides feedback to the deposition conditions (i.e. deposition rate, substrate temperature, etc...) for improving device electrical and light-emission properties.

Among all the organic materials showing semiconducting properties, thiophene derivatives have always attracted attention since the implementation of linear α-conjugated thiophene-based oligomers as active materials in the first field-effect transistors [13, 14].

The versatility of thiophene chemistry allows a great diversity of thiophene-based

chemical structures. Thiophene can be functionalized in positions α and β to sulphur or at the sulphur atom itself [15], regioregular oligomers and polymers with extremely varied functionalizations can be prepared, oligomers can be linear, branched, or star-shaped, and even-all thiophene dendrimers can be prepared [16].

The driving force behind the continuous creation of new thiophene-based structures is that they allow fine-tuning of charge-transport and light-emission properties and, more importantly, that understanding of the structure-property relationship is still dramatically scarce, particularly in the solid state.

Given the multi-functional properties of many classes of organic compounds, the full exploitation of these properties requires the realization of devices that are able to integrate electronic functions (e.g., transistors) with optical functions (e.g., light sources and light detectors). Light-emitting field-effect transistors (OLET) provide a very simple integration scheme for combining the switching properties of transistors with the emission properties of light-emitting diodes [17].

Organic semiconductors are ideal candidates for light emission applications since many small molecules and conjugated polymer semiconductors show very high photoluminescence and electroluminescence efficiencies over the whole visible spectrum coupled to charge transport properties, that allowed the realization of efficient light-emitting diodes [18]. In recent years, many research groups have worked to achieve light emission from organic field-effect transistors [19–24]. Ambipolar OFETs can provide an effective pn-junction within the transistor channel that allows exciton formation and radiative recombination [25]. Compared to light-emitting diodes (OLEDs), organic light-emitting transistors (OLETs) present some intriguing characteristics which overcome many physical and technical withdraws in the realization of nano-scale integrated electro-optical devices. Some of these characteristics include: control over the position of the emission zone, emission far away from injecting metal electrodes, high

current densities, low charge concentration within the emission zone, and perfectly balanced hole and electron currents.

Therefore, OLET planar structure is not only a convenient platform for investigating charge carrier recombination processes in organic semiconductors with spatially resolved probes, but it is also attractive for the realization of integrated electro-optical switches.

Considerable effort has been devoted to increasing the electroluminescence efficiency of thin films of organic materials within the OLET device structure. In particular, a range of strategies, including the dispersion of laser dyes in a host matrix, have been developed to control intermolecular interactions and prevent light emission quenching.

The thesis is organized as follows:

In **Chapter 2** a general description of the physics of organic semiconductors is introduced. Then a description of the theoretical aspects of the charge transport and light generation is given.

In **Chapter 3** is introduced a detailed description of the structure of a transistor, the working principles of single layer, bi-layer vertical heterojunction OFETs and OLETs and the tri-layer vertical heterojunction OLET.

In **Chapter 4** the experimental setups used for this thesis are described. They concern optoelectronic measurements and probing tools for thin film morphological characterization.

Chapter 5 introduces the organic materials and dielectrics used for the device fabrication with a description of their known properties.

In particular, for the active organic materials, the description will be separated in two different categories. Transport materials, with a brief description of oligothiophenes as a class of organic compounds displaying multifunctional properties, host matrices

materials and guest photo-emissive dyes to be used in host-guest systems.

In **Chapter 6** the characteristics of single layer devices fabricated with the studied materials and dielectrics will be reported with the purpose of determining the optimal packing and grow conditions for the best device performances. Then, in the same chapter will be presented the fabrication of bi-layer vertical heterojunction OFETs using the best combination of materials, in order to understand, in a more complex structure, the compatibility among different compounds grown in a vertical stack. This preliminary study is essential for finding the best material combination to be implemented in the new structure of tri-layer OLET reported in chapter 6.

In **chapter 7** the best combination of materials will be selected, according to the previous studies, to be implemented in a number of tri-layer OLET structures. The results are then compared with the objective of finding the best materials combination for the best efficient OLET in terms of light emission.

Chapter 8 presents a description of the perspectives in terms of applications of the tri-layer OLET platform. These applications will range from the realization of devices that, in combination with photo-sensors, could be used as lab-on-a-chip for biological analysis, to the organic lasing systems. Within the chapter will be also presented some critical issues that must be overcome in order to develop further this technology.

1.1 REFERENCES

[1] Pochettino A. Atti della r. accademia di lincei. *Rendiconti della classe di scienze fisiche matematiche e naturali*, 15:355, 1906.

[2] F Pope and C. E. Swenberg. *Electronic processes in Organic Crystals 2nd ed.* Oxford University Press, USA, 1999.

[3] G. Horowitz. Organic field-effect transistors. *Adv. Mater.*, 10(5):365–377, 1998.

[4] J. H. Burroughes, D. D. C. Bradley, A. R. Brown, R. N. Marks, K. Mackay, R. H. Friend, P. L. Burns, and A. B. Holmes. Light-emitting-diodes based on conjugated polymers. *Nature*, 347(6293):539–541, 1990.

[5] C. J. Brabec, N. S. Sariciftci, and J. C. Hummelen. Origin of the open circuit voltage of plastic solar cells. *Adv. Funct. Mater.*, 11(5):15, 2001.

[6] B. Crone, A. Dodabalapur, A. Gelperin, L. Torsi, H. E. Katz, A. J. Lovinger, and Z. Bao. Electronic sensing of vapors with organic transistors. *Appl. Phys. Lett.*, 78(15):2229–2231, 2001.

[7] A. R. Brown, A. Pomp, C. M. Hart, and D. M. Deleeuw. Logic gates made from polymer transistors and their use in ring oscillators. *Science*, 270(5238):972–974, 1995.

[8] O. D. Jurchescu, J. Baas, and T. T. M. Palstra. Effect of impurities on the mobility of single crystal pentacene. *App. Phys. Lett.*, 84:3061–3063, 2004.

[9] D. J. Gundlach, Y. Y. Lin, T. N. Jackson, S. F. Nelson, and D. G. Scholm. Pentacene organic thin-film transistors - molecular ordering and mobility. *IEEE Electron Device Lett.*, 18(3):87–89, 1997.

[10] R. Kersting, U. Lemmer, R. F. Mahrt, K. Leo, H. Kurz, H. Bssler, and O. Gbel. Femtosecond energy relaxation in pi-conjugated polymers. *Phys. Rev. Lett.*, 70(24):3820, 1993.

[11] R. N. Marks, R. H. Michel, W. Gebauer, R. Zamboni, C. Taliani, R. F. Mahrt, and Hopmeier M. The origin of photoluminescence from alpha-sexithienyl thin films. *J. Phys. Chem. B*, 102(39):7563, 1998.

[12] H. Sirringhaus, N. Tessler, and Friend R. H. Integrated optoelectronic devices based on conjugated polymers. *Science*, 280(5370):1741, 1998.

[13] X. Z. Peng, G. Horowitz, D. Fichou, and F. Garnier. All-organic thin-film transistors made of alpha-sexithienyl semiconducting and various polymeric insulating layers. *Appl. Phys. Lett.*, 57(19):2013–2015, 1990.

[14] M.A. Loi, E. Da Como, F. Dinelli, M. Murgia, R. Zamboni, F. Biscarini, and M. Muccini. Supramolecular organization in ultra-thin films of alpha-sexithiophene on silicon dioxide. *Nat. Mater.*, 4(1):81–85, 2005.

[15] G. Barbarella, L. Favaretto, G. Sotgiu, M. Zambianchi, A. Bongioni, C. Arbizzani, M. Mastragostino, M. Anni, G. Gigli, and R. Cingolati. Tuning solid-state photoluminescence frequencies and efficiencies of oligomers containing one central thiophene-s,s-dioxide unit. *J. Am. Chem. Soc.*, 122(48):11971–11978, 2000.

[16] T. Benincori, M. Capaccio, F. De Angelis, L. Falciola, M. Muccini, P. Mussini, A. Ponti, S. Toffanin, P. Traldi, and F. Sannicolo. Spider-like oligothiophenes. *Chem. Eur. J.*, 14:459–471, 2008.

[17] Muccini M. A bright future for organic field-effect transistors. *Nat. Mater.*, 5(8):605–613, 2006.

[18] C. W. Tang and S. A. Vanslyke. Organic electroluminescent diodes. *Appl. Phys. Lett.*, 51(12):913, 1987.

[19] A. Hepp, H. Heil, W. Weise, M. Ahles, R. Schmechel, and H. von Seggern. Light-emitting field-effect transistor based on a tetracene thin film. *Phys. Rev. Lett.*, 91(15):157406, 2003.

[20] C Rost, S Karg, W Riess, M.A. Loi, M Murgia, and M. Muccini. Ambipolar light-emitting organic field-effect transistor. *Appl. Phys. Lett.*, 85(9):1613, 2004.

[21] L Edman, B. Liu, M. Vehse, J. Swensen, G.C. Bazan, and A.J. Heeger. Single-component light-emitting electrochemical cell fabricated from cationic polyfluorene: Effect of film morphology on device performance. *J. Appl. Phys.*, 98(4):044502, 2005.

[22] J. Zaumseil, R. H. Friend, and H. Sirringhaus. Spatial control of the recombination zone in an ambipolar light-emitting organic transistor. *Nat. Mater.*, 05(01):69–74, 2006.

[23] R. Capelli, S. Toffanin, G. Generali, H. Usta, A. Facchetti, and M. Muccini. Organic light-emitting transistors with an efficiency that outperforms the equivalent light-emitting diodes. *Nat. Mater.*, 9(6):496–503, 2010.

[24] T. Takenobu, S. Z. Bisri, T. Takahashi, M. Yahiro, C. Adachi, and Y. Iwasa. High current density in light-emitting transistors of organic single crystals. *Phys. Rev. Lett.*, 100(6):066601, 2008.

[25] A. Dodabalapur, H. E. Katz, and L. Torsi. Molecular orbital energy level engineering in organic transistors. *Adv. Mater.*, 8(10):853–857, 1996.

Chapter 2

Organic Materials

2.1 Electronic structure

The 21^{st} century could be considered the beginning of a new electronic revolution that has become possible thanks to the development and comprehension of a new class of carbon based materials, known as organic semiconductors. Most of their opto-electronic properties arise from the carbon atom features. In its ground state, the carbon atom has this classic electronic structure: $1s^2 2s^2 2px^1 2py^1$ (see fig.2.1). This means that carbon has two electrons in orbital 1s, two in orbital 2s and 2 in orbitals 2p. Since the s orbitals are totally filled, an atom carbon should form only two bonds involving the two unpaired electrons in 2p orbitals. Instead, it is well known that carbon is tetravalent and forms four bonds. This can be explained using the valence bond theory [1].

This theory asserts that a chemical bond is formed by the overlapping of the atomic orbitals which contain the electrons participating in the bond, in order to lower the total energy of the system. Since the atomic orbitals are the wave functions solving the Schrödinger equation for an atom, the overlapping between atomic orbitals corresponds to the combination of the wave functions describing the two electrons

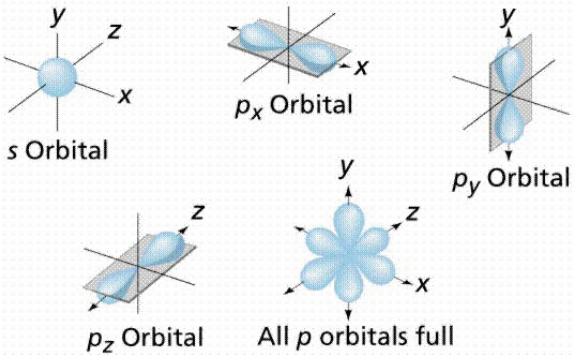

Figure 2.1: Geometrical representation of orbitals: s-orbitals are spatially spherical, while p-orbitals are shaped like a dumbbell

involved in the bond. The overall normalized wave function describing a molecular system (molecular orbital) can be expressed as:

$$\Psi = \sum_i a_i \phi_i \qquad \text{with } \sum_i a_i^2 = 1$$

in which ϕ are the solutions of the atomic Schrödinger equation, i.e. one-electron functions centered on the nuclei of the component atoms of the molecule. So the molecular orbital Ψ is the linear combination of n atomic orbitals ϕ (LCAO), each multiplied by a corresponding coefficient a_i. The coefficients are weights of the contribution of n atomic orbitals to the molecular orbital. The molecular orbital is expressed as linear combination of basis functions. By minimizing the total energy of the system an appropriate set of the linear combinations is determined. For of carbon atom the linear combination is defined as hybridization and can be between 2s orbital and one, two or three 2p orbitals [2]. If the hybridization occurs between the 2s orbital and all the 2p orbitals, we obtain four degenerate sp3 hybrid orbitals lying in a tetrahedral geometry around the central carbon atom ($109,47°$ between bond axes). This hybridization is the one found in diamond, in which every carbon atom is bonded to other four carbons.

Hybridization can also occur between 2s orbital and one 2p orbital to form 2 equivalent sp orbitals. The latter are on the same plane passing through the nucleus, and lie at $180°$ from each other. The 2 pure orbitals p remaining lie in a plane which is perpendicular to the former.

In the case of the sp2 hybridization, the 2s orbital is mixed with two 2p orbitals, for example the 2px and the 2py in fig.2.1. From this hybridization, three new states are formed in the XY plane, leaving the 2pz orbital unchanged as it can be seen in fig.2.2. The phenomenon of sp^2 hybridization is the fundamental basis for understanding the

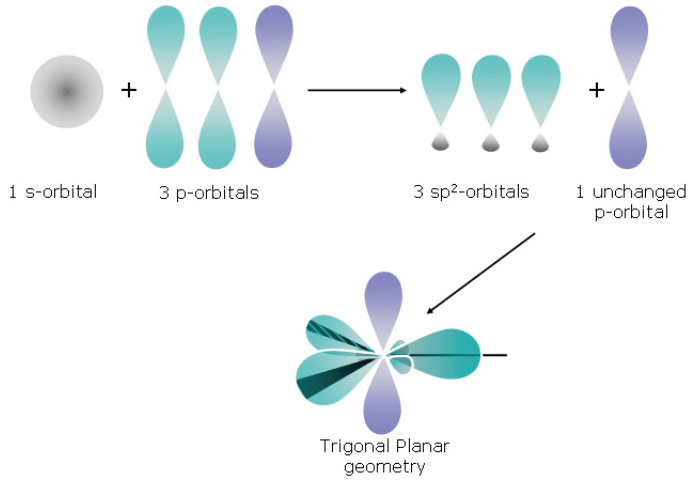

Figure 2.2: Scheme of an sp^2 hybridization of a carbon atom. The resulting structure is composed by the union of 3 sp^2 orbitals with one unchanged p orbital

charge transport properties of the organic materials. Indeed, when two hybridized carbon atoms meet, their wavefunctions could overlap forming a new shared molecular orbital state called σ-*bond*. From this condition, then, the unchanged p orbitals of the two atoms, could overlap forming other two bonds called π (see fig.2.3). The newly formed molecule will have a weaker force compared to the σ-bond, since the high directionality of the latter and the double bond, is consisted of a π-bond and a σ-bond with a shared electron. Furthermore, since the minor localization of the π-bond, rather than σ-bond, due to the different electronic distribution, the energy

difference between the ground and excited states is smaller. As a consequence of this distribution, the electrons of the π-bond, are not confined as happens for other bonds, but they form a density cloud above and below the plane formed by the σ-bond.

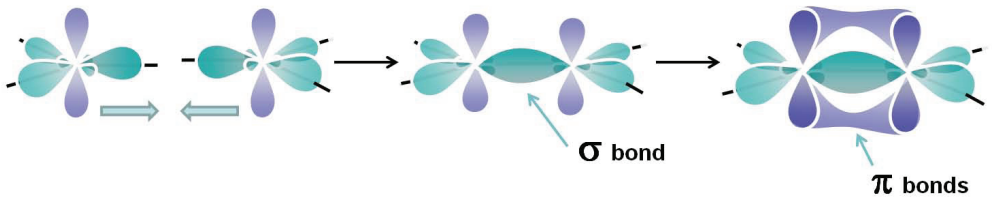

Figure 2.3: Scheme of the formation of π-bonds between two carbon atoms

Ideally this cloud should be delocalized over the entire molecule, but in real systems, this delocalization is limited in some parts of the molecule. The π-conjugated double bonds between carbon atoms are the basic structures that form the organic semiconductors. The delocalization of the electrons in these π orbitals is the responsible for having charge transport and injection delocalization. However, beside the strong intramolecular forces in the molecular structure, usually the crystals and, in general, the solid state aggregations, are held together by weak Van der Walls forces [3]. It is thanks to these weak interactions that also in solid films, the properties of the single molecule is mostly retained. For this reason, in many cases is possible to tune the properties of macroscopic solid systems, by chemical tailoring directly the molecule structure. Of course, also the molecular order of the film in solid state, is an important aspect to be considered for the charge transport and light generation optimization. Two main classes of π-conjugated materials can be considered, according to the molecular weight. Low molecular weight materials are usually called *small molecules*, while materials with high molecular weight, up to many thousand of g/mol are called *polymers*.

2.2 Electrical Properties of Organic Semiconductors

The semiconductive properties of organic materials are tightly related to the presence of the electrons delocalized cloud consisting of the molecular π-bonds, as we discussed before. As a consequence of this ideal delocalization over the entire molecule, the resulting one dimensional band has a certain band width and the conjugated chain can be viewed as a semiconductor with a filled valence band and an empty conduction band, called respectively *highest occupied* (HOMO) and *lowest unoccupied molecular orbital*(LUMO). In this band-like configuration the charge injection and transport phenomena can be easily demonstrated. The limitation to these considerations, comes when charge transport happens not only within the unity but it involves charge transport between different molecules, since there is a low inter-molecular orbital overlapping.

2.2.1 Charge Transport

When we consider the transport of hole or electrons in an organic semiconductor, the first concept that must be taken into account is the fact that charge movement involves ionic molecular states. Thus in order to generate an hole, an electron must be removed from a molecule to form a radical cation and vice versa for the case of electron generation. In general, depending on the degree of molecular order (e.g. from molecular crystals to disordered organic solids) the charge transport mechanism can be either *band-like* or *hopping*.

Band-like Transport

Band transport is typically referred to the mechanism occurring in highly crystalline inorganic solids like metals and semiconductors. The same happens in highly purified molecular crystals at room temperature, but, since their electronic delocalization is

weaker, usually the band width is smaller compared to the inorganic counterpart. Briefly, band theory could be explained in the following way: the electrons of a single isolated atom occupy atomic orbitals, that form a discrete set of energy levels. When several atoms are brought together into a molecule, their atomic orbitals split. The number of molecular orbitals formed are proportional to the number of atoms. When a large number of interactive atoms are brought together to form a solid, the number of orbitals becomes very large, and the difference in energy between them become smaller. Thus, in solids the levels form continuous bands of energy rather than the discrete energy levels of the isolated atoms. Of course, some intervals of energy contain no orbitals, no matter how many atoms are aggregated, forming, namely, the band gaps. The statistic that rules over the filling of a band is the Fermi-Dirac. At a zero kelvin temperature, the bands are filled with electrons up to the Fermi Energy level (EF).

$$f(E) = \frac{1}{1 + \exp\left(\frac{E - E_f}{KT}\right)} \tag{2.1}$$

This energy defines a general distinction between two different classes of materials. A solid, is considered an insulator when, at a certain temperature, the conduction band (lowest unoccupied band) is empty and the valence band (highest occupied band) is completely filled by electrons. A solid is, instead, called a conductor when the conduction band, at a certain temperature, is partially filled. In the middle of these two cases are the semiconductor materials, in which the energy gap between the top of the valence band and the bottom of the conduction band is small enough (< 4 eV). At non-zero temperature, the change in the Fermi-Dirac distribution causes a certain number of electrons to fill the bottom of the conduction band, thus leaving the top of valence band empty. The first model developed for band charge transport in a solid

state systems, is the Drude model. This model assumes the hypothesis that, under an applied electric field, the carriers are free to move through the solid and they are subject only to collisional damping forces due to the presence of scattering centers (phonons) or impurities. A statistical equation for determining the drift velocity of the carriers in the direction of the electric field could be expressed as

$$\frac{d}{dt}\langle v_x \rangle = \frac{q}{m^*} F_x - \frac{1}{\tau}\langle v_x \rangle \tag{2.2}$$

where q is the charge unity, τ is the mean free time of the moving charges between two collisions and m^* is the effective mass. Under steady state condition, the solution of the previous equation is:

$$\langle v_x \rangle = \frac{q\tau}{m^*} F_x = \mu F_x \tag{2.3}$$

where μ is defined as the mobility of the semiconductor. Mobility can also be defined as:

$$\mu = \frac{q\lambda}{m^* \nu_{tv}} \tag{2.4}$$

where q is the charge unity, λ is the electron mean free path, m^* is the effective mass of charges and ν_{tv} is the electron thermal velocity. Regarding the temperature dependence of the mobility, it is possible to define the following general law, according to phenomenological observations.

$$\mu(T) \propto T^{-n} \tag{2.5}$$

Where *n* is a positive number. This law shows how the mobility increases with decreasing temperature and, usually, when the behaviour is well matched by the experimental data, it can be considered as a proof of band transport. Of course this happens only for rather low temperatures ($<$ 100 K) since, when the electron mean free path is lower than the distance between molecules, the conditions for having diffusion transport are not met.

Transport by Hopping

The main reason why the band model is unable to describe clearly the charge transport in organic semiconductors is that it fails to account for polarization in these materials. Polarization was studied in detail by Silinsh and Cápek [4]. A charge carrier residing on a molecular site tends to polarize also its neighbours. As a consequence there is a polarization cloud that moves together with the charge. Thus, the travelling charge is no longer a single entity, but a *dressed* charge. The quasi-particle so formed is called *polaron*. In conjugated solids, the main polarization effect is that on clouds formed by π-electrons, as shown in fig.2.4. In order to estimate the polaron stability, it is

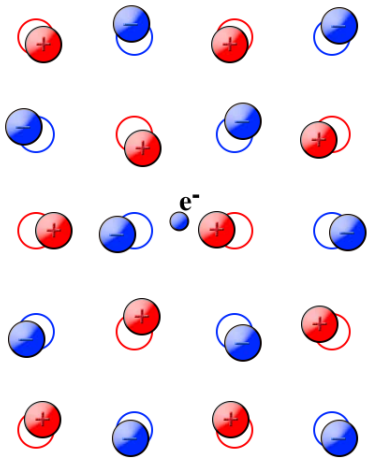

Figure 2.4: Picture of a polaron effect created by the passage of a negative charge.

possible to define two different typical times: the residence time τ_{res} that corresponds to the average time a charge will reside on a molecule and the electronic polarization time τ_{el} that is the time it takes for the polarization cloud to form around the charge. Both time scales can be estimated by using the Heisenberg uncertainty principle.

$$\tau = \frac{\hbar}{\Delta E} \tag{2.6}$$

For the residence time (τ_{res}) the energy considered is the width of the allowed band, typically 0.1 eV for organics and 10 eV for inorganics, thus, the resulting

τ_{res} is respectively 10^{-14} s and 10^{-16} s. For the electronic polarization time (τ_{el}) the energy taken into account is the electronic transition ($\sim$1eV) and the corresponding time scales are 10^{-15} s for both organic and inorganic materials. The result of these considerations is that for inorganics, the charge localization is shorter than the time of any polarization effects that could form (included in the band theory as *rigid-band approximation*). In organics, instead, charges move through the sites, slower than the electronic polarization time (τ_{el}) and therefore a polarization cloud is formed in the molecular site. Through this process charge transport is allowed by polarons movement along the conjugation and, of course, by the jump of the charges from different molecular neighbours. The weak point of the approach developed by Silinsh and Cápek is that it is phenomenological.

An alternative approach that helps to describe charge transport in a polarizable media is the Marcus model [5]. Initially, this model was used to describe electron transfer from an electron donor to an electron acceptor in solution. In general, each polaron residing in a molecular site can be described by its generalized configurational coordinate Q and its Hamiltonian operator H(Q). In the case of a localized state without interactions with nearby systems, the Hamiltonian can be expressed as:

$$E(Q) = E_0 - AQ + BQ^2 \tag{2.7}$$

where A is a positive number and it is the local electron-phonon coupling constant. The element BQ^2 represents the elastic energy produced by lattice distortion and E_0 is the carrier energy in absence of phonons.

The linear electron-phonon interaction element alters the local configuration of lattice, thus, lowering the carrier energy by $E_b = \frac{A^2}{4B}$. This corresponds to a modification of the equilibrium position from $Q = 0$ to $Q = \frac{A}{2B}$. The electron together with its associated local distortion is called *polaron*. Transfer between different molecular sites occurs when the configuration of lattice atoms presents the same energy on

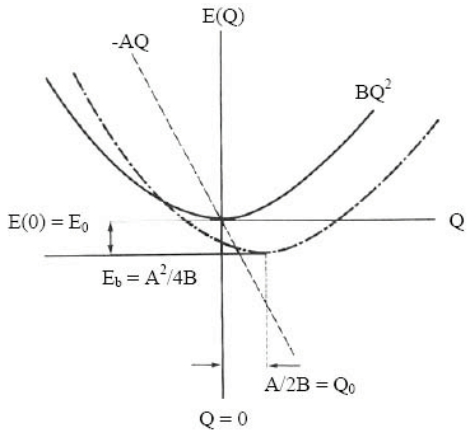

Figure 2.5: Graphical representation of the polaron energy as a function of generalized configurational coordinate Q.

both sites. The phonon frequency is not altered by the linear phonon coupling [6], therefore the factor B remains unchanged and the condition of equivalent electron energy for two different sites is $Q_1 = Q_2$. The energy, needed to create a distortion in both the molecules for obtaining this configuration, is:

$$W_a = B(Q_0 - Q)^2 + BQ^2 \tag{2.8}$$

Looking at the formula, it appears clear that the minimization occurs when $Q = \frac{Q_0}{Q} = \frac{A}{2B}$. So far the discussion was limited to the case of a localized small polaron. When there is an interaction energy (J) between neighbouring molecules, the degeneracy at X is lifted, leading to new states called X1 and X2. The activation energy for transfer is then lowered from X to X1 level and the new potential barrier for the charge movement is W_a (see Fig.2.6). If the magnitude of J is so large that the transition between E- and E+ is improbable, the carrier moves adiabatically [7]. Otherwise, if J is small enough to allow the transition, the transfer is called non-adiabatic [8]. The general form of this model defines an important principle for determine the difference between band-like transport, that occurs when $J > \omega\hbar$ and localized-type transport,

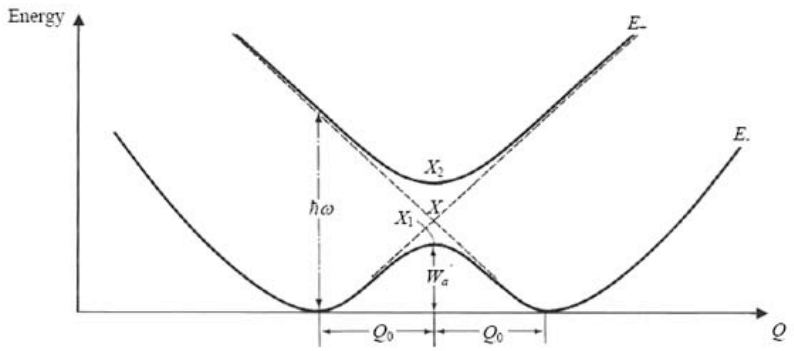

Figure 2.6: Representation of the lowered activation energy (W_a) for a small polaron in a two-site system

when $J < \omega\hbar$. Moreover, the mobility as a function of the temperature (T) is different in the two cases. At low T, J dominates over the other factors and we have band-like transport, on the contrary as T increases, the polaron bandwidth narrows until, after a certain threshold T, lifetime broadening is comparable to the polaron carrier bandwidth, thus leading to an inelastic scattering process with a consequence emission and absorption of phonons. Several models tried to explain the way hopping transport occurs, each based on different physical approximation and introducing different assumptions in order to give emphasis to some aspects respect to other, but in most cases temperature functional dependence of charge carrier mobility is defined as

$$\mu = \mu_0 \exp\left[-\left(\frac{T_0}{T}\right)^{\frac{1}{\alpha}}\right] \qquad with\ \alpha \in [1,4] \tag{2.9}$$

In this equation α is defined as the dimensionality of the system, T_0 is a parameter inversely proportional to the density of states at Fermi Level (E_F) and μ_0 is a mobility correction factor. A useful model to determine charge transport in real systems with

limitation due to localization of state induce by defects is the MTR model (*Multiple Trapping and Release Model*).

MTR Model

This model has been developed, initially, by Shur and Hack in order to give a description of the mobility of amorphous silicon. Then, Horowitz et al. expanded the model to describe also organic semiconductors in which thermal activated transport has been observed [9]. The model is based on the hypothesis that there is a distribution of localized energy levels situated below the extended states in which charge transport occurs. In general, the carriers, injected in the semiconductor and transiting in the delocalized band, interact with localized states and become trapped in the forbidden gap. These traps can be *deep*, if their energy level is far below the transport band, or they can be *shallow*, if located in vicinity of transport band edge (see fig.2.7).

The model place an assumption for the trapping and release mechanisms. Carriers

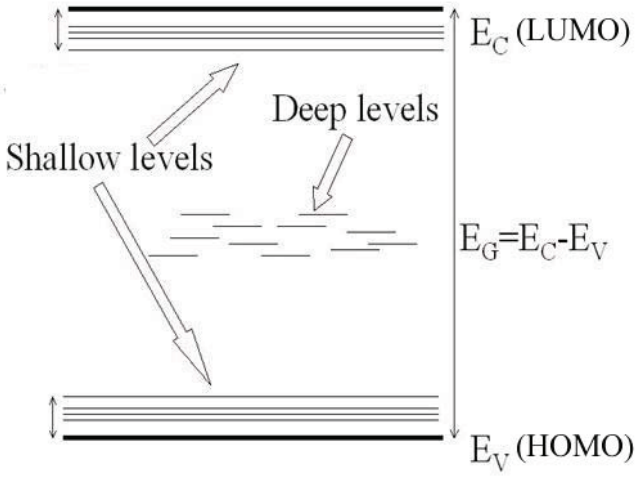

Figure 2.7: Representation of deep traps and shallow traps between the HOMO and LUMO level. Shallow traps are just few KT far from the bands edge, while deep traps are mostly in the middle of the band-gap.

that arrive at a trap are instantly captured with a probability close to one, and the

release of trapped carriers is controlled by thermally activated process. The model shows a dependence of carrier mobility from the temperature, from the energetic level of traps and from the carrier density of the semiconductor. For a single trap-level with energy define as E_{tr}, the mobility can be defined as

$$\mu = \mu_0 \alpha \exp\left(\frac{E_c - E_{tr}}{KT}\right) \tag{2.10}$$

in which E_c is the energy corresponding to the transport band edge and α is the ratio of the trap density of state to the effective density of states (DOS) at the transport band edge. The dependence from the temperature, decreases with temperature itself. For low T, the polycrystalline semiconductor is described by trap-free domains separated by boundaries with high trap density. If this size is lower than Debye length, the traps distribution can be considered uniform. If, on other hands, the grains size is larger than Debye length, charges move through grain boundaries. At high T, the transport of charges happens through thermally activated tunnelling and increased T dependence is observed. It is worth of noting that with MTR model, for an energy distributed DOS, mobility depends from gate voltage [10], and that in single crystals semiconductors, mobility is found to be rarely gate dependent, indicating how the gate voltage dependence originates from localized levels associated with impurities and defects.

Polaron Model

In the polaron model, introduced in 1958 by Yamashita for inorganic semiconductors and improved by Holstein and Fesser et al. for organics, charge transport can be described using the polarons concept, introduced before. The idea was that the charges move by thermally activated hops between adjacent sites. Holstein proposed a model to determine the mobility of polarons as a function of the lattice constant a, the electron transfer energy J, the reduced mass of the sites M, the frequency of the

molecules harmonic oscillator ω_0, the polaron binding energy and the temperature T.

$$\mu = \sqrt{\frac{\pi}{2}} \frac{qa^2}{\hbar} \frac{J^2}{\sqrt{E_b}} (kT)^{-3/2} \exp\left(\frac{E_b}{kT}\right) \tag{2.11}$$

2.2.2 Charge Injection

If we consider a metal and a semiconductor in contact, a barrier is formed at the interface. This barrier is responsible for controlling the current conduction behaviour. In the ideal case, it is defined as the difference between the metal work function (W_f) and the semiconductor HOMO level, for p-type injection, or LUMO level for n-type injection. A good ohmic contact is present when this barrier is as low as possible, contrarily, if there is an high barrier there is a poor charge injection and thus, namely, a bad ohmic contact is present. The most common model for defining the charge injection mechanism between the metal/semiconductor interface, is the Mott-Schottky model. In the simplest formulation of the model, it is supposed that both vacuum levels of the metal and of the semiconductor are at the same level. Indeed, when the metal and the organic semiconductor come in intimate contact, the organic material is in the potential rise of the tail of the metal electron distribution. Thus, both the vacuum levels get aligned in a very narrow interfacial gap. However, in this configuration the two Fermi energy-levels (E_f) are not aligned, thus a so-called built-in barrier is present. This leads to a charge flow from one material to the other, in order to compensate this unbalance. There are two extreme cases to consider, depending on whether the transferred charge forms an interfacial dipole within the first molecular layer of the semiconductor or occupies only dopant levels in the bulk. The latter case yields the Mott-Schottky rule, which states that the vacuum levels align at the interface, and then the additional charge resides in a depletion zone

created by ionizing donor or acceptor dopants and causes band bending. As a result a diffusion layer is formed to align the Fermi energies of the two solids. The barrier is formed after the contact between the metal and the semiconductor, and physically consists of a region of uncompensated charge. This space charge causes a voltage drop at the interface. From the energetic point of view, there is a bending of the energetic levels of the semiconducting material at the interface, as metal creates a gap with respect to its work function (see fig.2.8). The charge injection barriers

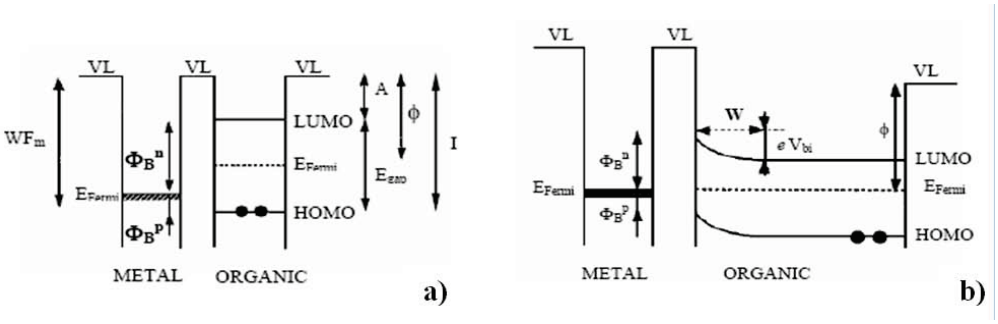

Figure 2.8: Scheme of an energy level diagram for an ideal metal-semiconductor interface, when the two solids are not in contact(a), in which they have the same vacuum levels and when they form an interface(b). VL is the vacuum level, WF_m is the metal work function, A and I are the electron affinity and ionization energy of the semiconductor, respectively. When the two solids are in contact a diffusion layer with a thickness of W is formed.

can be easily obtained by simply determining Φ_B^n for electrons and Φ_B^p for holes, as follows:

$$\Phi_B^n = WF_m - A \tag{2.12}$$

$$\Phi_B^p = I - WF_m \tag{2.13}$$

with I and A as ionization energy and electron affinity of the semiconductor, respectively. However in the real cases most of organic semiconductor/metal interfaces don't follow the Mott-Schottky model since the electronic structure is more complex with respect of represented in 2.8. Often an interface dipole Δ is present with the effect of shifting upward the semiconductor vacuum level with respect to the metal one.

The interface dipoles have different potential origins. They can be formed by a charge transfer effect between the semiconductor molecules and the metal or by a reduction of the metal work function due to an absorption of the organic layer and population of metal-induced mid-gap (new energy levels) at the interface. Sometimes, simple chemical notions (e.g., high or low electron affinities) can be used to predict the sign of the dipole (i.e., whether it points to the metal or to the semiconductor), but the prediction of its magnitude is a difficult computational problem.

2.3 Optical Properties of Organic Semiconductors

The optical properties of organic semiconductors are mainly determined by their fundamental photo-excitations. In solids with a long-range translational order, the quantum of excitation is able to move in different molecular units. This aspect leads to define a quasi-particle called *exciton*. A basic definition of exciton can be found in the book of Dexter and Knox [11]. *It is a quantum of electronic excitation travelling in a periodic structure, whose motion is characterized by a wave vector*. In Van Der Walls solids, due to the weak intermolecular interactions, the fundamental excitations are Frenkel excitons [12]. These are characterized by a very small radius of the electron hole pair (< 5Å) due to a strong binding energy between them ($\sim$1 eV). The opposite case is represented by Wannier-Mott excitons, typical of covalent solids (inorganic semiconductors), where electron and holes are delocalized on many molecular or atomic sites of the solid. The Wannier–Mott exciton radius has values in the range 40-100 Å.

According to the electronic structure of the molecule and to the molecular packing in the solid, excitons can have different properties. A first very simple classification involves, as for molecular excitation, the electron/hole total spin moment that divides excitons in triplet and singlet. Other types of excitons have been found in organic

π-conjugated materials: charge transfer excitons, excimers and surface excitons.

In charge transfer exciton (CTE) electron and hole are more delocalized, usually spreading on the nearest neighbour molecules. They remind the Frenkel excitons in inorganic semiconductor and are of primary importance in the photoconduction processes (i.e. exciton dissociation and electron-hole separation). CTE have a weak oscillator strength and are usually detected with electroabsorption spectroscopy or non-linear spectroscopy such as photoinduced absorption spectroscopy [13]. Excimers (Excited-Dimers) are formed by an excited pairs of molecules. They consist of an excited state which form a complex between two molecules. This complex is unstable (dissociative) when the molecules are in their ground states. As a consequence, the ground state potential energy surface is lacking of any minima and has higher energy with respect to that of the isolated molecule ground state. Thus, the excimer photoluminescence (PL) is characterized by a broad (unbound ground state) red-shifted band and a longer PL decay with respect to the isolated molecule. Molecules that show typical excimer emission are perylene and pyrene, in which the pair-like solid state packing is highly favorable for excimer formation. Surface excitons are quite rare states and can be observed only in molecular crystals at very low temperature (below 10 K). The appearance of these states is related to the abrupt change in the molecular environment for molecules at the crystal surface with respect to that in the bulk. This influences strongly the PL features, according to the unit cell geometry and the exposed surface. They have been observed in highly pure anthracene and tetracene crystals.

2.3.1 Excitons in thin films

The excitonic energy levels of a molecular solid are strongly influenced by the molecular arrangement. In thin films, according to the preparation procedure, it is possible to obtain different degrees of molecular order. As a consequence the film morphology

has a direct impact on the optical properties of the film [14, 15]. Also the substrate on which the film is prepared has a role in the molecular ordering. Epitaxial growth or quasi-epitaxy has been demonstrated by using single crystal substrates [15].
As a general rule, if the film has a crystalline morphology, the exciton levels and the optical properties will be very similar to those of the corresponding single crystal. In the case of amorphous films, intermolecular interactions are relaxed or even absent and the absorption or PL spectra will resemble those of the isolated molecule [16].
Between these two extreme there are a plenty of cases in which the film morphology tunes the optical properties. One of the most common situation is the concomitant presence of ordered crystallites and disordered or amorphous regions. In this case excitons that are generated in the crystalline domains diffuse (if they do not decay) with a thermally activated hopping process till they find a low energy level. Then excitons are trapped if the thermal energy is not sufficient for detrapping. These trapping sites can be created by a more disordered molecular aggregation with respect to that of the crystal.

Exciton Generation

An exciton can be generated exciting the crystal or the thin film with an electromagnetic wave. This light must have a frequency resonant with the energy gap and the right polarization with respect to the transition dipole moments. Moreover, in order to have light absorption and exciton creation, optical selection rules must be satisfied. In particular, the photon momentum q must be equal to the k wave vector of the electronic level. Since in the UV/VIS region $q \sim 0$, only $k = 0$ states are probed. If the crystal has an inversion center then states are classified as gerade (g) and ungerade (u) and only $u \leftarrow g$ transition are allowed. Two photon absorption (i.e. absorption of light through a mid gap virtual state), being a second order process, is

capable to perform g $\leftarrow$ g transitions [17].

Either Davydov components of a particular singlet component can be produced, but the lowest-lying singlet exciton represents the surviving state after about a picosecond. Thus, while a triplet exciton can be generated directly, the absorption coefficient for this transition can be quite small; for example in anthracene the singlet-singlet transition rate is 10^8 higher than the singlet-triplet one. An electrical way to generate excitons is by charge carrier recombination. This process involves: the injection of holes and electrons in the material by means of electrodes, their diffusion in the presence of an electric field, charge recombination and exciton formation. In this case both triplet and singlet exciton are created with a ratio $3/1$, respectively. Light emission of electrically generated exciton is called electroluminescence (EL) and in organic semiconductors was first observed by Pope [18]. Electroluminescence is at the basis of the operation of optoelectronic devices such as organic light-emitting diodes (OLEDs) [15] and organic light-emitting field-effect transistors (OLETs) [19].

Exciton Migration

As pointed out in the definition of exciton, this quasiparticle is characterized by a wave-like motion. This aspect is relevant not only from the fundamental viewpoint of the energy transport but also because of its importance in opto-electronic device realization. The absorption of a photon by the organic solid creates a Frenkel state with **k** wave vector near to zero. Immediately after exciton creation, the phases of the wave functions of all excited molecules have a unique defined relationship to each other. If the phases are maintained during the excitation migration, the exciton moves as a wave and is said to be coherent. However, because of the interactions with lattice modes (phonons) and imperfections (physical and chemical) in the crystal, transitions are induced among the various state accessible to the exciton and the

coherence may be lost. For time greater that the coherence time (time for which the exciton remains coherent) the exciton is viewed as a localized excitation undergoing a random hopping-like motion. Typical values of the exciton diffusion coefficients for single crystals are $10^{-3} - 10^{-5} cm^2 sec^{-1}$. During hopping movement, excitons can encounter sites with an energy lower than the exciton band edge. In this case, if the thermal energy is not sufficient to promote the hopping, the exciton is trapped. Then it can relax with emission of radiation or with a non radiative pathway. An analysis of the exciton absorption line width can provide a measure of the degree of the exciton coherence if the magnitude of the homogeneous line width can be estimated. Homogeneous line broadening is caused by local site energy fluctuation from site to site due to thermal effects and natural isotopic impurities thus reflecting the motion of the individual (as opposed to ensemble) molecular excitation. So in the case of highly delocalized exciton and weak exciton-phonon coupling, Lorentzian optical absorption line shape is expected. The presence of Gaussian line shapes is interpreted as from the statistical nature of phonon effects on the local site energy of the electronic excited state, i.e. inhomogeneous line broadening. This line shape is indicative of localized, incoherent exciton motion corresponding to strong exciton-phonon coupling [3].

Energy Transfer

The term *energy transfer* is used to describe a process that involves one donor molecule and one acceptor molecule, whereas energy migration refers to the process of movement of the exciton. Usually migration involves a series of transfers if no intervening trap hinders the process [20]. The process of photon re-absorption, sometimes called cascade or trivial energy transfer, is important at long distances typically more than 100Å from the site of the excitation. In this process fluorescence is emit-

ted from a donor and reabsorbed by the acceptor. Reabsorbed fluorescence can play a significant role in increasing photo-conductivity produced by highly absorbed light since the fluorescent light can de-trap carriers, removed from the illuminated surface that ordinarily could not be de-trapped either thermally or by exciton interactions. The second mechanism of transfer, known as resonant or Förster transfer, depends upon the overlap between the absorption spectrum of the acceptor (A) and the fluorescence spectrum of the donor (D). This transfer occurs without the appearance of

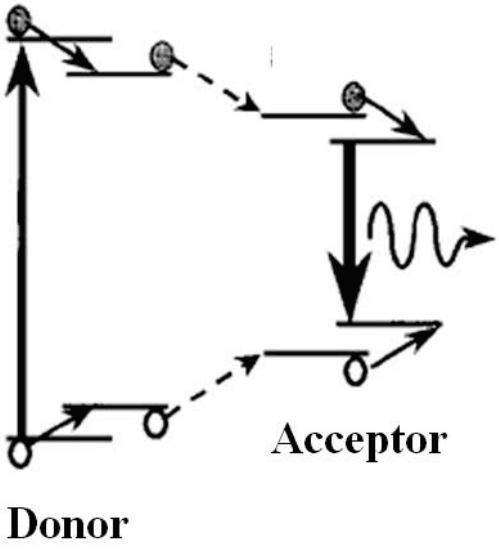

Figure 2.9: Energy level diagram of a donor-acceptor system in which a Förster energy transfer can occur. Non-radiative Förster energy transfer from donor molecules is reported with dashed arrows, while the Franck - Condon shift with solid arrows.

a photon, and is primarily a result of a dipole-dipole interactions between the donor and the acceptor. The rate of energy transfer depends upon the extend of overlap of the emission spectrum of the donor with the absorption spectrum of the acceptor, the relative orientation of the donor and the acceptor transition dipole moments, and the distance molecules. It is this latter dependence upon distance which has resulted in a widespread use of the energy transfer to measure distances between donors and

acceptors. The rate of energy transfer from a specific donor to a specific acceptor is given by

$$K_T = \frac{1}{\tau_D}\left(\frac{R_0}{r}\right)^6 \tag{2.14}$$

in which τ_D is defied as the lifetime of the donor in absence of acceptor, r as the distance between the donor and the acceptor and R_0 as a characteristics distance called the Förster radius at which the efficiency of the transfer is 50%.

Exciton Relaxation

There are many pathways that an exciton can undergo in order to relax to the fundamental ground state. The investigation of the energetics and the dynamics involved in these processes is the fundamental question of solid state photophysics. We will discuss in detail all the typical processes of relaxation pathways for an exciton which are reported in Fig.2.10. Initially, light with a resonant frequency is absorbed and an exciton is created in the upper or lower Davydov component (upward arrow) according to frequency and polarization. Few hundreds of femtoseconds later the exciton can either relax to the lowest Davydov component (curved arrow) or it can hop to the nearest sites (thick bended arrow) and eventually dissociate to the nearest or next-nearest molecular neighbours to form a charge transfer state. All these early stage processes are non-radiative. It is important to point out here that, according to the Kasha rule, radiative relaxation always takes place from the lowest state of the exciton band since the internal conversion from higher singlet excited states to the lowest takes place in less than 10ps. As a consequence, we expect light emission from the lowest excitonic level and eventually from *relaxed states* that lie just below the exciton band. In fig.2.10 it is shown that is possible to observe fluorescence (downward arrow) from the above mentioned singlet states and eventually phosphorescence (oblique arrow) from triplet exciton states. The fluorescence is a process that occurs

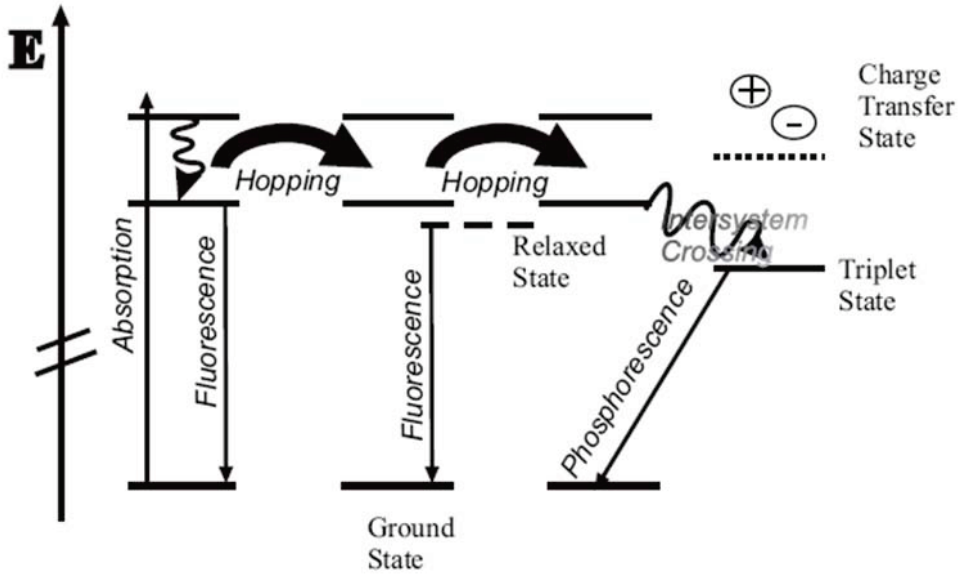

Figure 2.10: Scheme of the energy diagram for a molecular solid with two Davydov components, a charge transfer state and a relaxed state. Upward arrow shows the absorption of a photon to an higher Davydov band energy level. Thick bend arrows show the exciton hopping between adjacent molecular sites. Wavy downward arrows show non-radiative processes (internal conversion and inter-system crossing) while straight downward arrows represent radiative processes.

spontaneously. The radiationless transition from an excited singlet state to a triplet state can be induced by internal perturbations (spin-orbit coupling, substituents containing nuclei with high atomic number) as well as by external perturbations (paramagnetic collision partners, like O_2 molecules in the solution, or solvent molecules containing nuclei of high atomic number). These radiationless transitions are called intersystem crossing. The transition from the first triplet state to the singlet ground state has a much longer lifetime (ranging from milliseconds to several seconds) with respect to fluorescence process since it is a forbidden transition. As it can be seen in fig.2.10, all the transitions are characterized by a rate constant **k** that is defined as the sum of at least two components $k = k_r + k_{nr}$, that take into account both radiative and non-radiative deactivation processes. In the case of fluorescence the measured lifetime is the reciprocal of **k**. In order to obtain k_r, a measure of the

fluorescence quantum yield Φ_F must be carried out, given the following relation

$$k_r = \Phi k \tag{2.15}$$

The fluorescence quantum yield is a number ranging between 0 and 1 and indicating the ratio between the numbers of photons emitted in the fluorescence process and the photons absorbed.

2.4 REFERENCES

[1] A Sacco. *Fondamenti di chimica*.

[2] C Cohen-Tannoudji, B Diu, and F Laloe. *Quantum Mechanics: Volume I*. 1992, 2nd ed.

[3] F Pope and C. E. Swenberg. *Electronic processes in Organic Crystals 2nd ed.* Oxford University Press, USA, 1999.

[4] E. A. Silinsh and V. Cpek. *Organic molecular crystals: Interaction, localization and transport properties*. 1994.

[5] Z Bao and J Locklin. *Organic field-effect transistors*. 2007.

[6] A.A. Maraudin, Montrol E.W., and G.H. Weiss. *Theory of Lattice Dynamics in the Harmonic Approximation, 2nd edition, Solid state Physics Suppl. 3*. 1963.

[7] I.G. Austin and N.F. Mott. Polarons in crystalline and non-crystalline materials. *Adv. Phys.*, 18(71):41, 1969.

[8] T. Holstein. Studies of polaron motion : Part ii. the small polaron. *Ann. Phys.*, 8(3):343, 1959.

[9] M. Shur and M. Hack. Physics of amourphous silicon based alloy field-effect transistors. *J. Appl. Phys.*, 55(10):38313842, 1984.

[10] A. Miller and E. Abrahams. *Phys. Rev.*, 120:745, 1960.

[11] D.L. Dexter and R.S. Knox. *Excitons*. 1965.

[12] D.P. Craig and S.H. Walmsley. *Excitons in molecular crystals: Theory and Applications*. 1968.

[13] G. Lanzani, S.V. Frolov, P.A. Lane, Z.V. Vardeny, M. Nisoli, and S. De Silvestri. Transient spectroscopy of frenkel and charge transfer excitons in alpha-sexithienyl films. *Phys. Rev. Lett.*, 79(16):3066–3069, 1997.

[14] F Meinardi, M. Cerminara, A. Sassella, A. Borghesi, P Spearman, G Bongiovanni, A Mura, and R Tubino. Intrinsic excitonic luminescence in odd and even numbered oligothiophenes. *Phys. Rev. Lett.*, 89(15):157403, 2002.

[15] S. R. Forrest. Ultrathin organic films grown by organic molecular beam deposition and related techniques. *Chem. Rev.*, 97(6):1793, 1997.

[16] E. Lunedei. *PhD thesis*. PhD thesis, Univ. Stuttgart, 2003.

[17] N. Periasamy, D Danieli, G Ruani, R Zamboni, and C. Taliani. Location of the low-energy ag-1 state in a polythiophene oligomer by 2-photon absorption-spectroscopy - alpha-sexithienyl. *Phys. Rev. Lett.*, 68(7):919–922, 1992.

[18] M. Pope, H. Kallmann, and P. Magnante. Electroluminescence in organic crystals. *J. Chem. Phys.*, 38(8):2042, 1963.

[19] Muccini M. A bright future for organic field-effect transistors. *Nat. Mater.*, 5(8):605–613, 2006.

[20] R. Lakowicz. *Principles of Fluorescence Spectrocopy*. 1983.

Chapter 3

OFETs and OLETs Working Principles

3.1 Organic Field-Effect Transistor (OFET)

A transistor is a semiconductor device commonly used as an amplifier or an electrically controlled switch. The first field-effect transistor (FET) was inorganic and was invented in 1947 by John Bardeen, William Shockley and Walter Brittain (Nobel prize, 1956). Since their discovery, transistors have dominated the mainstream microelectronics industry; in fact they are the fundamental building blocks for basic analytical circuits. An Organic Field-Effect Transistor (OFET) is a transistor based on organic semiconductors. The interest in using organic semiconductors as the active layers in FETs stemmed from the demonstration of field-effect conduction in small organic molecules and conjugated polymers [1]. In 1986 the first OFET was reported by A. Tsumara [2]. From that moment a huge improvement in materials performances and development of new fabrication techniques took place. OFETs are technologically attractive because all their layers can be deposited at low temperature and with low cost, in a large area and on a flexible substrate [3]. OFETs have also already been demonstrated in flexible electronic applications such as active matrix

electronic paper displays, sensors, and low-cost radiofrequency identification cards (RFIDs). In order to render these devices more suitable for various applications an important step is to increase the charge carriers mobility. Indeed, the performances of OFETs are still lower with respect to those of the amorphous silicon devices. Since conjugated organic solid are more similar to insulators than semiconductors, charge transport in these materials is much less efficient than in conventional semiconductors. Clearly, the problem is more crucial in transistors where charges have to travel along much longer paths than in diodes. At the current state of the art, mobility in organic thin-film transistor ranges between 0.01 and 10 cm^2/Vs, which is still much lower than what found in inorganic semiconductors (mobility is around 10^3 cm^2/Vs in crystalline silicon), but substantially higher than the typical values obtained in organic light-emitting diodes or photovoltaic cells. In particular, hole mobility on the order of 1 cm^2/Vs and 0.1 cm^2/Vs was reached using respectively small molecules [4] and conjugated polymers [5] as organic semiconductor materials. The highest mobility and most intrinsic charge transport properties in organic semiconductors are observed in single crystals, in particular, hole mobility of up to 20 cm^2/Vs is observed in rubrene [6]. High mobility in OFET is the result of large research efforts at improving structural order in the organic semiconductor film. In addition to high mobility values, the major objectives are: stability under ambient conditions and under bias stress, device to device fabrication reproducibility as well as easy processing, e.g., from solution, which would make organic semiconductors a viable alternative to amorphous silicon. Before explaining the OFETs working principles, we introduce the main structures that compose the device and define its working characteristics.

3.1.1 Gate Dielectric

The crucial process of charge accumulation and transport in OFET takes place at the interface between the gate dielectric and the semiconductor. Thus, the properties of this interface and the dielectric have a huge influence on device characteristics. Device parameters such as mobility, threshold voltage, sub-threshold swing, etc. depend not only on the nature of the semiconductor but also on the chemical structure and dielectric properties of the insulator. The requirements for gate dielectrics in OFET are rigorous. They should show high dielectric breakdown strength, contain only minimal concentrations of impurities, that could act as traps, easily processable and be environmentally stable. Apart from their breakdown strength, gate dielectrics are mainly characterized by their dielectric constant ϵ_r (also named κ), which determines the capacitance per unit of area $C_i = \frac{\epsilon_r \epsilon_0}{d}$ of a dielectric layer of thickness d (ϵ_0 is the permittivity of vacuum) and thus the amount of induced charges per applied V_g. Hence, in order to achieve a certain amount of charges in the transistor channel, one can either reduce the dielectric thickness or use a dielectric with a higher ϵ_r. Since the ready availability of doped silicon wafers with high quality, smooth, thermal silicon dioxide that can also be used as substrates and give reproducible results for many semiconductors, typically organic semiconductors are grown on SiO_2 ($\epsilon_r = 3.9$) for testing purpose. Many groups investigated the influence of surface treatments of SiO_2 (e.g., with hexamethyldisilazane (HMDS) or self-assembled monolayers of different silanes) on the performance of organic transistors, looking at the change of morphology of semiconductor film, number of trap states, and dipoles at the surface [7]. Other metal oxides with higher ϵ_r such as, e.g., Al_2O_3 ($\epsilon_r = 10$) [8] and Ta_2O_5 ($\epsilon_r = 10$) [9] have also been investigated as possible gate dielectrics for organic transistors. Nevertheless, for the application of organic semiconductors in flexible electronics, SiO_2 and other oxides are not ideal dielectrics. In order to use

them on flexible substrates, they usually need to be sputtered or anodized, which leads to inferior device performance. Another option are insulating polymers that can be processed from solution, that do not require high temperature processing, and whose characteristics can be tuned over a wide range by changing their chemical structure. Polymer gate dielectrics have been used in top as well as bottom gate transistors, and their impact on morphology and mobility was investigated [10]. They are easily applied in top gate transistors, where they are spun on top of the semiconductor, from solvents orthogonal to the semiconductor in order to prevent any influence of the interface morphology or damage the semiconductor [11].

3.1.2 Charge Injection from Metal

Despite the fact that significant potential barriers ($> 0.3eV$) exist at metal-organic semiconductor interfaces, it is possible to obtain ohmic source and drain contacts in OFETs. A likely explanation for such a behaviour is that the charge injection mechanism is probably not simple thermionic emission in which carriers must overcome the full potential barrier. Instead, at intense interfacial electric field, field emission (tunnelling) through the barrier can become possible thus lowering effectively the potential barrier. Another possible injection mechanism involves defect-assisted transport in which carriers bypass the barrier by hopping through mid-gap states. In Fig.3.1 we report simple comparison of these different charge injection mechanisms. Measurements on the source contact resistance as a function of temperature reveal that the injection process is indeed thermally activated (which is consistent with thermionic emission), but the activation energies are generally much smaller than the estimated energy potential barriers determined by photo-emission spectroscopy. In some cases, the activation energy associated with the source contact resistance is very similar to the activation energy associated with the carrier field-effect mobil-

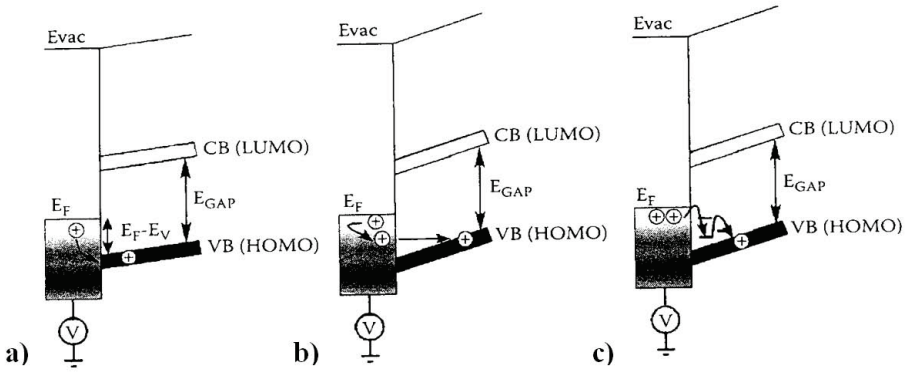

Figure 3.1: Comparison of different charge injection mechanisms at a biased metal-semiconductor contact: (a) thermionic emission, (b) field emission (tunnelling), (c) defect assisted injection.

ity, thus suggesting that transport of charge in the semiconductor near the contact (depletion region) is the limiting bottleneck. Moreover the source and drain contact resistances are strongly gate voltage dependent; specifically, they decrease with increasing gate voltage. The variation of the contact resistance with gate voltage is essentially identical for both the source and the drain, and it is also similar to the variation of the channel resistance. The close tracking of the gate voltage dependence on the source, drain and channel resistances also indicates that resistance depends on the film transport properties and morphology near the contact.

3.1.3 Active Materials

A detailed description of the semiconducting properties of the active materials have been already reported in the previous chapter. In general the majority of Organic Semiconductors (OS) are p-type, but in the last years a number of n-type materials have been produced [12, 13]. Typical OS feature relatively wide band gap: in the range of $2 - 3\ eV$. The synthesis of new n-type or ambipolar OS involve the presence of high electron affinity groups in the material, comprising specific electron

withdrawing groups [12] (as -F, -CO, etc). It was recently clarified that not only does the chemical structure of the organic material determine its behaviour, but also processing conditions, the choice of electrodes and the dielectric species are relevant for the OFET operations. The material transport properties strongly depend to the interfaces present in the device in which it is used. Therefore, instead of p-type or n-type OFET, one should better refer to p-channel or n-channel transistors.

3.1.4 OFETs Working Principles

A field-effect transistor is composed by a semiconducting material working as a channel in which current flows. At one extremity of the channel there is an electrode called source and at the opposite side there is a second electrode called drain. The physical dimension of the channel are fixed but the portion of the active material actually used for the conduction can be varied by applying a voltage to a third electrode called gate. The FET conductivity depends on the portion of the channel open to the current. Little changes in the gate voltage can involve great changes in the current flowing from the source to the drain, thus amplifying the signal. If the channel is composed by an organic material, we have an organic field-effect transistor (OFET). The channel is in contact with a dielectric layer working as a capacitor, and allows current modulation through the gate voltage. The main constituting elements of an OFET are: three contacts (source, drain and gate), an active semiconducting material and a dielectric layer. These key elements can be differently combined to obtain different device structures. The most common configurations are: bottom gate - bottom contact (in which the drain and source electrodes are positioned directly on the dielectric film), bottom gate - top contact (in which the source and drain electrodes are grown on the organic semiconductor) and top gate - bottom contact (in which the dielectric film is deposited on the organic semiconductor and the gate contact is placed on top

of it). Since throughout this thesis we deal only with bottom gate-top contact configuration (Fig.3.2), we use this simple configuration to discuss briefly how a classic OFET works. The physical dimension of the channel is fixed and it is described by the channel length (L) and the channel width (W). We refer to the voltage applied between drain and source as V_{ds}, while the voltage applied to the gate is labelled as V_{gs}. By convention, the source is generally considered grounded and the voltage is applied to the drain contact. The current flowing through the channel is called Ids and it is a strong function of V_{gs}. The dielectric is sandwiched between the gate and

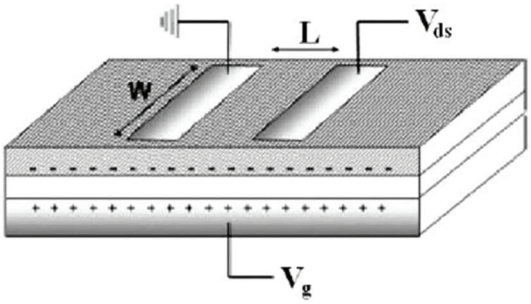

Figure 3.2: Classic BG-TC geometry with physical channel dimensions labelled: W as channel width, L as channel length.

the organic semiconductor, and they work as two plates of a plane capacitor. Thus, when a V_{gs} is applied, charges of different sign are accumulated at gate/dielectric and dielectric/organic semiconductor interfaces (as in a classic capacitor, in Fig.3.2 a positive gate voltage applied as an example). Much of this accumulated charge in the active material is mobile and moves in response to the applied V_{ds}. When no V_{gs} is applied there are ideally no free charge carriers, and the device is off. Otherwise, with applied V_{gs} the device is on. This gate-induced charge carrier creation is called field-effect, and it is the key-idea of the working principle of FETs [14]. An n-channel OFET (i.e., electrons are transported through the channel) can be used as an example to understand the basic device operational regimes due to the gate

voltage dependence of the distribution of "free" charges in the active material [15]. If we assume ohmic contacts and no trap presence (ideal case), when a $V_{gs} > 0$ is applied, free electrons start accumulating at organic semiconductor/dielectric interface. Without any voltage difference between drain and source ($V_{ds} = 0$), this negative charge density is uniform along all the active material, thus having a uniform conduction channel. If a positive V_{ds} is applied, the induced charge superficial density in a certain position x of the semiconductor is described by:

$$q_{ind} = n(x)et = C_i \left[V_{gs} - V(x)\right] \tag{3.1}$$

where t is the thickness of the charge layer in the channel, $n(x)$ is the number density of charges in the channel, e is the electron charge and C_i is the insulator capacitance per area unit. However, real devices are far from being ideal and not all induced charges are mobile; a large number of deep charge traps are present in the film (deep enough to effectively immobilize electrons trapped in them). Deep traps have to be filled before the additionally induced charge can move. Thus, a minimum gate voltage has to be applied to obtain free electron density in the channel, the threshold voltage, V_{th}. Obviously, in n-channel OFETs V_{th} is higher than zero (for a p-channel OFETs, V_{th} is lower than zero since the charges flowing are positive). If we include the threshold voltage in the previous equation:

$$q_{ind} = n(x)et = C_i \left[V_g - V_{th} - V(x)\right] \tag{3.2}$$

As V_{th} is not ideally a function of x, with $V_{ds} = 0$ and $V_{gs} > V_{th}$ a homogeneous charge density is present in the channel. When a small source-drain voltage is applied ($V_{ds} << V_{gs} - V_{th}$) a linear gradient of charge density is formed. The voltage drop between organic semiconductor and gate is larger at the source, where $V(x) = 0$ (grounded), than at the drain, where $V(x) = V_{ds}$. This is the linear regime in which the current flowing through the channel is directly proportional to V_{ds} (Fig.3.3a).

When the source-drain voltage is further increased, we reach a point where a potential

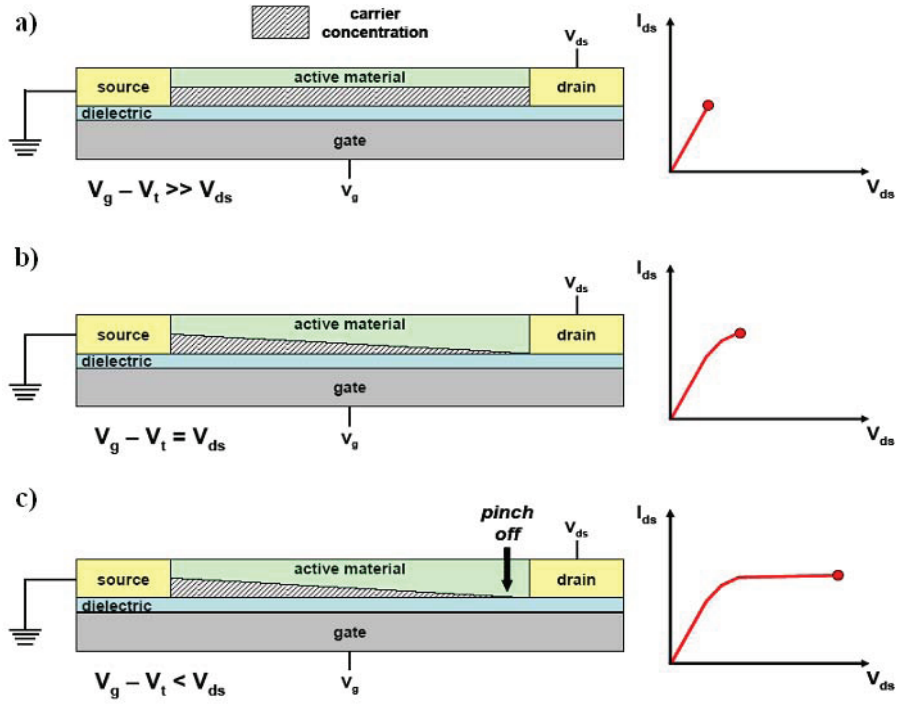

Figure 3.3: Schematic structure of an OFET. a) Carrier concentration profile in the linear regime; b) Carrier concentration profile when the pinch off occurs near the drain electrode (V_{gs}–V_{th}=V_{ds}); c) Carrier concentration profile in the saturation regime.

difference between the gate and the part of the channel near the drain no longer exists, the channel is pinched off. This means that a charge carrier depletion region is formed next to the drain, because the difference between the local potential $V(x)$ and V_{gs} is lower than the threshold voltage. A space-charged-limited saturation current can flow across this narrow depletion zone. Carriers are swept from the pinch point to the drain by a comparatively high electric field in the depletion region (Fig.3.3b). A further increase in V_{ds} pushes the pinch-off point further away from the drain (Fig.3.3c). However the length of the channel (L) shortens only slightly, as it is infinitely larger than the width of the depletion region, and the integrated resistance of the channel from the source to the pinch point remains more or less the same.

For these reasons once pinch off condition is met, current saturates at I_{ds}^{sat}. From a mathematical point of view, pinch off is reached when $V_{ds} = V_{gs} - V_{th}$. The current-voltage characteristics in the different operating regimes of an OFET can be described analytically, in a simplistic way assuming that (1) the transverse electric field induced by the gate voltage is largely higher than the longitudinal field induced by the gate bias (gradual channel approximation) and (2) the mobility is constant all over the channel. Assumption (1) is justified by the geometry of the device since the distance from source to drain is often much larger than the thickness of the insulator. Assumption (2) is almost always fulfilled in inorganic semiconductors. However, this is far from true in organic solids as we pointed out. In short, I-V characteristics can be drawn by either varying the drain voltage at a constant gate voltage (output characteristics) or changing the gate voltage at a fixed drain voltage (transfer characteristics). Locus characteristics are obtained by varying simultaneously drain voltage and gate voltage and keeping them at the same value so that the pinch-off condition is always reached in the reached the drain electrode. In the output characteristics, the curves are divided into a linear regime at low V_{ds} that turns into the saturation regime when $V_{ds} > V_{gs}$. The current Ids in both regimes is given by the equations

$$I_{ds}^{lin} = \frac{W}{L} C_i \mu \left[(V_{gs} - V_{th})\, V_{ds} - \frac{V_{ds}^2}{2} \right] \qquad Linear Regime \tag{3.3}$$

$$I_{ds}^{sat} = \frac{W}{2L} C_i \mu \, (V_{gs} - V_{th})^2 \qquad Saturation Regime \tag{3.4}$$

in which μ is the charge carrier mobility.

A widely used method for parameter extraction from the characteristics curve consist of plotting the square root of the saturation current as a function of gate voltage. As it is clear from the saturation-regime curve, the square root of the saturation regime is supposed to give a straight line whose slope is an estimation of the mobility while its extrapolation to the x axis corresponds to the threshold voltage. Mobility

value can be calculated also in the linear regime but often is different from the one calculated in the saturation regime (usually it is higher). This happens because the conduction channel resistance in saturation is higher than in the linear case, hence contact resistance is less critical than in the linear region. However, the two mobility values must be equal in devices with good injection contacts. Since the mobility is gate-bias dependent, an exact estimation of the saturation current would require integrating the mobility all along the channel, which does not appear feasible given that the gate-bias dependence of the mobility for a device is not known before-head.

3.2 Ambipolar OFETs

While the development of ambipolar (both hole- and electron-transporting) OFETs is still at early stages, it is certainly an exciting subject within the OFET community. These devices offer not only new possibilities for complementary logic circuit design, but also the potential to control electron-hole recombination within the semiconductor channel to afford light emission. In general, an organic transistor is called ambipolar when it shows a current flow when biased in p-type polarization (negative bias) as well as in n-type polarization (positive bias). The ambipolar condition can be obtained either by intrinsic properties of the organic semiconductor, or by superimposing organic semiconductors of opposite charge carriers or by blending of two opposite charge carriers organic semiconductors.

The mathematical description of the ambipolar curves is the same for each case. Instead the interpretation of the device main parameters behaviour must take into account the charge injection, charge accumulation and recombination phenomena that depend on the structure.

3.2.1 Intrinsic Ambipolar OFET

To better understand how an ambipolar works, let's consider the simplified case in which the source electrode is kept at ground and we vary the drain and gate voltages with respect to the source. In an intrinsic ambipolar OFET (extended also to an ambipolar thin-film blend OFET) in order to inject electrons in the channel, a locally negative potential between the gate and the injecting electrode, is necessary. Similarly, in order to inject holes in the device, there must be a locally positive potential between the gate and the injecting electrode. If the absolute value of gate voltage (V_{gs}) is higher of the absolute value of drain-source potential (V_{ds}), ($|V_{gs}| > |V_{ds}|$), then the local potential at the electrodes has the same sign. In this condition only one type of charge carrier can be injected. The case is similar to a unipolar OFET, in fact the ambipolar OFET is said to be working in **unipolar region**. If, instead, $|V_{gs}| < |V_{ds}|$, then, the local potentials at the injecting electrodes have different signs. Since the semiconductor can transport holes as well as electrons, in this condition both charge carriers flowing in the device. The device is said to be working in **ambipolar region**. A detailed description of the working regions of an ambipolar OFET is reported in Fig.3.4. From the mathematical point of view, the model that describes an intrinsic ambipolar transistor is based on the coupling of two *non-interacting* unipolar OFET p-type and n-type. The coupling between the two OFETs is defined by the edge conditions defined by three contacts voltages. Let's consider as first, the case in which gate voltage is positive. The n-type unipolar OFET will be defined by the V_{gs} and V_{ds} potentials. The p-type unipolar OFET, instead, will be defined by the potentials V_{gd} ($V_{gd} = V_{gs} - V_{ds}$) and V_{ds}. The total current flowing in the ambipolar OFET is given by the sum of the unipolar currents. When the gate is negatively biased, the model is the same except that considerations done for the n-type and p-type OFET must be inverted. In equations 3.5 and 3.6

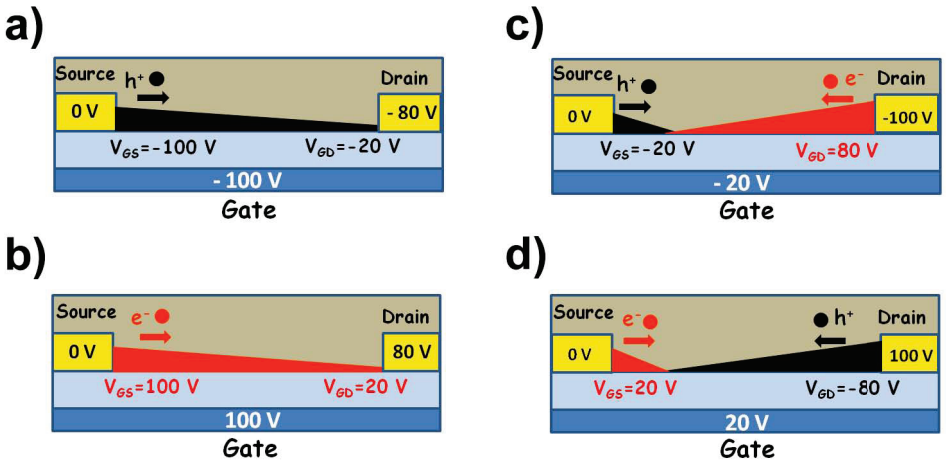

Figure 3.4: Example of an ambipolar OFET working in unipolar regime biased for hole transport (a) or electron transport (b). In this cases the V_{gs} and V_{gd} voltages have the same sign. In ambipolar regime, instead, there are two more cases, (c) when the gate is p-type (negative) polarized and (d) when gate is n-type (positive) polarized. These regimes are characterized by V_{gs} and V_{gd} voltages of opposite signs.

is reported the drain-source current (I_{ds}) model for the ambipolar case with positive gate voltage bias.

$$I_{ds} = I^n + I^p \tag{3.5}$$

with

$$\begin{aligned} I^n &= \mu^n C_i \frac{W}{L} \begin{cases} (V_{gs} - V_{th}^n)V_{ds} - \dfrac{V_{ds}^2}{2} & \text{for } |V_{ds}| < |V_{gs} - V_{th}^n| \\ \dfrac{1}{2}(V_{gs} - V_{th}^n)^2 & \text{for } |V_{ds}| \geq |V_{gs} - V_{th}^n| \end{cases} \\ I^p &= \mu^p C_i \frac{W}{L} \begin{cases} (V_{gd} - V_{th}^p)V_{ds} - \dfrac{V_{ds}^2}{2} & \text{for } |V_{ds}| < |V_{gd} - V_{th}^p| \\ \dfrac{1}{2}(V_{gd} - V_{th}^p)^2 & \text{for } |V_{ds}| \geq |V_{gd} - V_{th}^p| \end{cases} \end{aligned} \tag{3.6}$$

where

$$\mu^n \neq \mu^p, \qquad V_{th}^n \neq V_{th}^p, \qquad V_{gs} > 0$$

In a typical ambipolar OFET, the electrical curves show a characteristic effect not present in unipolar devices. Since both charge carriers can flow through the channel, the I_{ds} output current does not completely saturates but it is composed by two phases. In the first phase, when one charge carrier is flowing, the behaviour is similar to a unipolar OFET and eventually the current can reach a temporary plateaux. When the gate voltage reaches a local bias that permits the injection of the opposite charge carrier, the I_{ds} output current begin to raise quadratically (second phase). In I-V transfer curves in saturation regime, instead the behaviour of an ideal ambipolar OFET is represented by a typical *V-shaped* curve. Each branch of the curve represents a different charge carrier as a function of the polarity of the gate contact. When the gate voltage is biased at the edges of the curve, there is a unipolar current (I_{ds}) whose charge carrier type is defined by the local difference of potentials at the electrode V_{gs} or V_{gd}. When the curve reaches a minimum in terms of drain-source current (represented by the bottom of the V-shape), there is the maximum of ambipolar behaviour of the OFET, thus the two charge carriers currents have the highest balance. An example of the typical curves of an ambipolar OFET is showed in Fig.3.5

3.2.2 Bi-layer OFET

In bi-layer OFETs, the ambipolar behaviour cannot be classified within the model of two *non-interacting* OFETs, since the electrical characteristics can change noticeably from the "ideal" situation. In the system previously described, the two OFETs were aligned and, thus, they have the same organic/dielectric interface where accumulation takes place and the same metal/organic injection interface. Moreover in the previous system all the injected charges recombined within the channel. In a bi-layer (or in a generic multi-layer) device, instead, the two OFETs, representing the model, are superimposed. Then, in this case the charge accumulation and charge injection

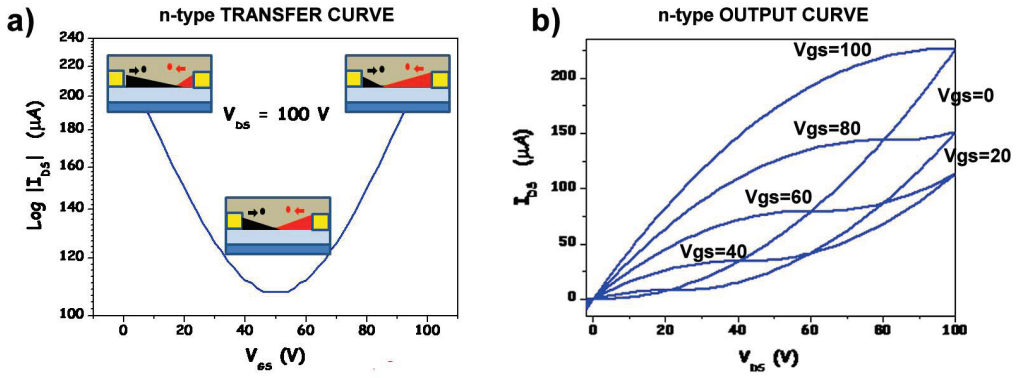

Figure 3.5: Typical curves of an ambipolar OFET with $|V_{th}^n| = |V_{th}^p| = 2V$ and $\mu^n = \mu^p = 0.1\ cm^2/Vs$. (a) represents an n-type transfer saturation curve. Superimposed on the curve are present schemes of devices along the currents flowing through the device in each region.(b) represents multiple IV output curves at different gate voltages.

interfaces are different for each OFET, therefore charge transport and charge accumulation of a layer could affect charge injection and charge accumulation of the other one.

From the mathematical point of view, the description is almost identical to the non-interacting case, if the distance between the two OFETs or their energetic levels permit to presume that there is not any vertical charge percolation between the devices.

In general, this "cross-talking" effect between the two systems can be a positive opportunity, e.g. it is possible to decrease V_{th} of the lower transport layer with an improved charge carrier injection assisted by the presence of the upper layer. However, for determining the overall characteristics of a bi-layer device, it is important also to consider the problem of growth compatibility of the active layer at the organic/organic interface that can either yield to a poor OFET or improve the positive effects mentioned before.

3.3 Organic Light-Emitting Field-Effect Transistor (OLET)

OLETs based on molecular and polymeric organic semiconductors are multifunctional devices that integrate light emission with the current modulating function of a transistor. The planar geometry of OLET offers direct access to the light emission region, providing a unique experimental configuration to investigate fundamental optical and electronic properties in organic semiconductors. Moreover, OLETs show great potential for technological applications such as active matrix full color electroluminescent displays.

In general, an OLET is a three-terminal device that couples the electrical characteristics of an OFET to the controlled radiative recombination of the electrons and holes injected in the channel via the drain and source contacts. Excitons are thus created by the recombination of in-plane moving electron- and hole-currents, which are controlled by the gate electrode. In order to understand the lighting characteristics of the OLET, it must be compared to the up-to-date state of the art in terms of organic light emission, the light-emitting diode (OLED).

The main difference between the vertical (OLED) and planar (OLET) device geometry is a direct consequence of the different device structures. In OLED, charge transport occurs perpendicular to the organic layers (bulk charge transport) while in OLET the transport occurs horizontally (field-effect charge transport). In Fig.3.6 we report the scheme of an OLED structure compared to a single-layer and single-material BG-TC OLET for showing the devices typical dimensions. Under the typical biasing conditions, the electron and hole mobility can be about four orders of magnitude higher in OLETs than in OLEDs, thus affecting directly the material lifetime and exciton emission. In a typical OLED structure, the minority carriers travel only a few

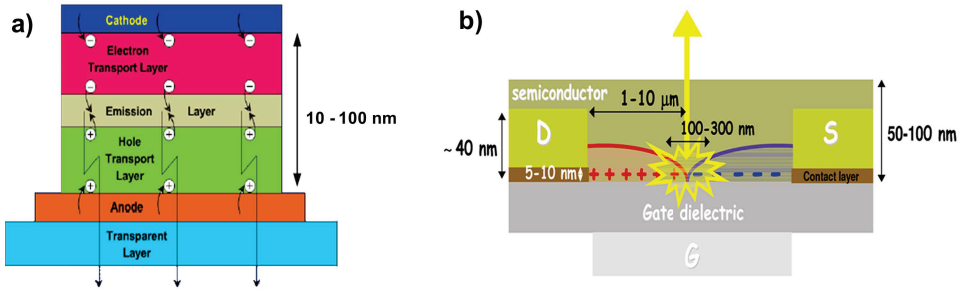

Figure 3.6: Schemes of an OLED (a) and an OLET (b) showing for each the typical dimensions.

tens of nanometers to encounter the opposite sign carrier and to recombine radiatively. On OLETs, instead, both carriers must travel longer distances (typically tens of microns), which imposes more requirements on the organic semiconductors charge transport properties. A clear advantage of the OLETs is the virtually higher electroluminescence quantum efficiency inherent to the device structure. Indeed, in OLETs it is possible to drastically reduce the exciton quenching by interaction with charge carriers and with metal contacts. For what concerns the exciton-charge interaction, even though the current density in an OLET is expected to be higher (1-10 A/cm^2, for a 1-nm-thick accumulation layer) compared to OLEDs ($10^{-3}10^{-2}A/cm^2$), the spatial localization of charge carriers in an OLET could favor an effective separation between the exciton population and the charge carriers thus avoiding any quenching for that kind of interaction. The presence of a third electrode helps to achieve a balanced charge carriers current, therefore further reducing exciton-charge quenching. In OLET, compared to OLED, all the operational requirements of the basic electronic and optoelectronic elements in active matrix displays, are satisfied in a single device structure. Indeed in conventional OLED electronics, such a high degree of integration cannot be achieved and, for each pixel, an electrical switch and a separate light source must be combined. Lastly, in OLETs is possible to control the position of the emission zone inside the channel length.

According to the previous discussion, it turns out how the OLET structure has more intriguing potentiality compared to OLED. However, the actual degree of exploitation of this technology depends on the development of new organic materials combining multiple functionalities and high performances. Moreover, many structure-related issues are to be considered in order to get good electrical properties and high light emission from the device. Indeed, since FETs (and thus OLETs) are considered as truly interface devices, processes that take place in the device active region, like charge transport, energy/charge transfer, exciton formation, charge trapping, are strongly dependent on interfaces. In recent years it has been demonstrated that the chemical structure of the organic semiconductor is not the only factor that determines whether an organic FET exhibits predominantly p-channel or n-channel behaviour. Processing and characterization conditions, device architecture, and choice of electrodes are important as well. To get an insight into the main phenomena that happens at the interfaces, many aspects must be taken into account: the chemical and electronic interaction taking place at the different interfaces (dielectric/organic, organic/organic and organic/metal), the modulation of the molecular electronic structure in the active material due to the proximity with other functional layers (polarization, relaxation), the bonding and ordering of molecules at the interface (which strongly determine the growth morphology). For example, one of the crucial processes of charge accumulation and transport in OLETs takes place at the interface between the gate dielectric and the semiconductor. Thus, the properties of this interface and the dielectric will have a huge influence on device opto-electronic performances. Device parameters such as mobility, threshold voltage, sub-threshold swing, etc. depend not only on the nature of the semiconductor but also on the chemical structure and dielectric properties of the insulator.

The requirements for gate dielectrics in OFET are rigorous. They should show high

dielectric breakdown strength, contain only minimal concentrations of impurities, that could act as traps and must be easily processable and be environmentally stable. From the point of view of light emission, the requirements depend on the structure used for fabricating the OLET, but regardless the implemented architecture, it is absolutely important to use high efficiency luminescent organic materials. In the next sections we will discuss some issues related to the emission in different OLET approaches, each with its points of strength and weaknesses.

3.3.1 Unipolar OLETs

Historically the first demonstrated OLET was achieved from unipolar charge carriers transistors made from tetracene by Hepp et al. in 2003 [16]. The device was fabricated on Si/SiO_2 substrates in bottom-gate bottom-contact configuration, with gold electrodes. The material was chosen because of its good charge carrier transport and EL properties. The electrical characteristic of the OLET were typical from an unipolar p-type transistor and can be seen in Fig.3.7, along with a picture of the illuminated channel (located near the drain contact). Despite the electrical unipolar

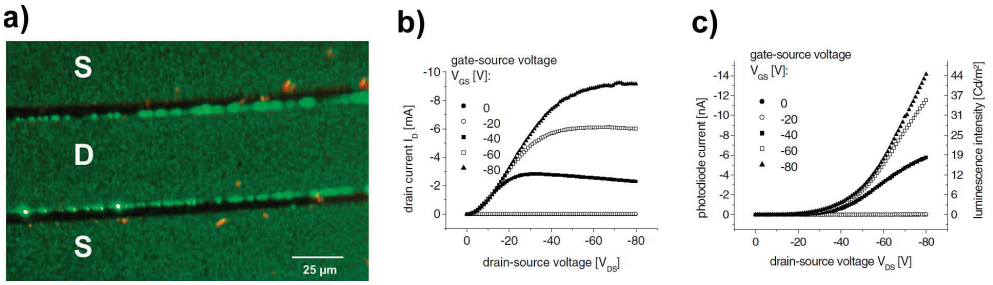

Figure 3.7: Image of the illuminated channel with the typical green-light emission of tetracene (a), I-V characteristic (b) and electro-luminescence (c) measurement of the device, in the negative bias region [16].

behaviour, the observation of light emission from tetracene proved an undoubted presence of opposite charges recombining inside the material. Given the inhomoge-

neous illuminated channel area, Hepp et al. introduced then an empirical model in which they supposed different injection mechanisms at the source or drain electrodes as a consequence of the thin-film physical imperfections. In particular they assumed that, due to under-etching problems of the electrodes that act as a shadow mask, a thinner tetracene layer is formed at the organic/electrode interface resulting in a poor electrical contact. During device operation, the channel is filled with holes. However due to imperfections of the electrode, holes cannot directly reach the drain through the channel, but they must travel a certain distance in the tetracene bulk film. On the other side, since the gate field is screened by holes at the dielectric/organic interface, there is a high electric field at the drain electrode. This strong field, magnified by the local spikes due to the imperfections on the contact, could be enough to allow injection of electrons into the organic [17]. For more details, see Fig.3.8. A successive

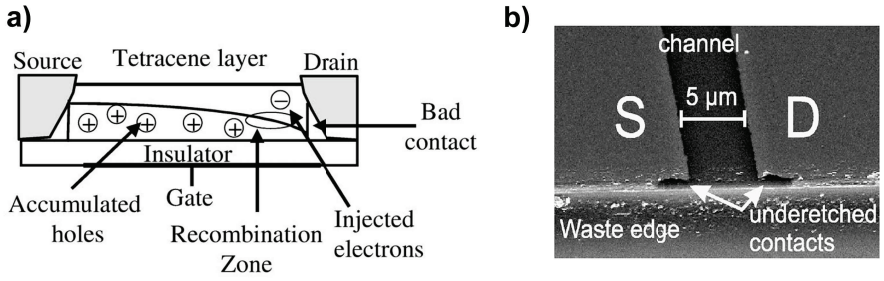

Figure 3.8: Scheme of the device with the edge effect at the contacts, proposed to demonstrated the electrons injection from the drain contact (a) [16], example of a SEM image showing the under-etching effect (b) [18].

study, proposed a new phenomenological model to explain the working mechanism of the OLET. The model assumed that the voltage drop at drain electrode, caused by a contact barrier, induces a distortion of the Highest Occupied (HOMO) and Lowest Unoccupied (LUMO) Molecular Orbital levels of tetracene near the contact, thus determining the conditions for the tunnelling of electrons from the drain to the LUMO of the organic [19]. In the proposed model, the external quantum efficiency

(EQE) of light emission, which is defined as the ratio of the number of photons emitted outside the device or in a particular viewing direction to the number of flowing electrons in the device channel, is proportional to the tunneling probability and thus proportional to the drain-source voltage (V_{ds}), but it is independent from gate voltage (V_{gs}). Indeed, increasing V_{gs} leads to an overall increase of the electroluminescence (EL) but leaving unaffected the EQE. Several other approaches have been performed on unipolar OLETs using spin-coated or drop-casted polymers like *poly-phenylenevinylene*, *poly-fluorene* or *poly-arylenevinylene* derivatives [18, 20, 21] as active layer. These experiments, besides showing a possible extension of the concept of unipolar OLET, demonstrated the feasibility of wet-technique fabrication process that could open up many possibilities of large-area and low cost devices. Within the same studies, it was demonstrated also that using different metals for drain-source contacts could lead to a considerable increase of EL. Generally, despite the enhancement in EL in unipolar devices, the EQE achieved is still too low for any practical application. Indeed, some problems arisen from the type of architecture, limit drastically its potentiality. First of all the EL emission takes place in proximity to the metal electrode with a consequence quenching due to the interaction between exciton and metal surface plasmons. Moreover, the exciton formation and recombination occurs in the same spatial region where charges flow, so leading to a significant exciton-charge quenching. In practice, unipolar OLETs suffer from the same negative effects of OLEDs.

3.3.2 Ambipolar OLETs

So far we showed a possible approach to fabricate OLETs, using a unipolar organic material (polymeric or small molecule) as the active single layer. In this case the emission is localized in a small region below the metal contacts. Indeed, most of the

scientifically and technologically remarkable properties that make light-emitting transistors desirable are, however, only present in ambipolar OLETs since they can provide an effective pn-junction within the device channel that allows exciton formation and radiative recombination. The most simple structures are composed by a single organic material capable of transporting electrons as well as holes (single component approach) or by a combination of two unipolar transport materials (multi-component approach).

Ideal Single Layer Ambipolar OLETs

In an ideal ambipolar transistor with just one semiconducting layer, that could be formed by a small molecule or by a semiconductor polymer, the ambipolar regime is characterized by a hole and an electron accumulation layers, next to the respective electrode, that meet at some point within the transistor channel. There, oppositely charged carriers recombine. In electroluminescent materials, this leads to light generation within the channel. The length of each channel and thus position of the recombination zone depends on the applied gate and source-drain voltage and mobility ratio. The behaviour of an ambipolar field-effect transistor in ambipolar regime can roughly be imagined as that of a saturated hole and electron channels in series within the field-effect transistors. In general, ambipolarity in FETs is an attractive characteristic since it enables the fabrication of complementary logic circuits like CMOS transistors and permits an higher light emission efficiency due to the maximization of the exciton recombination through a better electron-hole charge balance. In addition, with an opportune tuning of the gate voltage, is possible to move the emission through the channel length. On other hands, one of the limiting aspect of this class of devices remains the poor mobility of charge carriers, usually of the order of $10^{-4} cm^2/Vs$.

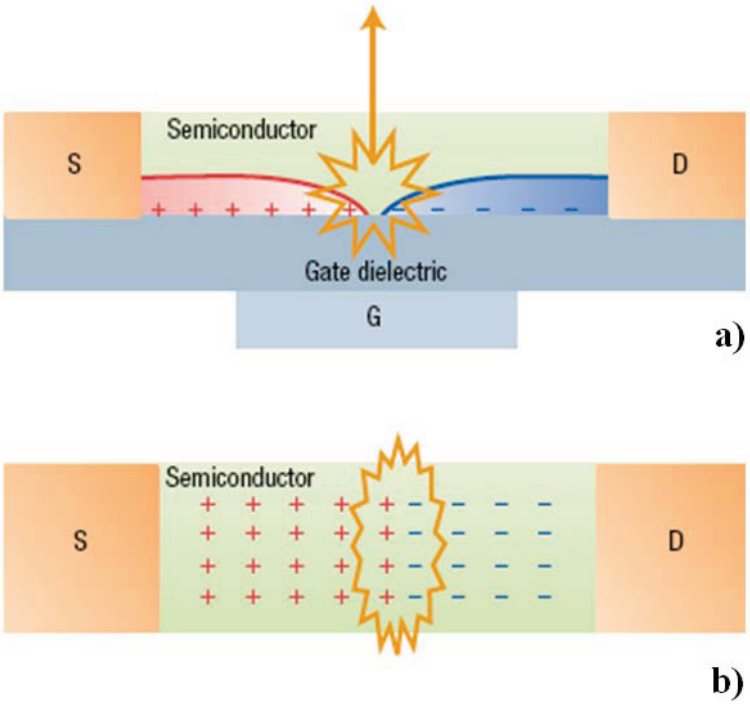

Figure 3.9: Scheme of a light-emitting ambipolar field-effect transistor. (a) Side view. (b) Top view. In a simple model, the device can be modelled as a sort of a two-dimensional forward-biased pn junction. Electrons and holes are injected from the drain (D) and source (S) contacts and recombine within the channel position controlled by the gate (G).

Ambipolar Polymer OLET

The first research showing the feasibility of an ambipolar single layer OLET, was done by Swensen et al. [22]. The material used was a *poly-phenylenevinylene* (PPV) derivative polymer, called SuperYellow (SY) and the device was done on a Si/SiO_2 substrate. Previous studies on the same class of material/substrate FETs showed only p-type mobility. It was just after the discovery of the hydroxyl groups trapping effect for electrons and the consequent SiO_2 surface passivation process implementation [23], that it was possible the realization of electroluminescent ambipolar polymer transistors. In particular, the presence of a so called two-color geometry of the device was the key feature for enabling ambipolar transport from SY. In this

reported geometry, they implemented the use of a low work-function metal (Ca) for the n-type injection electrode and an high work-function metal (Ag) for the p-type injection electrode. A spatially resolved recombination zone, controlled by gate voltage, was then observed under ambipolar conditions. The emission zone moved across the channel as the gate bias swept (see Fig.3.10) and when the electron and hole currents were balanced the recombination was located at the channel centre. Almost contemporarily, another group achieved the same results using a spin-coated

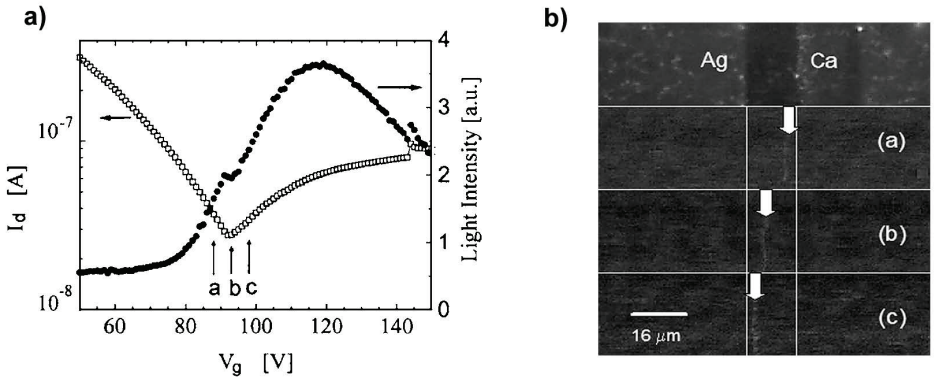

Figure 3.10: Transfer characteristic of the SY OLET along with EL intensity (a), image of EL inside the channel at different spatial positions depending on gate bias (b) [22].

layer of a different conjugated polymer, *poly(2-methoxy-5-(3,7-dimethyloctoxy)-p-phenylene-vinylene)*(OC1C10-PPV) [24]. Also in this case, to obtain a good ambipolar behaviour, with balanced electron-hole charge densities, two different work function metals were used. For this material, the reported EQE was 0,35%, thus similar to the EQE of a bulk LED based on the same polymer. Recently in 2008, again Zaumseil et al. fabricated ambipolar OLETs with *poly(9,9-di-n-octylfluorene-alt-benzothiadiazole)* (F8BT) and *poly((9,9-dioctylfluorene)-2,7-diyl-alt- [4,7-bis(3-hexylthien-5-yl)-2,1,3-benzothiadiazole]-2,2-diyl)* (F8TBT) (see Fig.3.11) [25]. In their study, through the use of theoretical models they showed that the ambipolar regime can be thought of as a saturated electron channel and a saturated hole

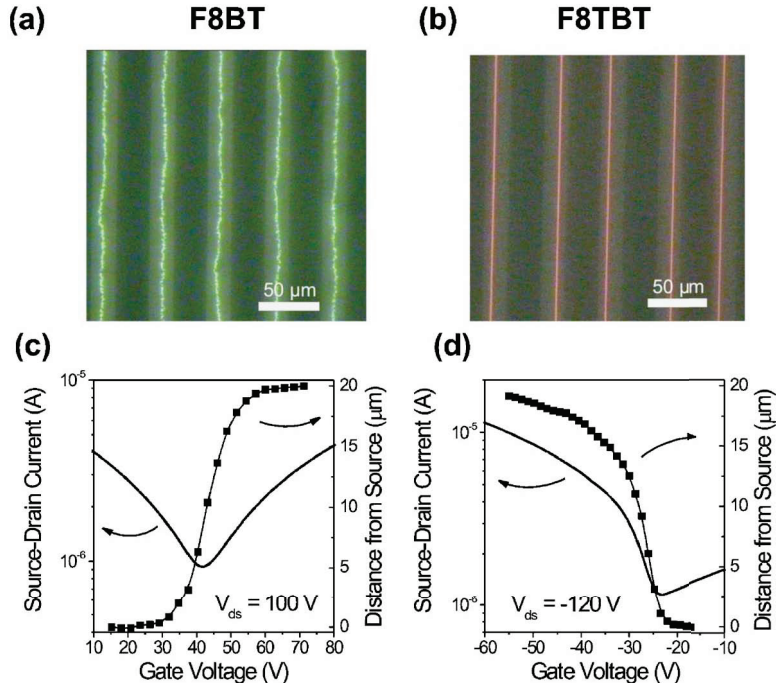

Figure 3.11: Image of light emission from an interdigitated source-drain OLET made with F8BT (a) and F8TBT (b). Transfer curves and position of the light with respect of source contact for F8BT (c) and F8TBT (d) [25].

channel in series within the OLET channel. Within the model, EQE was expected to be constant, depending only on singlet-triplet ratio and not from, for example, voltage conditions. The increase of EQE with current density up to saturation, measured during the experiments, was considered as a consequence of trap-assisted non-radiative decay mechanisms at the semiconductor-dielectric interface. Furthermore, they demonstrated that, when complete recombination of all charges happened the maximum saturated EQE of F8BT, in top gate OLET configuration, is 0,8%. This conclusion signed a very important step in OLET fabrication, showing, clearly, for single layer devices, that an EQE of 0,8% is the highest limit.

Ambipolar Small Molecule OLET

Another approach in the realization of ambipolar single layer OLETs, using an intrinsic ambipolar light-emitting small molecule, was explored by Capelli et al., describing the realization of α,ω-*dihexyl-carbonyl-quaterthiophene* (DHCO4T) based device [13]. The advantage in using a physical vapour deposited (PVD) small molecule instead of a polymer deposited by solution-processes is that, in the first case, the resulting film presents a more ordered and crystalline structure and thus, in principle, higher hole-electron mobilities due to larger charges delocalization.

Unfortunately electro-luminescence was present mainly in unipolar region (see Fig.3.12). In order to have a better understanding of the phenomena, they tested the material

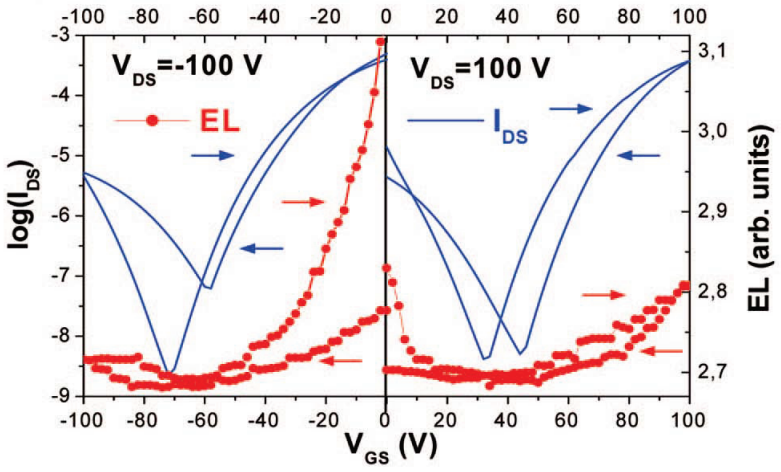

Figure 3.12: Example of transfer characteristics of a DHCO4T OLET on SiO_2/*poly-methyl-metacrylate* (PMMA) substrate. The left plot is in p-type bias mode, while the right one is in n-type bias mode.

in different conditions, changing dielectrics and metal contacts. Through this study, they showed the strong dependence of DHCO4T-based OLETs performances from the dielectric-organic interface. This aspect profoundly affects the electrical properties of both charge carriers in terms of mobility and threshold voltage and thus electro-luminescence. They identified this main issue as the first cause of limited

optoelectronic performances of their device.

Multi-layer Ambipolar OLETs

In multi-component approach, OLETs can be obtained either by simultaneous co-evaporation of two unipolar materials realizing a bulk hetero-junction or by superposing two layers of unipolar materials in a bi-layer structure.

Bulk Hetero-Junction OLETs

In bulk organic hetero-junction approach, exciton formation and charge transport are competitive processes due to the dispersed interface between the p-type and n-type transport materials. Clearly, the wider the interface surface is, the higher the probability that electrons and holes recombine forming excitons. Nevertheless, connected percolative paths are needed for the charges to migrate by hopping so that interface can represent a physical obstacles for efficient charge transport. Furthermore, even if the interface morphology is precisely controlled during vacuum sublimation, well-balanced ambipolar behaviour has not yet been achieved. The first documented fabrication of an ambipolar device belonged to this class of OLETs. In 2004, for the first time, Rost et al. proposed a new structure made by a co-evaporation with 1:1 ratio of *N,N-ditridecylperylene-3,4,9,10-tetracarboxylic diimide* (P13) for n-type transport and α-*quinquethiophene* (T5) for p-type transport (see Fig.3.13) [26]. These two materials are known for their good hole-transporting (T5, with mobility of $10^{-2}cm^2/Vs$) and electron-transporting (P13, with mobility of $10^{-1}cm^2/Vs$) properties. Of course, one of the most important prerequisite for having exciton formation and thus light formation, is the relative positions of the materials energy levels of highest occupied (HOMO) and lowest unoccupied molecular orbital (LUMO). Indeed, there must be the conditions to allow recombination in the material with smaller en-

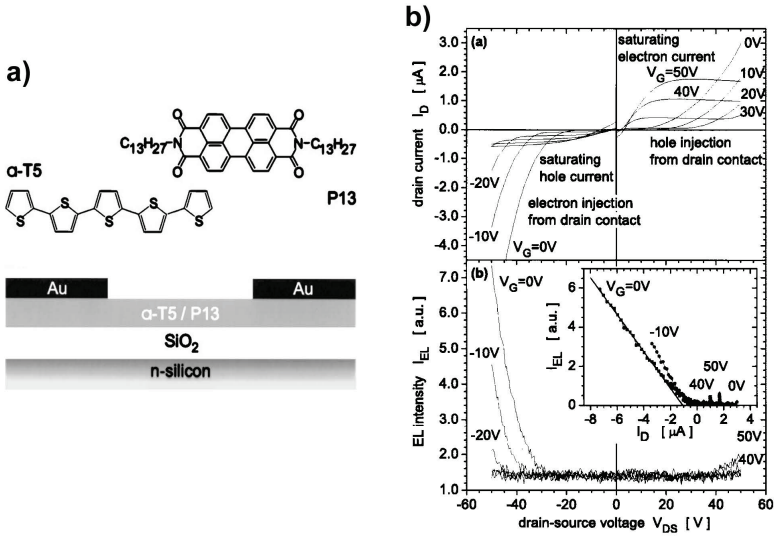

Figure 3.13: Device and molecules chemical structures (a), I-V characteristic with EL emission at different gate biases.

ergy gap. Through a fine control of the two materials co-evaporation, it is possible to obtain a good tuning of both charge carriers mobilities and quite good EL. However, in general, in this kind of device structure, the absolute mobility values are definitely lower, if compared to other fabrication strategies. In particular, Rost et al., after a deep investigation, found the best deposition parameter tuning in order to obtain very high mobility of both layers, though with low EL emission. Mobilities achieved were, respectively, $10^{-4}cm^2/Vs$ for hole transport and $10^{-3}cm^2/Vs$ for electron transport.

Bi-layer Vertical Hetero-Junction OLETs

In this structure the organic layers are deposited in a vertical stack. Each layer is devoted to a single functionality and can be optimized by controlling the growth conditions of the different organic/organic, organic/contact and organic/dielectric interfaces. This approach, compared to others, presents the advantage of fabricating devices with good charge transport. It is known that in OFETs the charge transport is confined to the first few layers next to the dielectric. Thus, electron and hole

paths are confined at the interface between the first layer and the substrate and at the interface between the two organic films. If the two films are continuous, the charge transport should be uniform in both films over all the device channel area and therefore good mobilities are expected. Dinelli et al. reported on a bi-layer of α,ω-*dihexylquarterthiophene* (DH4T) and P13 OLET, on silicon substrate, that showed good ambipolar behaviour and light emission [27]. They demonstrated, studying two different possible organic configurations (DH4T-P13 or P13-DH4T), that the device, in which DH4T was evaporated directly on the dielectric surface, had the best balanced mobility in ambipolar region ($10^{-2}cm^2/Vs$ for both charge carriers). Through analysis of the interfaces of the two cases, they underlined the importance of having the best growth compatibility between the hole and electron transport materials in order to form continuous films and thus determining the optoelectronic responses. They observed also that EL occurs only when the device is biased with FET transport in the bottom layer and that the light emission originates, from P13, as expected from energetic considerations. In the bi-layer approach, the spatial separation between charge carriers mainly prevents excitons formation inside the device channel, and so, EL is present only in unipolar bias region. This means that the pn-junction forms only underneath the electrodes as in the case of single layer unipolar OLETs. However, this structure has, up to date, the highest balanced ambipolar mobility ever obtained in OLETs. Instead of implementing n-transport and p-transport materials in the bi-layer device realization, Heeger et al. utilized a structure comprising a hole transporting polymer, *poly(2,5-bis(3-tetradecylthiophen-2-yl)thieno[3,2-b]thiophene)* (PBTTT-C14) and a light emitting polymer, Super Yellow (SY), a *polyphenyleneviny-lene* derivative showing good output characteristics and brightness. Both materials were deposited by wet techniques (see Fig.3.14) [28]. It is well known that, in OLET devices, light emission is quite low due to the fact that the organic materials present

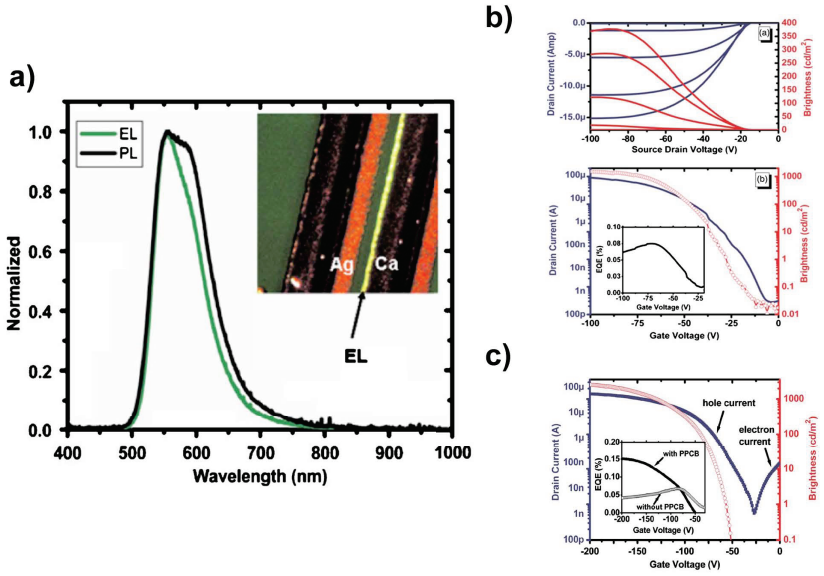

Figure 3.14: Image of the EL emission spectrum of the device compared to PL emission of SY, along with a picture of the luminescent channel (a), I-V characteristic, transfer characteristic and EL curve of the bi-layer device(b) [28].

either low carrier mobility with high photoluminescence (PL), i.e. amorphous materials, or high mobility with weak PL, i.e. crystalline materials. In order to obtain good performances, materials should be capable of good ambipolar behaviour and have an high PL efficiency in thin film. In this case, although they did not achieve good ambipolarity, since electron transport was significantly lower than hole one, using two different metals as drain-source electrodes (Ag for hole injection and Ca for electron injection), they obtained a device showing intense EL, independent from the gate bias, with an efficiency of 0,35% and located under the electrode.

3.3.3 Tri-layer Vertical Hetero-Junction OLETs

Here we present a novel strategy in OLET realization, the tri-layer vertical heterojunction whose study and development is at the basis of the work done in this thesis. So far, we have seen OLETs based on unipolar single layer which reached high bright-

ness but EQE as low as 0,2% due to exciton-charge and exciton-metal quenching effects. Then it has been reported of ambipolar single layer OLETs that enable, under proper bias conditions, the spatial localization of the EL far from the electrodes, but since charge carrier and exciton coexists in the same region, large exciton-charge quenching happens. Finally it has been reported of ambipolar bi-layer approaches for OLETs, but in each of the two cases proposed (superposition of either two unipolar semiconductors of different charge transport or a highly efficient luminescent layer over a unipolar conductive layer) the device architecture does not offer any control on the exciton quenching due to charge and metal electrodes interactions. This new tri-layer hetero-structure OLET enable simultaneous control of the electrode induced photon losses, the exciton-metal and the exciton-charge interactions.

In the trilayer configuration the first organic thin-film in contact with the device dielectric layer is devoted to the unipolar field-effect transport. The second layer deposited onto is the recombination layer which presents high emission quantum efficiency and OLED-like vertical bulk mobility value. The third layer is devoted to unipolar charge transport complementary to that of the first layer (see Fig.3.15a). The key idea of the vertical tri-layer heterojunction approach in realizing OLET is that each layer has to be optimized according to its specific function (charge transport, energy transfer, radiative exciton recombination). Clearly, matching the overall device characteristics with the functional properties of the single materials composing the active region of the OFET, is a great challenge that requires a deep investigation of the morphological, optical and electrical features of the system. In this structure, the main aim is to enable charges to percolate into the middle emitting layer. In order to do so, first of all, material energetic levels must be considered. The LUMO level of the n-type transport layer should be equal or higher than the LUMO level of the guest matrix of the host-guest system consisting the middle layer, while the

HOMO level of the p-type transport layer should be less or equal than the guest matrix HOMO level (see Fig.3.15b). In addition to these considerations, attention must be paid to the control over the interfaces morphologies, in order to allow the formation of the most continuous stack. Indeed, in this approach more than in oth-

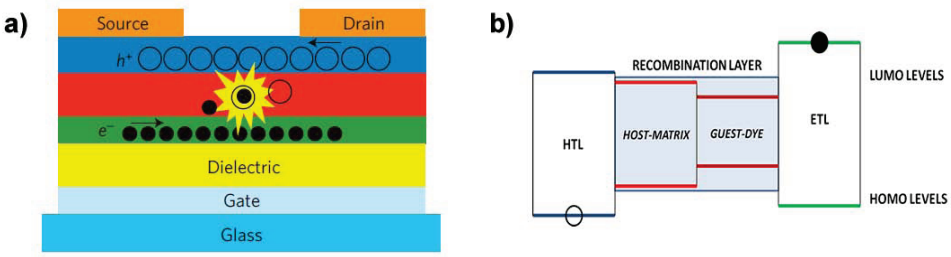

Figure 3.15: Example of a tri-layer device structure along with HOMO and LUMO energy levels of the materials (b). In this case, the recombination layer (middle layer) is composed by an host matrix-guest dye blend.

ers, functional interfaces play the predominant role in determining the performance of vertical tri-layer heterojunction. As in the case of the bilayer-based OLETs, it is clear that the interfaces between the dielectric and the bottom transport layer and between the recombination and the top transport layers are crucial for guaranteeing good ambipolar field-effect electrical characteristics. Moreover interfaces between the bottom transport and the recombination layer and between the recombination and the top transport layer should provide the favourable conditions for the charge percolation to happen in the recombination layer and form excitons. For what concerns light emission, in ambipolar region EL is located inside the device channel far from electrodes, thus preventing photon losses due to exciton-metal quenching. Moreover, since the emission layer is separated from charge flows, the exciton-charge quenching is also prevented. The light generation process is based on the percolation of the opposite charges from the transport layers into the recombination layer. This percolation is made easier due to the transverse electric field generated by electrons and holes in the respective transport layers. In the tri-layer structure charges recombine

in the middle layer because they cannot travel through several microns of opposite charge accumulation layer without recombining, similarly to what happens in ambipolar single-layer OLETs in which charges recombine in the middle of the channel. Indeed, a self-regulated equilibrium exists between the amount of charges located in the transport layers and those entering the recombination one that prevents any possible exciton-charge interaction.

3.4 REFERENCES

[1] G. H. Heilmeier and L. A. Zanoni. Surface studies of α-copper phthalocyanine films. *J. Phys. Chem. Solids*, 35:603, 1964.

[2] A. Tsumara, H. Koezuka, and T. Ando. Macromolecular electronic device: Field-effect transistor with a polythiophene thin film. *Appl. Phys. Lett.*, 49(18):1210, 1986.

[3] S. R. Forrest. The path to ubiquitous and low-cost organic electronic appliances on plastic. *Nature*, 428(6986):911, 2004.

[4] M. M. Payne, S. R. Parkin, J. E. Anthony, C. C. Kuo, and T. N. Jackson. Organic field-effect transistors from solution-deposited functionalized acenes with mobilities as high as 1 cm2/vs. *J. Am. Chem. Soc.*, 127(14):4986, 2005.

[5] H. Sirringhaus, P. J. Brown, R. H. Friend, M. M. Nielsen, K. Bechgaard, B. M. W. Langeveld-Voss, A. J. H. Spiering, R. A. J. Janssen, E. W. Meijer, P. Herwig, and D. M. de Leeuw. Two-dimensional charge transport in self-organized, high-mobility conjugated polymers. *Nature*, 401(6754):685, 1999.

[6] E. Menard, V. Podzorov, S.H. Hur, A. Gaur, M.E. Gershenson, and J.A. Rogers. High-performance n-and p-type single-crystal organic transistors with free-space gate dielectrics. *Adv. Mater.*, 16(23-24):2097, 2004.

[7] F. Dinelli, R. Capelli, M. A. Loi, M. Murgia, M. Muccini, A. Facchetti, and T. J. Marks. High-mobility ambipolar transport in organic light-emitting transistors. *Adv. Mater.*, 18(11):1416–1420, 2006.

[8] J. Lee, J. H. Kim, and S. Im. Pentacene thin-film transistors with al2o3+x gate dielectric films deposited on indium-tin-oxide glass. *Appl. Phys. Lett.*, 83(13):2689, 2003.

[9] L. A. Majewski, M. Grell, S. D. Ogier, and J. Veres. A novel gate insulator for flexible electronics. *Org. Electron.*, 4(1):27, 2003.

[10] X. Z. Peng, G. Horowitz, D. Fichou, and F. Garnier. All-organic thin-film transistors made of alpha-sexithienyl semiconducting and various polymeric insulating layers. *Appl. Phys. Lett.*, 57(19):2013, 1990.

[11] H. Sirringhaus, T. Kawase, R. H. Friend, T. Shimoda, M. Inbasekaran, W. Wu, and E. P. Woo. High-resolution inkjet printing of all-polymer transistor circuits. *Science*, 290(5499):2123, 2000.

[12] J.A. Letizia, A. Facchetti, C.L. Stern, M.A. Ratner, and T.J. Marks. High electron mobility in solution-cast and vapor-deposited phenacyl-quaterthiophene-based field-effect transistors: Toward n-type polythiophenes. *JACS*, 127(39):13476, 2005.

[13] R. Capelli, F. Dinelli, S. Toffanin, F. Todescato, M. Murgia, M. Muccini, A. Facchetti, and T. J. Marks. Investigation of the optoelectronic properties of organic light-emitting transistors based on an intrinsically ambipolar material. *J. Phys. Chem. C.*, 112(33):12993–12999, 2008.

[14] C. R. Newman, C. D. Frisbie, D. A. da Silva Filho, J. L. Bredas, P. C. Ewbank, and K. R. Mann. Introduction to organic thin film transistors and design of n-channel organic semiconductors. *Chem. Mater.*, 16:4436–4451, 2004.

[15] J. Zaumseil and H. Sirringhaus. Electron and ambipolar transport in organic field-effect transistors. *Chem. Rev.*, 107(4):1296, 2007.

[16] A. Hepp. Light-emitting field-effect transistor based on a tetracene thin film. *Phys. Rev. Lett.*, 91(15):7406–1 7406–4, 2003.

[17] K. Murata, S. Cina, and N. C. Greenham. Barriers to electron extraction in polymer light-emitting diodes. *Appl. Phys. Lett.*, 79(8):1193–1195, 2001.

[18] M. Ahles, A. Hepp, R. Schmechel, and H. von Seggern. Light emission from a polymer transistor. *Appl. Phys. Lett.*, 84(3):428–430, 2004.

[19] C. Santato, R. Capelli, M. A. Loi, M. Murgia, F. Cicoira, V.A.L. Roy, P. Stallinga, R. Zamboni, C. Rost, S.E. Karg, and M. Muccini. Tetracene-based organic light-emitting transistors: optoelectronic properties and electron injection mechanism. *Synth. Met.*, 146(3):329–334, 2004.

[20] T. Sakanoue, E. Fujiwara, R. Yamada, and H. Tada. Visible light emission from polymer-based field-effect transistors. *Appl. Phys. Lett.*, 84(16):3037–3039, 2004.

[21] J. Swensen, D. Moses, and A. J. Heeger. Light emission in the channel region of a polymer thin-film transistor fabricated with gold and aluminium for the source and drain electrodes. *Synth. Met.*, 153(1-3), 2005.

[22] J. Swensen, C. Soci, and A. J. Heeger. Light emission from an ambipolar semiconducting polymer field-effect transistor. *Appl. Phys. Lett.*, 87(25):3511–1 3511–3, 2005.

[23] L.L. Chua, J. Zaumseil, J.F. Chang, E.C.W. Ou, P.K.H. Ho, H. Sirringhaus, and R.H. Friend. General observation of n-type field-effect behavior in organic semiconductors. *Nature.*, 434(7030):194–199, 2005.

[24] J. Zaumseil, R. H. Friend, and H. Sirringhaus. Spatial control of the recombination zone in an ambipolar light-emitting organic transistor. *Nat. Mater.*, 05(01):69–74, 2006.

[25] J. Zaumseil, C.R. McNeill, M. Bird, D.L. Smith, P.P. Ruden, M. Roberts, M.J. McKiernan, R. H. Friend, and H. Sirringhaus. Quantum efficiency of ambipolar light-emitting polymer field-effect transistors. *J. Appl. Phys*, 103(06):4517–1 4517–10, 2008.

[26] C. Rost, S. Karg, W. Riess, M. A. Loi, M. Murgia, and M. Muccini. Ambipolar light-emitting organic field-effect transistor. *Appl. Phys. Lett.*, 85(09):1613–1615, 2004.

[27] F. Dinelli, J. F. Moulin, M. A. Loi, E. Da Como, M. Massi, M. Murgia, M. Muccini, F. Biscarini, J. Wie, and P. Kingshott. Effects of surface chemical composition on the early growth stages of alpha-sexithienyl films on silicon oxide substrates. *J. Phys. Chem. B*, 110(1):258, 2006.

[28] E. B. Namdas, P. Ledochowitsch, J. D. Yuen, D. Moses, and A. J. Heeger. High performance light emitting transistors. *Appl. Phys. Lett.*, 92(18):3304–1 3304–3, 2008.

Chapter 4

Experimental Setups

In this chapter the experimental facilities and techniques used for OFETs fabrication and characterization will be presented. We will start from the description of the main techniques used for film deposition, like *physical vapour deposition* (PVD) and spin-coating, giving attention to the facilities used for fabrication. Then, the main measurement and characterization instruments, like *atomic force microscopy* (AFM) for surface scanning, parametric analyzer and calibrated spectrometer for opto-electronic measurements, will be introduced.

4.1 Films Deposition

The deposition processes for the materials (organics semiconductors, metals or dielectrics) are the fundamental steps for the fabrication of organic electronic devices. Thin films are grown by a number of different processes that are chosen by the chemical nature of the source material and the desired properties of the deposited films. Among many growing techniques two are considered as the most important, the *physical vapour deposition* (PVD) and *spin coating deposition* (SCD) that will be briefly reviewed in this section.

4.1.1 Physical Vapour Deposition

PVD is a process in which atoms or molecules from a thermal vaporization source reach and impinge the substrate without collisions with residual gas molecules in the deposition chamber. This type of process requires a relatively good vacuum inside the growing chamber. Indeed vacuum evaporation technology has experienced an enormous diffusion after the invention of Sprengel mercury column vacuum pumps. In 1879 Edison used this type of pump to evacuate the first carbon-filament incandescent lamps and, in 1887, Nahrwold performed the first vacuum evaporation. Vacuum deposition of metallic thin films was not common until the 1920s, since it normally requires a vacuum of better than 10^{-6} mbar. In general the main advantages of this kind of technique consist of providing sub-monolayer thickness control during deposition and low level of contamination due to moisture or impurities, depending on the vacuum level. Other advantages of this technique are: the *line-of-sight* deposition allows the use of masks to define area of growth, very high and very low deposition rates can be obtained, this technique is relatively inexpensive compared to other techniques. The main drawbacks of this process are: sometimes the line-of-sight deposition gives poor surface coverage and poor deposit uniformity over a large surface area without complex fixturing and tooling, high radiant heat loads during processing (for metal deposition), impossibility of processing polymers and, in general, high molecular weight materials [1]. A typical vacuum evaporation chamber is equipped with a vacuum pump, a crucible (where the material is held and heated to sublimation temperature), a heater cell in which the crucible is placed, a substrate mount (also called *target*), a shutter to control the open/close processes of the substrate target and, in some cases, of the source heater in order to have a better control of the deposition and a quartz crystal micro-balance for measuring the film thickness. Once the crucible is filled with the material, it is heated since it

reaches the sublimation temperature. Then, after opening the eventual shutters, the sublimed materials exits the crucible aperture and reach the target. In particular, our film deposition is made in two different vacuum chambers of which we represent the schemes in Fig.4.1, below.

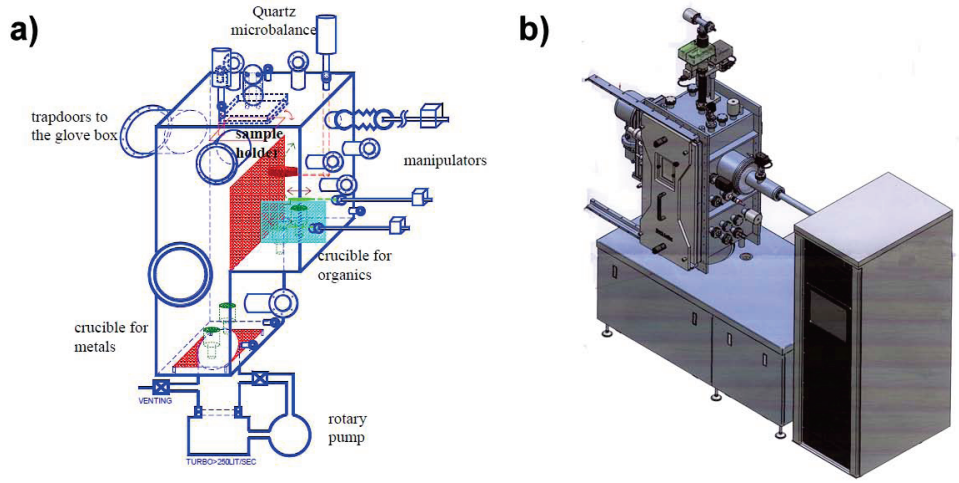

Figure 4.1: schemes of the vacuum chamber used for the PVD processes. The left chamber (a) is home-made, while the right chamber (b) is a custom made model from KJL. Both models are attached to a glove-box system.

Growth Modalities

When molecules impinge the substrate, the film growth can evolve essentially in three possible modalities. The mode of growth is dependent on the growth conditions used, the strengths of the interactions between the substrate and the molecules diffusing on it and the interaction strength between the molecules diffusing and the solid islands of material already deposited. These growth modes can be seen in Fig.4.2. The Frank/van der Merwe mode of growth is the most desired for transistor applications because it leads to large, well-connected domains that facilitate charge transport parallel to the substrate. Layer-by-layer growth is thermodynamically favourable for systems where the sum of the surface energy (tension) of the adsorbate and the

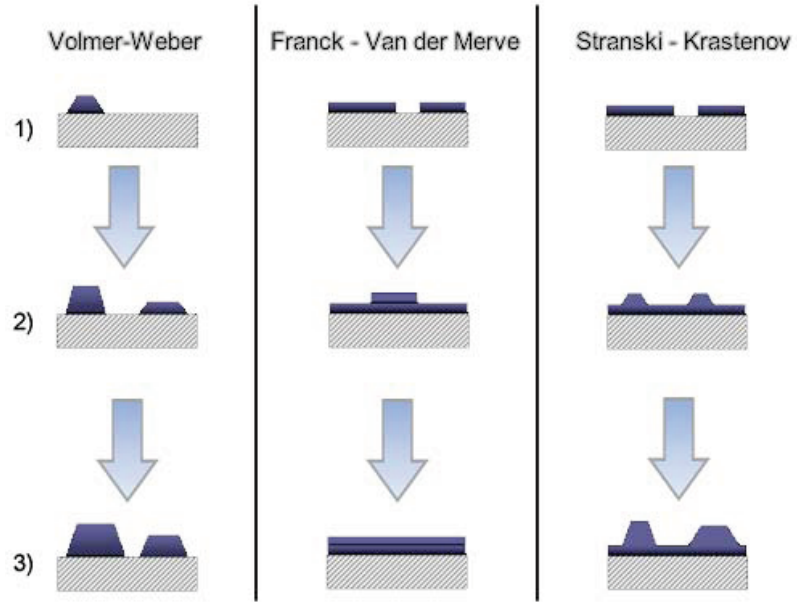

Figure 4.2: Representation of the growth modes. This idealized simple model of a growing crystal is known as a Kossel crystal and is useful for simple calculations. In figure 1 the early stage of growth is represented (less than a mono-layer thick films) and the evolution of growth is showed in figures 2 (between 1 and 2 mono-layers thick) and 3 (more than 2 mono-layers thick films), respectively. In each case is presented a different mode of growing. The first column shows a complete three-dimensional island formation (Volmer/Weber), the second one shows a layer-by-layer growth (Franck/Van der Merwe) and the latter shows an intermediate case between the two, so a layer-by-layer growth followed by an island formation (Stranski/Krastanov).

interfacial energy between the substrate and the film is less than or equal to the surface energy of the substrate. As the film grows thicker, the effective value of the substrate-film interfacial energy may increase enough (possibly due to the formation of strains) to make layer-by-layer growth unfavourable and, eventually, lead to what is known as Stranski/ Krastanov growth whereby islands form on top of one or several complete monolayers. The growth scenario of Volmer/Weber, three-dimensional, or island, occurs when the interfacial energy and the film surface energy are higher than the subtrate surface energy [2, 3].

4.1.2 Spin-Coating

Spin-coating technique has been widely studied since the beginning of 20th century [4–6]. It consists of a process where a solution is applied to a horizontal rotating disc, resulting in ejection and evaporation of the solvent and leaving a liquid or solid film. Through the use of this process it is possible to obtain a highly uniform film to a planar substrate over a large area, with highly controllable and reproducible film thickness. Typically spin-coating is used in various application, such coatings of photoresist on silicon wafer for photo-lithography processes, or protective or optical coatings. Recently spin-coating has expressed its high usefulness in microelectronic applications [7] and in particular for coatings of polymers whose solubility is high in many solvents. Deposition a viscous fluid over a horizontal surface must be done by tuning some critical parameters defined by the physics that lies behind this technique [8]. This physics involves a balance between a controlled centrifugal force of the rotating disk, the viscosity of the fluid and the adhesive forces at liquid-substrate interface. This results in a strong sheering of the liquid which causes a radial flow in which most of the polymer is quickly ejected from the disc (almost 99%) [9]. This process, combined with the solvent evaporation produces a decrease of the remaining film-solution thickness. After the evaporation of the rest of solvent, a uniform solid polymer film is obtained (see Fig.4.3). The spin speed of the disc affects the degree of centrifugal force applied to the solution and its evaporation rate. As the solution dries, viscosity increases until the radial force of the spin can no longer move the solution toward the edges of the disc [10]. An empirical correlation between experimental parameters and film thickness exists. Indeed, it is known that solution viscosity, angular velocity, angular acceleration, spin time and solution volume affect the film thickness. In general the viscosity parameter is often related to the dilution of the solution. Very dilute solutions tend to form thinner films rather than viscous (or

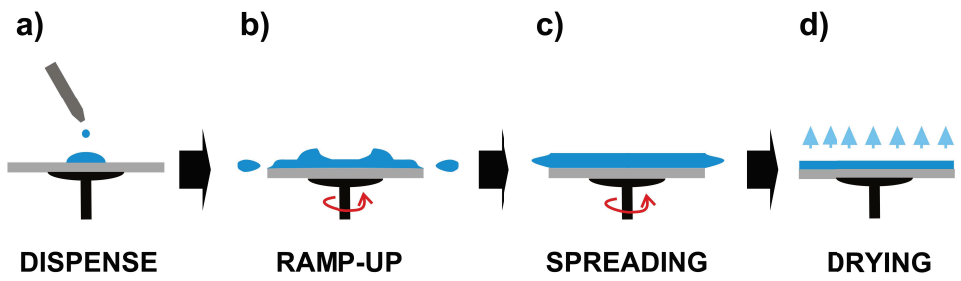

Figure 4.3: Representation of the processes occurring during spin-coating.

concentrated) solutions. The correlation between angular velocity and concentration has been widely reported in literature and an example of it is shown in Fig.4.4. The

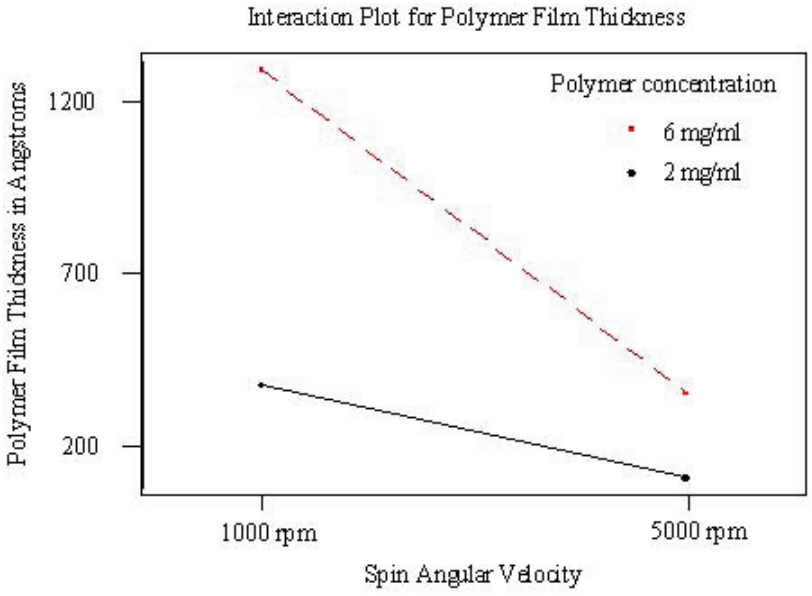

Figure 4.4: Graph representing the behaviour of film thickness Vs. angular velocity of spin, at different concentrations. The picture was taken from [11]

acceleration of the disc to reach the maximum angular velocity can also affect the coated film properties, since the solution starts to dry during the first part of the spin cycle (in some cases, more than 50% of solvent evaporates after few seconds of

spin). Lastly, the spin time must be sufficient to permit to complete evaporation of all molecules of solvent.

4.2 Opto-electronic Device Characterization

After the device fabrication, one of the most important steps, is its functional characterization. This process is distinguished in two parts: electrical and optical measurements. Both of them require a suitable detector or analyser, for collecting EL, in one case and, the flowing current through the working device, in the other case. Moreover, often these instruments must work in synchronization, since the EL is always correlated to the presence of current in an organic light-emitting transistor. Usually all measurements are performed in a controlled atmosphere (in a vacuum or inert gas atmosphere), since air and moisture could be disastrous in terms of device performances due to interaction with the organic layers. The setup we used to carry out some of the opto-electrical measurements in inert atmosphere is composed by a parametric analyser connected to a low noise probe station (provided with a photodiode) inside an inert-gas dry box. The analyser has the purpose of supplying the set voltage to the device contacts in order to obtain the current flowing. Furthermore, it allows to collect the intensity of the current flowing through the OFET channel. All operations are software-controlled. As analyser we used the Agilent B1500A system. In order to permit the existence of the devices also outside the glovebox, another step in the fabrication process is required, the encapsulation. By means of a UV resin and chemical etched glass caps, it is possible to isolate the OFETs active area from polluting environment. With this technique it has been possible to do more complex optical measurement on the devices, like measurement of EL spectra by means of a spectro-radiometer. We will speak in detail of the instrumentations used in the next sections.

4.2.1 Probe Station

For performing opto-electronic device characterization immediately after fabrication without any interaction of devices with atmosphere, we set-up a Sss PM5 Analytical Probe System (see Fig.4.5) in the nitrogen-atmosphere glove-box system which is coupled to the growth vacuum chamber. In a probe station by micrometric positioning

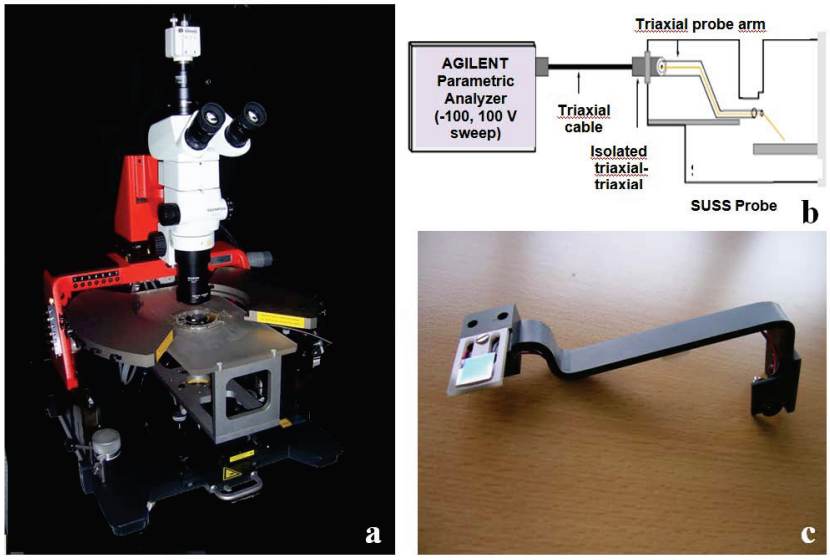

Figure 4.5: a) Sss PM5 Analytical Probe System. b) Scheme of the triaxial cable connection between the Semiconductor Device Analyser and the Analytical Probe System. c) Hamamatsu photodiode used for electroluminescence measurements. In order to collect the electro-luminescence two Hamamatsu photodiode (S1337) are mounted on two are arms (c) that can be positioned over and underneath the device substrate by two probe-heads with micrometric X,Y, Z stages. Thus, in the case of all-transparent devices it is possible to collect photons emitted upward and downward through the transparent substrate are easily collected. The photodiode effective area is $100mm^2$ and photosensitivity at 633 nm (He-Cd laser) is 0.6 A/W.

of tungsten tips on the device pads we are able to apply voltage to device and collect low-current signal (noise level tens of pA) that can be correlated to the device electro-luminescence because of the presence of photodiodes in the proximity of the device active area. The probe platen has enough area and heavy mass to provide extreme

rigidity and accessibility to the probe-heads. Platen can travel vertically along Z axis for 40 mm with a 0.2 mm contact/separation stroke. The chuck is mounted on a rigid X/Y table with ergonomic coaxial controls. The chuck position can be finely tuned in the Z direction. A pull-out stage moving along the Y axis permits quick and safe device loading as well as superior positional repeatability for packaged devices and substrates. For locating accurately the tungsten tips on the three device electrodes manual probeheads are magnetically blocked onto the base plate. The probe-head arms are connected to triaxial wires. The probe-head incorporates an independent X, Y and Z stage system with a maximum mechanical cross-talk deviation of 3 microns. Each stage incorporates hardened steel rails and ball bearings assembled to strict specifications. Each axis has 8 mm of travel with the choice of either 50 or 100 tpi (threads per inch) resolution. The triaxial-chuck connection (Fig.4.5b) is created to minimize the chuck leakage current. It is guarded and completely separated from the base machine by a Teflon insulation. The guard has an insulation resistance value of 1.0 TΩ. The chuck guard must be connected to the instruments guard connection to guarantee accurate and ultra low-current measurements. A 70X-magnification optical microscope is mounted vertically on the chuck plate to allow precise positioning of the probing tungsten tips.

4.2.2 Glove Box

A glove box is a sealed container designed to allow one to manipulate objects while being in a different atmosphere with respect to the object one, that is usually a very high purity inert atmosphere (such as argon or nitrogen). This is useful for working with oxygen sensitive substances. Inert atmosphere glove boxes are typically kept at a higher pressure than the surrounding environment, so any microscopic leaks are mostly leaking inert gas out of the box instead of letting air in. Built into the sides of the glove box are gloves, arranged in such a way that one can place his hands

into them and be able to perform tasks inside the box without breaking the seal or allowing potential injury to the worker. Part or all of the boxes are usually transparent to allow one to see what is being manipulated. This instrument is important because most organic materials are oxygen and moisture sensitive; measurements performed inside the glove-box are intrinsic, as the environment does not influence them. Our instrument is an EC-MECABOX from MECALAB labortechnologie AG. This glove box is composed of two containers coupled together by the main access entry chamber (Fig.4.6). Each container also presents a small entry chamber to introduce small objects. The left module contains the spin coater and is used for wet chemical pro-

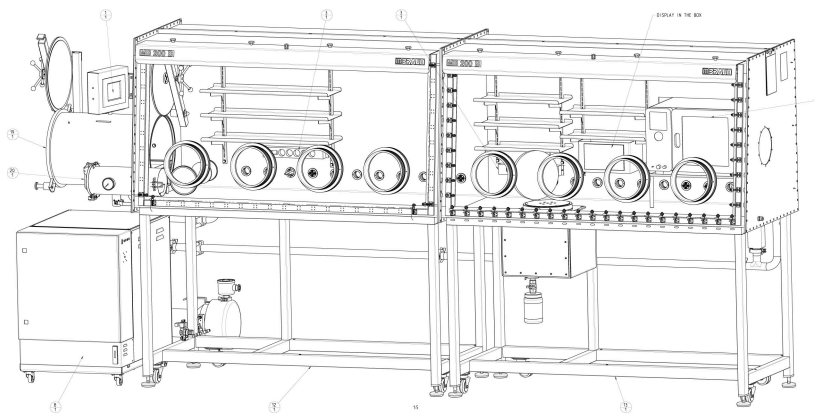

Figure 4.6: Scheme of the glove-box used for devices fabrication and characterization.

cessing. The right module contains the probe station for the electrical measurements and is linked to a growth chamber. This permits electrical characterization immediately after the device growth, without any air and oxygen exposure. Our glove box ensures oxygen and water presence below 1 ppm.

4.2.3 Integrating Sphere

For performing device electrical characterization in a 10^{-6} mbar vacuum atmosphere an integrating sphere is used (see Fig.4.9). Moreover this set-up allows to perform

Photo-Luminescence (PL) and Electro-Luminescence (EL) quantum yields. The setup

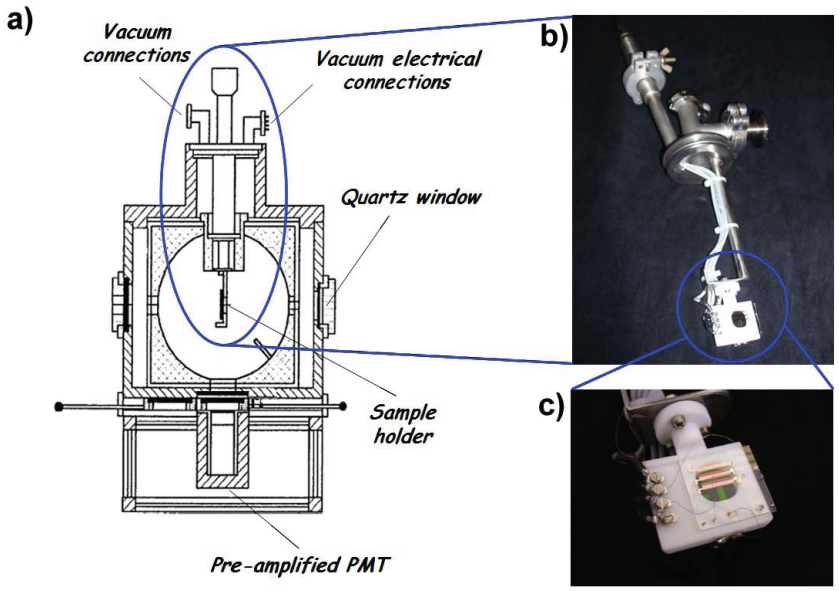

Figure 4.7: Left picture: Scheme of the vacuum integrating sphere used for EL measurements. Right top picture: particular of the sample holder with the feed-through connections. Right bottom picture: Zoom of the teflon sample holder.

consists in a Labsphere-manufactured 12 in-diameter integrating sphere made of a material reflecting 99.8 % in the spectral range 300-900 nm. Thus, the internal surface of the integrating sphere can be considered a Lambertian surface which distributes homogeneously within the sphere volume the total amount of light that hits the surface itself. Therefore, the flux received at an aperture of the sphere is proportional to the total light emitted from the sample, irrespective of its distribution. Thus, knowing all the geometrical parameters of the sphere it is possible to obtain a quantitative measurement of the EL quantum yield just by having a calibrated detector and supposing the emitting sample as a point-like source. A vacuum chamber is built to contain the sphere with optical quartz windows corresponding to the horizontal and the meridial apertures. Both the apertures allow us to check if the light emitted by the devices may be visible by naked eye. The vacuum chamber has a removable

top cover for inspection and cleaning of the internal part and of the sphere. The top cover is designed to fit a sample holder endowed with suitable electrical feed-throughs which permit to carry out electrical measurements in vacuum (Fig.4.7b). The sample holder enters the sphere placing the sample at the center of the sphere. The sample is located in a teflon clamp which present a central hole (Fig.4.7c), thus minimizing any perturbation on the distribution of the emitted light induced by the sample holder. The electrical cables for applying tensions and collecting currents are fixed in the teflon clamp. Thin copper threads welded by tin on the incoming signal cables are electrically connected to the device-under-test pad by silver paste. Device pad are properly engineered to facilitate this operation. At the meridial aperture of the vacuum chamber a photomultiplier for the detection of integrated signal is screwed. The photomultiplier is a pre-amplified head-on R347 photomultiplier tube (PMT) from Hamamatsu, whose sensitive part is set 5 mm apart from the internal surface of the sphere. The radiant cathode and anode sensitivity at 420 nm is 64 mA/W and $3.4 \cdot 10^4$ A/W respectively. Although the head-on configuration of the PMT helps to overcome the dependence of the measured signal from the spatial distribution of the light intensity on the sensible area of the PMT, a spectral diffuser between the surface of the sphere and the PMT is set. A mechanical and turbo pump system is connected to the vacuum chamber and to the sphere through an aperture located near the sample holder. A vacuum of 10^{-6} mbar is guaranteed by mechanically pressed O-rings at each quartz window, at the interface between the cryostat and the cover of the chamber, as well as between the cover of the chamber and the chamber itself.

4.3 Surface Analysis

4.3.1 Atomic Force Microscopy

Atomic force microscopy (AFM) belongs to the family of the Scanning Probe Microscopy (SPM) techniques. SPM are based on 3-D scanning of a sample surface, through a probe which locally interacts with the surface [12**?** , 13]. The probe is placed near the surface (d $<$ 100 nm). An electronic system measures the surface-probe interaction at every (x,y) point in the sample [14]. The probe is moved on top of the sample by a piezoelectric actuator, in order to cover a path called raster. The interaction strength (whatever its nature is, depending on the SPM techniques) depends on the sample-probe distance. By mapping the strength in the (x,y) points, we could obtain an image of the sample surface. AFM was invented by G. Binning, C. Gerber and C. Quate [15]. It overcomes the limits of other SPM (like Scanning Tunneling Microscopy, STM) because it permits the analysis of all type of samples (insulator, semiconductor, etc). Furthermore, it allows processing in air, vacuum or liquid environment [16–19]. The main components of an AFM are schematically showed in Fig.4.8.

- The probe which can interact with the surface (shown in Fig.4.9). The different interactions (magnetic, electric, etc) settled between the surface and the probe are strictly dependent on the nature of the probe itself.

- The piezoelectric transducer (also called scanner) which permits probe or sample movements. Movements are possible in all the three spatial directions with an accuracy in the order of 10^{-12} m. Vertical movements are guided by a feedback system which keeps the surface-probe interaction fixed. These movements are recorded and used to determine the topological profile of the surface.

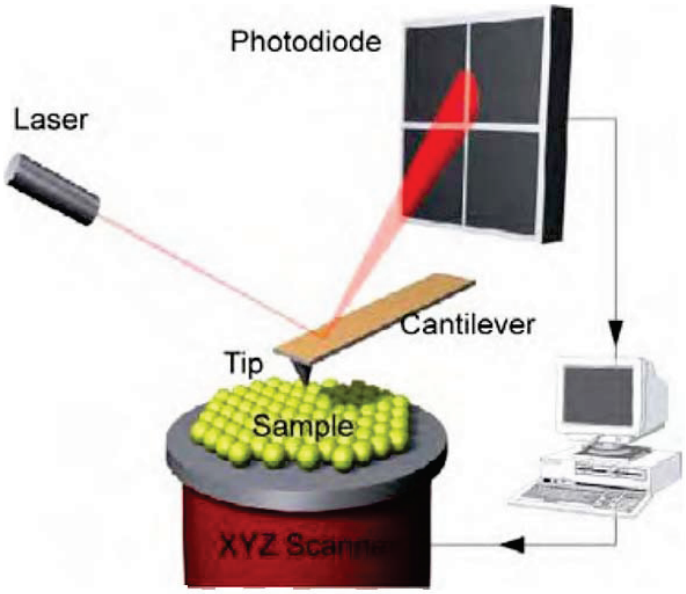

Figure 4.8: Scheme of the working principle of the AFM. The scanner moves the sample thereby changing the tip/surface interaction and the optical path of the laser beam, whose movement is collected by a photo-diode.

- An electronic system used to measure and to amplify the probe-surface interaction.
- A mechanical system, to damp the external vibrations; the above mentioned feedback system for keeping the signal with the physical information at a set value (setpoint).
- A control system for the acquisition and visualization of the data.

In the AFM technique, the probe is a very sharp pyramidal or conical tip fabricated on the edge of a lever called cantilever. When the tip and the surface interact, a force modifies the cantilevers mechanical balance. These change is detected by a laser beam focused on the back of the cantilever (Fig.4.8). The laser beam, after a convenient optical path, reaches a sensor (beam and bounce). During the surface scanning, the sensor (usually a photo-diode) reveals the different laser beam positions that, after a suitable amplification, are used to reproduce the surface topography. The

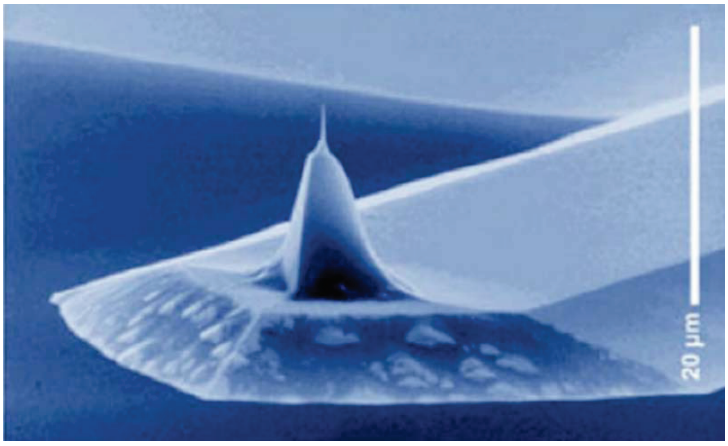

Figure 4.9: Scanning electron micrograph of a micromachined silicon cantilever with an integrated tip pointing in the [001] crystal direction (Wolter et al., 1991).

probe is the fundamental part of the instrument since it sets the minimal spatial resolution of the AFM. Ideally, it is conceived to be sensitive to a single chemical-physical interaction with the surface. But in practice this in not possible, so fabrication is important to minimize parasite interactions. There are rectangular or triangular shape levers with conic or pyramidal tip. Classic conic tips present these features: length around $100 - 130\mu$m, 35μm wideness, 2μm thickness, tip radius of curvature of 10 nm and an elastic constant less than 10 N/m. Several forces typically contribute to the deflection of an AFM cantilever. The force most commonly associated with atomic force microscopy is an interatomic force called the van der Waals force. The dependence of the van der Waals force upon the distance between the tip and the sample is shown in Fig.4.10.

Two distance regimes are labelled on Fig.4.10: (i) the contact regime; and (ii) the non-contact regime. In the contact regime, the cantilever is held less than a few angstroms from the sample surface, and the inter-atomic force between the cantilever and the sample is repulsive. In the non-contact regime, the cantilever is held on the order of tens to hundreds of angstroms from the sample surface, and the inter-atomic force between the cantilever and sample is attractive (largely a result of the long-

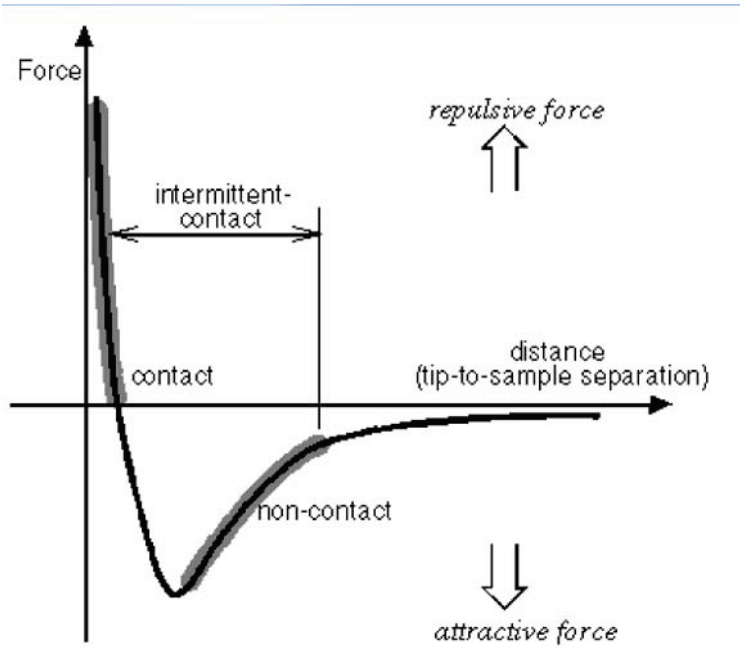

Figure 4.10: Graph showing the repulsive/attractive forces between the surface and the cantilever as a function of the distance.

range van der Waals interactions).

A third operation mode has been developed, between the contact and non contact modes: the semi-contact or tapping Mode (Fig.4.11). In Tapping Mode AFM the

Figure 4.11: Scheme of the AFM working modalities. In contact mode the topography is obtained by the cantilever bending; in no- contact mode and semi-contact (or tapping) mode the signal comes from the variation of frequency, magnitude and phase of the cantilever oscillation.

cantilever is oscillated at or near its resonance frequency with an amplitude ranging

typically from 20 to 100 nm. During the scan the tip lightly *taps* on the sample surface contacting the surface at the bottom of its swing [20, 21]. The feedback loop keeps constant the oscillation amplitude by maintaining a constant root-mean-mean value of the oscillation signal acquired by the split photodiode detector (setpoint). Then the vertical position of the scanner at each (x,y) data point is stored by the computer to form the topographic image of the sample surface. Clearly in this scanning modality a constant tip-sample interaction is maintained during imaging since a constant oscillation amplitude is maintained. Operation can take place both in ambient and liquid environments. When imaging in air, the typical amplitude of the oscillation allows the tip to contact the surface through the adsorbed fluid layer without getting stuck. The advantages of this procedure are low sample damaging and good lateral resolution. The semi-contact mode is usually employed for soft and biological materials.

4.4 REFERENCES

[1] K. Bobzin, N. Bagcivan, P. Immich, C. Pinero, N. Goebbels, and A. Kramer. Pvd - a success story with a future. *MaterialWiss Werkst*, 39(1):5–12, 2008.

[2] F. Schreiber. Organic molecular beam deposition: Growth studies beyond the first monolayer. *Phys Status Solidi A*, 201(6):1037–1054, 2004.

[3] A. Sassella, M. Campione, M. Moret, A. Borghesi, C. Goletti, G. Bussetti, and P. Chiaradia. Tuning the growth mode in organic molecular-beam epitaxy. *Phys. Rev. B*, 71(20), 2005.

[4] W.W. Flack, D.S. Soong, A.T. Bell, and D.W. Hess. A mathematical-model for spin coating of polymer resists. *J. Appl. Phys.*, 56(4):1199–1206, 1984.

[5] Middleman S. The effect of induced air-flow on the spin coating of viscous liquids. *J. Appl. Phys.*, 62(6):2530, 1987.

[6] C. J. Lawrence. The mechanics of spin coating of polymer films. *Phys. Fluids*, 31(10):2786, 1988.

[7] D. E. Bornside and C. V. et al Macosko. On the modeling of spin coating. *J. Imaging Tech.*, 13:122, 1987.

[8] D. E. Bornside, C. W. Macosko, and L. E. Scriven. Spin coating: One-dimensional model. *J. Appl. Phys.*, 66(11):5185, 1989.

[9] N. Sahu, B. Parija, and S. Panigrahi. Fundamental understanding and modeling of spin coating process : A review. *Indian J. Phys.*, 86(4):493–502, 2009.

[10] Lawrence C.J. Spin coating with slow evaporation. *Phys. Fluids A-Fluid*, 2(3):453–456, 1990.

[11] M. Cecchi, H. Smith, and D. Braun. Method to optimize polymer film spin coating for polymer led displays. *Synth. Met.*, 121:1715–1716, 2001.

[12] O. Marti, H.O. Ribi, B. Drake, T.R. Albrecht, C.F. Quate, and P.K. Hansma. Atomic force microscopy of an organic monolayer. *Science*, 239(4835):50–52, 1988.

[13] C.B. Prater, H.J. Butt, and P.K. Hansma. Atomic force microscopy. *Nature*, 345(6278):839–840, 1990.

[14] J.B. Pethica and W.C. Oliver. Tip surface interactions in stm and afm. *Physica Scripta*, T19A:61–66, 1987.

[15] G. Binning, C.F. Quate, and C. Gerber. Atomic force microscope. *Phys. Rev. Lett.*, 56:930, 1986.

[16] O. Marti, B. Drake, and P.K. Hansma. Atomic force microscopy of liquid-covered surface - atomic resolution images. *Appl. Phys. Lett., YEAR =*.

[17] T.R. Albrecht and C.F. Quate. Atomic resolution imaging of a nonoconductor by atomic force microscopy. *J. Appl. Phys.*, 62(7):2599–2602, 1987.

[18] M.D. Kirk, T.R. Albrecht, and C.F. Quate. Low-temperature atomic force microscopy. *Rev. Sci. Instrum.*, 59(6):833–835, 1988.

[19] C.M. Mate, M.R. Lorenz, and V.J. Novotny. Atomic force microscopy of polymeric liquid-films. *J. Chem. Phys.*, 90(12):7550–7555, 1989.

[20] C.B. Prater and Y.E. Strausser. *Tapping Mode Atomic-Force Microscopy - Applications to Semiconductors*. Intitute of Physics Conference Series, 1994.

[21] P.K. Hansma, J.P. Cleveland, M. Radmacher, D.A. Walters, P.E. Hillner, M. Bezanilla, M. Fritz, D. Vie, H.G. Hansma, C.B. Prater, J. Massie, L. Fukunaga, J. Gurley, and V. Elings. Tapping mode atomic-force microscopy in liquids. *Appl. Phys. Lett.*, 64(13):1738–1740, 1994.

Chapter 5

Materials For OFETs Fabrication

In order to enable practical applications of OFETs, the electrical characteristics must be consistently improved through the development of high performance organic semiconductors, a better control of the morphology as well as of the electronic properties at the active interface between the semiconductor film and the gate dielectric [1]. In order to do so, it can be extremely helpful to perform an appropriate chemical tailoring of the molecular structure. The chemical engineering of the molecular structure is indeed one the most important steps for OFET optimization and allows to tune key molecular and film properties, such as solubility, position of energy levels, film morphology and transport capabilities [2]. Furthermore, since OFETs are truly interface devices, in which charge transport is confined at the organic-dielectric interface, the control of the degree of crystallinity and uniformity over a large area at the organic-dielectric interface is mandatory to improve the device performances. In this chapter is presented a detailed description of some organic materials, used for transport or charges recombination, and dielectrics that will be considered as possible candidates to be implemented in a tri-layer OLET structure.

5.1 Charge Transport Materials

5.1.1 Oligothiophenes

The largest oligomeric family so far among conjugated organic compounds is probably that of oligothiophenes. This is a direct consequence of the extremely rich chemistry of the aromatic thiophene ring which has been extensively used to synthesize a large variety of p-conjugated a-linked oligothiophenes (α-nT, with n=number of thiophene rings in the oligomeric sequence, see Fig.5.1) [3, 4]. The recent and spectacular

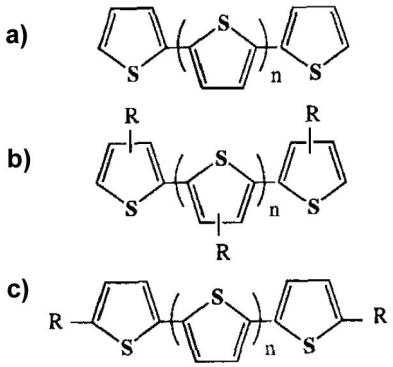

Figure 5.1: (a) Scheme of a generic oligo-thiophene α-nT (where "n" determines the length of the conjugated thiophene chain) along its derivatives functionalized at different positions with aryl groups (b,c).

development of conjugated oligothiophenes is essentially related to their use as active materials for electronic device applications [5]. In 1974 an initial article by H. Kuhn et al [6]. described photocurrent measurements on Langmuir-Blodgett films of $\alpha - quinquethiophene$ (α-5T). In the mid-1980's, conjugated all-α-linked oligothiophenes were used as model compounds and starting monomers for the preparation of electrically conducting polythiophenes [7]. Both in bulk and in thin-films the majority of unsubstituted conjugated organic thiophene oligomers (such as oligomers with four,five,six and eight thiophene rings [8–10]) crystallize into the monoclinic system with $P2_1$ space group ($P2_1/a$, $P2_1/b$, $P2_1/c$ according to the oligomer chain length) which is called herringbone structure (in Fig.5.2 is reported one of two polymorphs of

α-6T for example). Moreover they form polycrystalline films in which the molecule long axis is orientated perpendicularly to the substrate.

Molecules pack in this way in order to minimize π-orbital repulsion by adopting an

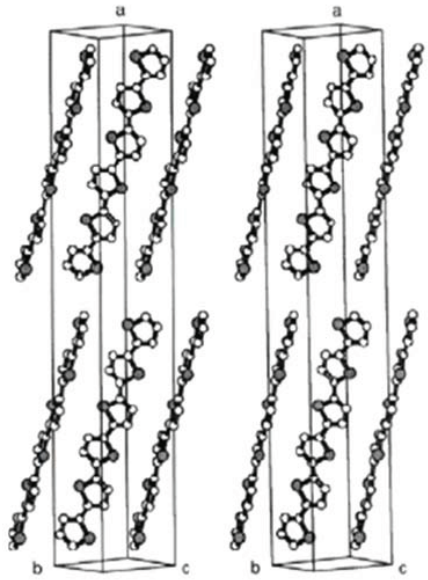

Figure 5.2: Crystal structure of $\alpha-6T$ deposited from the vapor phase, displaying a typical herringbone packing behaviour [11].

edge-to-face arrangement forming a two-dimensional layer [10]. The angle between molecular planes of side-by-side molecules is $40^\circ - 60^\circ$ and the distance between the sulphur atoms is around 3.6-3.9Å, depending on the length of the molecule [12]. This molecular arrangement is probably responsible for the reduction of the transport properties in the direction normal to the long molecular axis. It has been theorized that forcing the oligomers to adopt a face-to-face arrangement (π-stack) would increase the π-orbital overlap and thus enhance the charge mobility by maximizing electronic coupling between adjacent molecules [13]. Several oligomers that have been shown to adopt a co-facial packing arrangement include fused-ring oligomers [14], oligomers containing bulky substituents [15] and oligomers incorporating both electron-rich and electron-deficient aryl rings [16]. The electric performances of the devices obtained

from these oligomers are quite promising as compared with analogues that adopt a herringbone structure, but further investigations are needed to demonstrate conclusively that face-to-face π-stacking results in higher charge mobility.

This great interest in the study of the charge transport properties of semiconducting $\alpha - nT$ thin-films is due to the very promising implementation of linear oligothiophenes molecules as active materials in Organic Thin-film Transistor (OFET). In particular, it has been demonstrated that 6T-based OFETs show an improved carrier mobility when long range molecular ordering is achieved [17]. The highest mobilities ($\mu \sim 0.04\ cm^2/Vs$) are obtained in devices using highly oriented thin-films and are close to that measured on $\alpha - 6T$ single crystals ($\mu \sim 0.16\ cm^2/Vs$) [18]. This shows that charge transport between source and drain of an OFET occurs essentially through molecular channels of $\alpha - 6T$ molecules oriented perpendicular to the substrate and having the herringbone arrangement found in the single crystal. The highest reported mobility value for $\alpha - 8T$ is $0.33\ cm^2/Vs$ and was obtained when the substrate was heated to 120°C during deposition [19]. This mobility value is an order of magnitude higher than previously reported for $\alpha - 8T$ [8], and is attributed to the formation of elongated, terraced grains. The majority of the investigations on the transport properties of oligothiophene films do not show any effects that could be related to band-like descriptions of the excitonic or the charge carriers up to now. The strong thermal activation behaviour and the influence of the structure and the morphology of the polycrystalline oligothiophene films on transport processes establish a picture of the non-coherent hopping transport where different trapping levels dominate the motion of the charges [20]. In contrast to that, it was reported on the temperature dependence of field effect mobilities, which were attributed to a coherent carrier motion at very low temperature ($T < 50$ K) [21].

End-substitution of oligothiophenes by alkyl groups on the a-carbons of the terminal

rings is an efficient method to prevent chemical reactivity of these sites. In addition to enhanced chemical stability, end-substitution does not induce inter-ring torsion (as often does side-substitution) thus allowing retention of high π-conjugation and electroactivity.

α,ω-dimethyl-quaterthiophene (DM4T)

The first synthesis of this molecule was done by Hotta and Waragai by grafting methyl groups on the two α-carbons of the $\alpha - 4T$ and investigated the crystal structure of this compound in both its neutral [22, 23] and doped [24] forms (Fig.5.3). In con-

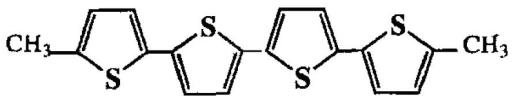

Figure 5.3: Chemical structure of α,ω-dimethyl-quaterthiophene (DM4T) molecule.

trast to non-substituted oligothiophenes, crystals of neutral DM4T are orthorhombic with a Pbca space group and Z=4. The molecules are almost coplanar, the two outer rings being slightly bent according to the mean plane of the two inner ones. Although packed in the herring-bone mode with an angle of about 59° between adjacent molecular planes, the molecules are aligned in an original zig-zag fashion, the molecular long axis being at an angle of 26° with the c axis (see Fig.5.4). The only reported electrical conductivity was done by Hotta and Waragai on blade-shape single crystals of DM4T doped with iodine [22, 23]. They found conductivities of $3.4{\cdot}10^{-5}\ S/cm$ along the c-axis, i.e. vertical to the crystal plane, and $1.2{\cdot}10^{-1}\ S/cm$ and $2.9{\cdot}10^{-2}\ S/cm$ for the directions longitudinal and transverse to the crystal plane respectively. The latter directions, however, do not coincide with either the a- or b-axis of the molecules. This also argues in favour of a preferred charge transport along

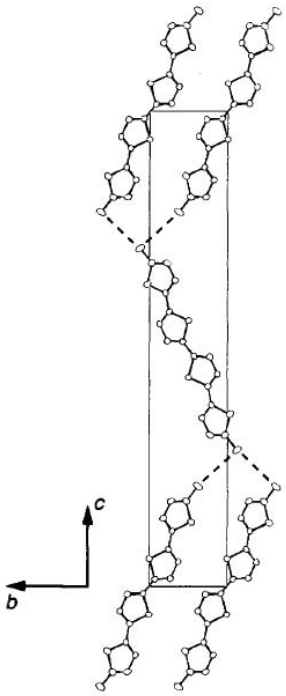

Figure 5.4: Crystal structure of α,ω-dimethyl-quaterthiophene (DM4T) [23].

the π-stacks rather than along the molecular axis. Nevertheless, Hotta and Waragai explain this as the effect of the iodine anions which are located between the ends of the molecules, thus preventing charge carriers from hopping from one site to the next. These conductivity results show that DM4T is a quasi two-dimensional conductor in which transport essentially occurs through face-to-face molecular arrays.

α,ω-dibutyl-quaterthiophene (DB4T)

The way in which the alkyl chain length affects the packing behaviour of molecules (in this case α-4T derivatives) in thin film and how it affects their transport characteristics is still almost unknown. For this reason, together with other well known α-4T p-type derivatives like DM4T and α,ω-dihexyl-quaterthiophene (DH4T), a material with an intermediate alkyl chain length, α,ω-dibutyl-quaterthiophene (DB4T) is also considered. Up-to-date, this kind of alkyl substitution at α-ω positions has not been

yet reported. Thus it is not possible to give any detailed description of the material except for its chemical structure (showed in Fig.5.5). In the following sections, we will report some detailed studies on the material properties from the electrical and morphological points of view.

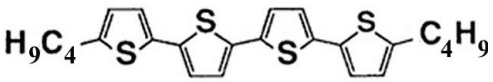

Figure 5.5: Chemical structure of α, ω-dibutyl-quaterthiophene (DB4T) molecule.

α, ω-dihexyl-quaterthiophene (DH4T)

Among all the alkyl end-substituted short oligothiophenes, we focus our attention on the study of α, ω-dihexyl-quaterthiophene (DH4T) (see Fig.5.6) since this molecule can organize in thermally grown polycrystalline thin-films presenting very high mobility and highly ordered structures. Transmission electron microscopy (TEM) [25]

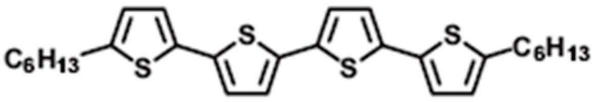

Figure 5.6: Chemical structure of α, ω-dihexyl-quaterthiophene (DH4T) molecule.

of the films on carbon grids reveals a very smooth and flat morphology of lamellar single crystals. At high deposition temperatures (e.g., 100°C) the flat crystals extend over many tens of micrometers without exhibiting substantial multi-layering. Their only distinguishing feature is the existence of transverse cracks. Because this feature is not seen for DH4T films deposited at lower temperatures, they are most likely the

result of contraction during cooling. Several groups investigated the ordering behaviour of DH4T in the last years. In particular two phase transitions were reported: from crystal phase to a mesophase at $84°$C and from mesophase to liquid phase at $181°$C. The mesophase is a highly ordered smectic phase [26]. Thin films deposited in mesophase can show long-range ordering over hundreds of μm [27]. Utilizing this mesophase of DH4T in thin film transistor manufacturing is a promising approach to obtain high molecular ordering and thus high mobility devices. X-ray diffraction (XRD) [25] of the films grown on Si/SiO_2 shows a series of sharp peaks, all corresponding to successive orders of the molecular repeat at 28.5Å. With increasing substrate temperature, the sharpness of the peaks increases, as it is expected, and the spacing between molecules shrinks. The 28.5Å molecular repeat is consistent with molecules being essentially normal to the substrate and with their hexyl chains directed toward the sulfur side of the 5 and $5'''$ positions of the quaterthiophene core. The spectrum at $180°$C is completely amorphous in agreement with a liquid phase. Picture of the crystal structure is reported in Fig.5.7.

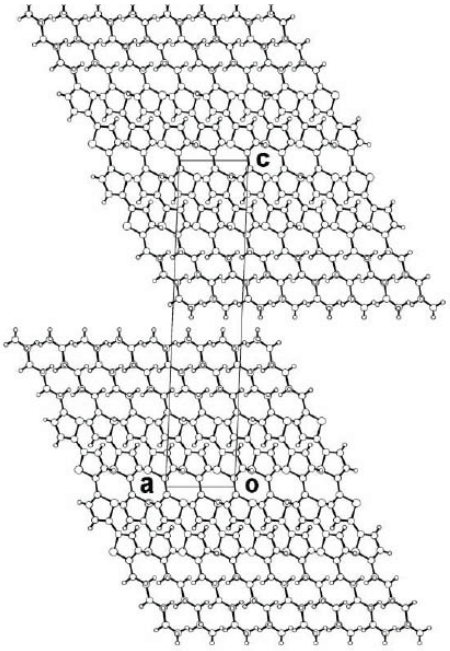

Figure 5.7: Crystal structure along unitary cell of α,ω-dihexyl-quaterthiophene (DH4T) [28].

α,ω-diperfluoro-quaterthiophene (DHF4T)

Facchetti and co-workers were the first to demonstrate that n-type behavior could be obtained in oligothiophenes through functionalization with perfluoroalkyl chains [29]. A series of oligomers was synthesized containing two to six thiophene rings functionalized in the α- or β-positions with perfluorohexyl chains [30, 31]. The introduction of perfluoroalkyl chains on the oligomer cores was found to increase the ionization potential and electron affinity but minimally affected the ground- and excited-state energies of the molecules. Organic thin-film transistor devices measured under nitrogen atmosphere only displayed semiconducting behaviour with positive gate voltages, indicating that these materials are exclusively electron conductors.

The complementary semiconductor behaviour of fluoroalkyl- (n-type) and alkyl- (p-type) α-nT is firstly due to the electron-withdrawing capacity of fluoroalkyl end-capping groups. Indeed, the thiophene ring is electron-rich and all the known thio-

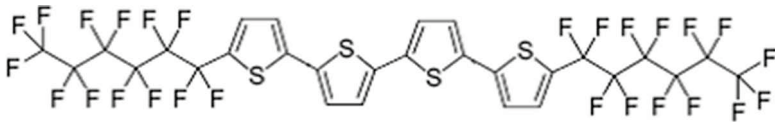

Figure 5.8: Chemical structure of α,ω-diperfluoro-quaterthiophene (DHF4T)

phene unsubstituted oligomers and polymers are hole-transport as thin-film. These systems are intrinsically p-type, and σ-electron donating alkyl substitution has the effect of enhancing this property. So, for all thiophene oligomers, fluoroalkyl substituents impart sufficient electron-withdrawing capacity lo lower the HOMO/LUMO core energy allowing electron injection to exceed hole injection [30].

Among fluoroalkyl thiophene oligomers, we focused our investigation on realization of devices based on α,ω-diperfluoro-quaterthiophene (DHF4T) whose chemical structure is reported in Fig.5.8. The molecular packing of DFH4T shares the familiar

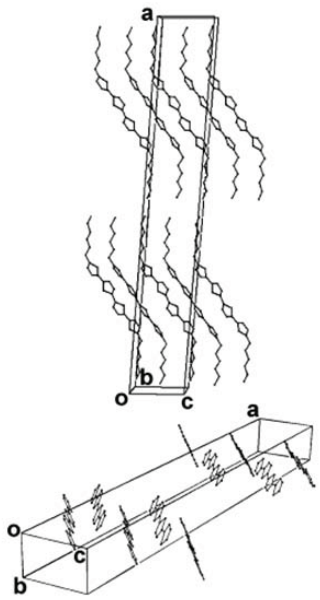

Figure 5.9: Crystal packing of DHF4T. Fluorine atoms (up) and fluorocarbon chains (bottom) are removed for clarity. The origin of the molecular angle, which is also typically found in many aromatic hydrocarbons crystal structures is principally due to intermolecular π-electron repulsion [31].

herringbone motif found in all members of the oligothiophenes series, with an angle of 50° between mean planes of adjacent molecules (Fig.5.9). Typical herringbone angles for oligothiophene α-nTs (with n = 4-6,8) range between 55° and 70°.

5.1.2 Perylene Derivatives

Up to now, many intensive studies have been done in the field of electronic materials, among which perylene diimide are one of the best n-type semiconductors due to their high electron affinity. As previously reported, organic semiconductors can conduct charges due to partial delocalization or charge hopping through molecules that are coupled by a relatively weak Van der Walls forces.

The electron-deficient character of perylene diimide is also a prerequisite for their high photochemical stability because photo-oxidation, as the major destructive mechanism for dyestuff, is disfavoured. Many perylene derivatives have been widely studied in OFETs since their well defined n-type behaviour. OFETs based on perylene derivatives (some of them are reported in Fig.5.10) show mobility values that can range from $0.1cm^2/Vs$ to $1.5cm^2/Vs$ and threshold voltages that range from 15V to 30V [32–34].

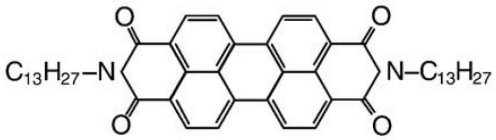

Figure 5.10: Chemical structure of the perylene diimide molecule used in this thesis (P13).

N,N'-ditridecylperylene-3,4,9,10-tetracarboxylic diimide (P13)

Among the many perylene derivatives studied, P13 is considered the most promising structure since it has the highest field-effect electron mobility due to the large

π-electron system and strong electron affinity.

From the crystal structure point-of-view it shows characteristic features of the polymorphous thin-film structure, even when the layer is deposited at only $30°$C. This structure is characterized by four reflection peaks at $3.43°$, $6.77°$,$10.11°$, and $13.57°$, which correspond to d-spacings of 25.7, 13.1, 8.77 and 6.5Å respectively. These peaks are associated to the (001), (002), (003) and (004) diffraction planes of the P13 crystalline structure [35]. P13 has been successfully used as a transport material

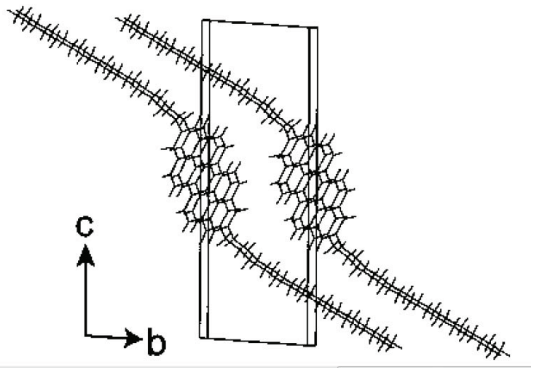

Figure 5.11: Crystal structure along unitary cell of N,N'-ditridecylperylene-3,4,9,10-tetracarboxylic diimide (P13) molecules. Perylene exhibits a peculiar crystal packing in which dimers (and not single molecules) are arranged in an herringbone fashion. The attachment of dianhydride (PTCDA) or diimide (PTCDI) moieties leads to compounds with good n-type properties.

for OFET fabrication [36] and, in a blend with pentacene, for efficient harvesting of light for solar cells applications [37].

5.2 Recombination and Light-Emitting Materials

The mechanism of electroluminescence (EL) in covalent bonded molecular system is often found among many molecular system, like π-conjugated organic materials. The process of charge recombination, thus exciton formation and relaxation in radiative pathways, was already described in the previous chapter. The following section will be devoted to the introduction of some materials mainly used as recombination layer

in our OLET structures.

Many organic dyes exhibit very high fluorescence quantum yields. However in the condensed phase, fluorescence quantum yield of molecular aggregates can be drastically reduced due to the formation of exciplexes. Because of this reason, fluorescence dye molecules are doped into a host matrix. Doping can be achieved by co-evaporating the dopant with the host and typical doping concentration of the fluorescent dye vary from a fraction of a percent to a few percents. Emission from dopant molecule can be obtained by two possible pathways. The first pathway is that electrons and holes recombine at host molecule site and generate excited electronic states. The excited state (exciton) are then transferred to the dopant molecules. This process is called Förster energy transfer. This way, emission is due to excited states of dopant molecules and independent of the host molecules. Another pathway is that electrons and hole are directly injected into the dopant molecules and recombination occurs at the dopant molecular site. Molecular doping enables the use of the same host materials with different color dopant molecules. E.g. Tris(8-hydroxyquinoline)-aluminum (Alq3) alone is a green emitter, but can be used as a host matrix for orange or red dopant dyes.

Considering the roles that must be fulfilled by the Emitting Layer (EML), many properties must be effectively combined.

- The layer should be able to transport charge both holes and electrons in order that the charge carriers are able to move through the layer and find each other.

- The recombined charges must then create an excited state in the material, which can collapse from this exciton state back to its ground state and in doing so emit a photon of light.

- All of this must occur efficiently with little to none of the input energy being

dissipated as heat or electrochemical transformations of the materials themselves.

- Furthermore, mixtures of materials, if used for long-lived devices, must remain uniformly dispersed (a high Tg and have good film forming properties as a solid solution) and not be subject to materials migration under an applied electric field (no electrophoresis).

5.2.1 Tris(8-hydroxyquinoline)-aluminum (Alq3)

The phenomenon of organic EL was first demonstrated using a small-molecule fluorescent emitter in a vapor-deposited OLED device. The Kodak group first used metal oxinoid materials such as the octahedral complex aluminum tris-8-hydroxyquinoline (Alq3)(Fig.5.12) as the fluorescent green emitter in their pioneering work on OLED architectures [38].

Alq3 is a stable emitter material in optoelectronic devices and metallic complexes of

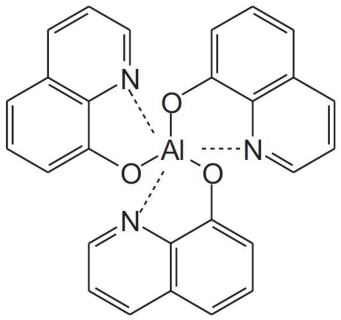

Figure 5.12: Chemical structure of Tris(8-hydroxyquinoline)-aluminum (Alq3)

this type have many of the desired stability and film-forming properties necessary to provide useful performance. The complex can exist as both fac and mer isomers and little attention is usually given to which isomer is present in the thin films of devices, although the starting material for the evaporation is usually predominantly mer. After Kodak group pioneering papers, Alq3, so far, is still considered a good emission

material (it has a solid-state fluorescence Quantum Yield (QY) of 25-32% [39]), it has electron transport properties and is an excellent host material for other more efficient dopant materials with lower emission energy.

As host material, Alq3 was the first OLED host material reported by Tang et al. [40]. The HOMO energy level is -5.95 eV and its LUMO energy level is -3.00 eV [41]. The triplet energy level of Alq3 was determined to be 2.0 eV. Singlet emission peaks centered at 560 nm make it suitable as a host for green and red emission. Alq3 has risen to a prominent position among OLED materials and remains the most widely studied metal chelate material. In Alq3 crystal structure, the distorted octahedral geometry of the 8-hydroxyquinoline ligands surrounding the Al^{3+} ion center makes it less prone to photoluminescence (PL) quenching in the solid state. It is thermally stable, has a T_g of $172°$C [42], and can easily be thermally deposited to form pin-hole free amorphous thin films due to its intrinsic polymorphic phase behavior [43]. The bulk electron mobility of Alq3 is $1.4 \cdot 10^{-6} cm^2/Vs$, far higher than its hole mobility $2.0 \cdot 10^{-8} cm^2/Vs$ as estimated by Time of Flight (TOF) measurements [44]. These electronic data together with the optical ones indicate that Alq3 is an electron acceptor.

Theoretical modelling work predicting the emission color of Alq3 derivatives has shown that the emission properties of the ligand dominate the fluorescence of the complexes [45, 46]. The electronic $\pi\pi^*$ transitions in Alq3 are localized on the quinolate ligands with the filled π orbitals (HOMOs) located on the phenoxide side of the quinolate ligand, and the unfilled π^* orbitals (LUMOs) are on the pyridyl side.

5.2.2 $4,4'$-bis[N-(1-naphthyl-1)-Nphenyl-amino]-biphenyl (α-NPD)

The most commonly used hole-transport materials (HTM) in OLEDs are triarylamine compounds. These compounds were developed as HTMs for photoconductive applications such as xerography [47]. They naturally have been selected as HTMs for

OLED applications largely because of their ready availability and their good electrochemical and thermal stabilities. The hole mobilities of these materials are also adequate for electronic applications. In addition, high purity, so as to ensure low hole-trap contamination, is believed necessary for long-lived devices performance and such materials may often be train sublimed to very high purity.

α-NPD has modestly high hole drift mobility, and was initially developed as charge

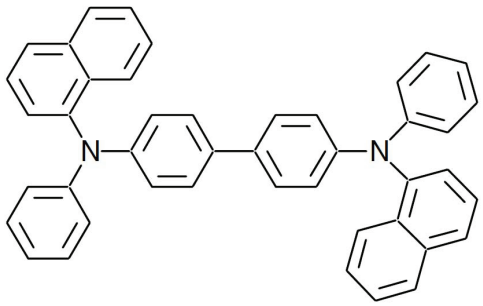

Figure 5.13: Chemical structure of $4,4'$-bis[N-(1-naphthyl-1)-Nphenyl-amino]-biphenyl (α-NPD)

transport layers in xerography (HOMO: -5.70 eV ; LUMO: -2.60 eV). However, α-NPD which has low glass transition temperature (Tg) of $95°$C, tends to crystallize or expand during device operation. For comparison, the Tg of Alq3 is $> 170°$C.

It is commonly believed that a good HTM should have both a low-energy barrier from the anode and a relatively high Tg. These properties will improve the hole injection efficiency, reduce the crystallization, and thus increase the lifetime of the device.

Adachi et al. showed that the ionization potential (relative to the molecule HOMO level) of HTM was found to be the dominant factor for obtaining high durability in organic EL devices [48]. The formation of the small energy barrier at the interface of a HTM and anode was required for high durability. However, their results showed that there are no straightforward relationships between melting point, Tg of the HTMs, and durability of the EL devices.

5.2.3 4-(Dicyanomethylene)-2-methyl-6-[p-(dimethylamino)styryl]-$4H$-pyran (DCM)

4-(Dicyanomethylene)-2-methyl-6-[p-(dimethylamino)styryl]-$4H$-pyran (DCM) (see Fig.5.14), is a bright and efficient red arylidene laser dye first synthesized in 1974 [49], and was the first dopant in host-guest system OLEDs introduced by Kodak researchers in 1989. The device ITO/hole transport layer (HTL)/Alq:DCM/Mg:Ag

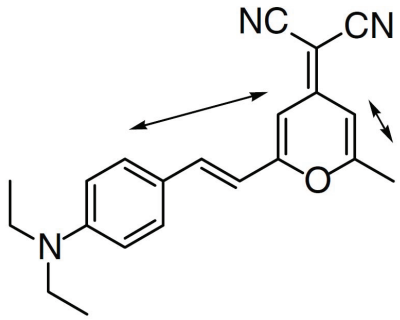

Figure 5.14: Chemical structure of 4-(Dicyanomethylene)-2-methyl-6-[p-(dimethylamino)styryl]-$4H$-pyran(DCM)

showed an EQE of 2.3%. The emission is orange-red with peak emission in the range of 570-620 nm for DCM depending on the concentration of the dopants. High concentration doping results in more saturated red emission, however, low efficiency due to concentration quenching becomes a factor at these high dopant levels [50]. The DCM molecule has an electrondonor π-acceptor (so-called push-pull) structure and it has an active methyl group, which can suffer further condensation reactions to form undesired bis-condensation by-products. This by-product shows a broad, very weak fluorescence. Consequently, during the synthesis of materials in the DCM, careful control of the reaction condition and repeated purification of the product is needed to get high-performance devices. The drawbacks of such a complex, synthetic protocol and tedious purification processes make it hard to be produced in large-scale manufacturing. The impurity issues of DCM materials have been solved through the elimination of the active methyl group by introducing unsymmetrical pyran moieties.

In our studies, DCM was used as a doping dye in a 3% wt host:guest blend with Alq3 or α-NPD as host matrices.

5.2.4 Pt(II) octaethylporphine (PtOEP)

Porphine complexes are known to possess long-lived triplet states useful in oxygen detection [51]. The addition of platinum to the porphyrin ring reduces the phosphorescence lifetime by increasing spin-orbit coupling; the triplet states gain additional singlet character, and vice versa. As described above, this also enhances the efficiency of inter-system crossing from the first singlet excited state to the triplet excited state. Transient absorption spectrometry gives a singlet lifetime in PtOEP of ~ 1 ps, and the fluorescence efficiency is extremely weak [52]. In contrast, the room temperature phosphorescence efficiency of PtOEP in a polystyrene matrix is 0.5% with an observed lifetime of 91 s [53]. PtOEP shows strong singlet absorption at 530 nm [54], corresponding to the peak emission of the electron transport material, Alq3. Thus it may be assumed that PtOEP is a suitable dopant for Alq3–based optoelectronic devices. Indeed, PtOEP was one of the first nonlanthanide phosphorescent organometallic complexes used in OLED devices [55]. It shows a very nice narrow red emission band centered at 650 nm. In our studies, PtOEP was used as a doping dye of a host-guest recombination system made of Alq3:PtOEP at 8% wt blend.

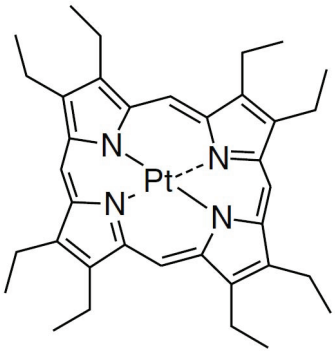

Figure 5.15: The chemical structure of platinum octaethylporphyrin (PtOEP)

5.2.5 Iridium bis(2-methyldibenzo-quinoxaline)(acetylacetonate) (IrMDQ(acac))

The first iridium complex used in OLED devices was fac tris(2-phenylpyridine) iridium $Ir(ppy)_3$ complex [55]. It has a short triplet lifetime (~ 1 ms) and high phosphorescent efficiency ($\phi_p = 40\%$ at room temperature in solution) [56]. However, in the solid state, most iridium complexes showed very low phosphorescent QE due to aggregate quenching. In most cases, the complexes have to be diluted in host materials to avoid reducing the phosphorescence efficiency. For example, $Ir(ppy)_3$ suffers aggregate quenching when the doping level is above 8 wt% in a CBP host [55]. An improved method to synthesize fac tris-ortho-metalated iridium complexes in high yield involves utilizing the commercially available starting material $Ir(acac)_3$ (acac=2,4-pentanedionate or acetylacetonate) [57]. This class of iridium complex has a red emission band (~600 nm). As for PtOEP, also IrMDQ(acac) was used, in our stud-

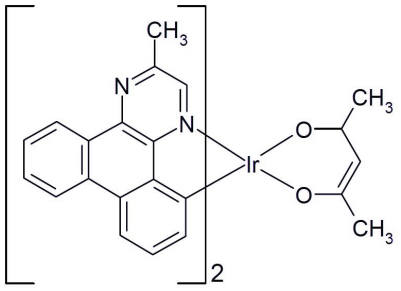

Figure 5.16: The chemical structure of iridium complex used in this thesis. The Iridium(III) bis(2-methyldibenzo-[f,h]quinoxaline) (acetylacetonate)(IrMDQ(acac))

ies, as a doping dye of a host-guest recombination system, whose the host matrices was α-NPD (10% wt. blend).

5.3 Gate Dielectric: Poly-Methyl-Metacrylate (PMMA)

Poly(methyl-methacrylate) (PMMA) is a transparent thermoplastic polymer, often used as a light or shatter-resistant alternative to glass. It is sometimes called acrylic glass. Chemically, it is the synthetic polymer of methyl methacrylate. The material was developed in 1928 in various laboratories, and was first brought to market in 1933 by Rohm and Haas Company, under the trademark Plexiglass. It has since been sold under many different names including Lucite and Perspex.

PMMA is an economical alternative to polycarbonate (PC) when extreme strength is not necessary. It is often preferred because of its moderate properties, easy handling and processing, and low cost, but behaves in a brittle manner when loaded, especially under an impact force, and is more prone to scratching compared to glass. PMMA

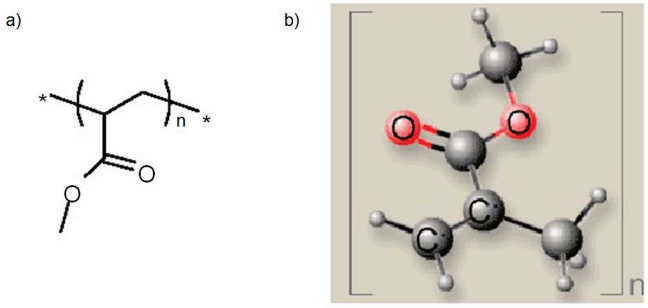

Figure 5.17: a) The chemical structure of PMMA repetition unit; b) 3D backbone structure of PMMA.

is commercially available in both pellet and sheet form. It is an amorphous polymer with a typical density of 1.17 g/cm^3. Its glass transition temperature is around $114°$C (depending on the molecular weight) and the monomer weight is 100.12 g/mol (see Fig.5.17). A 600K molecular weight PMMA in 3% wt. ethyl-lactate solution supplied by All Resist was used. The low frequency relative dielectric constant value of PMMA is 3.6. In our studies, films were obtained by spin-coating, after the wet cleaning of the substrates, using 400 μL of a 3% wt ethyl-lactate solution at 6000 rpm, yielding

about 450 nm thick films on transparent glass/Indium-Tin-Oxide(ITO) substrates. (See Fig.5.18).

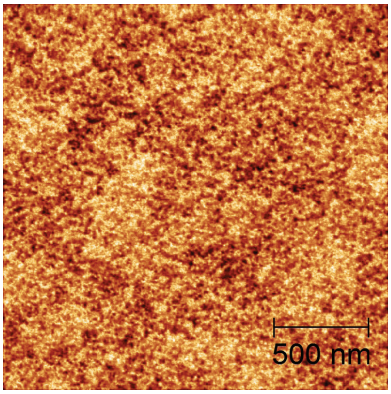

Figure 5.18: AFM image of PMMA surface deposited on a glass/ITO substrate.

5.4 REFERENCES

[1] M. A. Loi, E. da Como, F. Dinelli, M. Murgia, R. Zamboni, F. Biscarini, and M. Muccini. Supramolecular organization in ultra-thin films of alpha-sexithiophene on silicon dioxide. *Nat. Mater.*, 4:81, 2005.

[2] A. Facchetti. Semiconductors for organic transistors. *Mater. Today*, 10(3):28, 2007.

[3] J. Nakayama, T. Konishi, and M. Hoshino. Preparation of thiophene oligomers. *Heterocycles*, 27:1731, 1988.

[4] R. Hakansson. *Thiophene and its Derivatives*. S. Gronowitz, 1992.

[5] D. Fichou. *Handbook of Oligo- and Polythiophenes*. Wiley-VCH, 1998.

[6] U Schoeler, K.H. Tews, and H. Kuhn. Potential model of dye molecule from measurements of the photocurrent in monolayer assemblies. *J. Chem. Phys.*, 61(12):5009, 1974.

[7] M Akimoto, Y Furukawa, H Takeuchi, I. Harada, Y Soma, and M. Soma. Correlation between vibrational-spectra and eelectrical-conductivity of polythiophene. *Synth. Met.*, 15(4):353, 1986.

[8] R Hajlaoui, G Horowitz, F Garnier, A. Arce-Brouchet, L Laigre, A. El Kassmi, F. Demanze, and F. Kouki. Organic transistors using alpha-octithiophene and alpha,omega-dihexyl-alpha-octithiophene: Influence of oligomer length versus molecular ordering on mobility. *Adv. Mater.*, 9:389, 1997.

[9] A. Dodabalapur, L. Torsi, and H.E. Katz. Organic transistors - 2-dimensional transport and improved electrical characteristics. *Science*, 268(5208):270, 1995.

[10] D. Fichou. Structural order in conjugated oligothiophenes and its implications on opto-electronic devices. *J. Mater. Chem.*, 10(3):571, 2000.

[11] G. Horowitz, B. Bachet, A. Yassar, P Lang, F. Demanze, and F Fave, J.L.and Garnier. Growth and characterization of sexithiophene single-crystals. *Chem. Mater.*, 7(7):1337, 1995.

[12] A. Gavezzotti and G. Filippini. Crystal packing and lattice energies of polythienyls - calculations and predictions. *Synth. Met.*, 40(2):257, 1991.

[13] G. Horowitz, R Hajlaoui, R Bourguiga, and M. Haijlaoui. Theory of the organic field-effect transistor. *Synth. Met.*, 101(1-3):401, 1999.

[14] X.C. Li, H. Sirringhaus, F Garnier, A.B. Holmes, S.C. Moratti, N. Feeder, W Clegg, S.J. Teat, and R.H. Friend. Transition metal complex-doped hydroxyapatite layers on porous silicon. *J. Am. Chem. Soc.*, 120(45):2206, 1998.

[15] J.E. Anthony, J.S. Brooks, D.L. Eaton, and S.R. Parkin. Functionalized pentacene: Improved electronic properties from control of solid-state order. *J. Am. Chem. Soc.*, 123(38):9482, 2001.

[16] M.H. Yoon, A. Facchetti, C.E. Stern, and T.J. Marks. Nonlinear optical properties and excited-state dynamics of highly symmetric expanded porphyrins. *J. Am. Chem. Soc.*, 128(43):5792, 2006.

[17] F. Garnier, G. Horowitz, D. Fichou, and A. Yassar. Role of mesoscopic molecular organization in organic-based thin film transistors. *Supramol. Sci.*, 4(1-2):155, 1997.

[18] G. Horowitz, R Hajlaoui, and F. Kouki. An analytical model for the organic field-effect transistor in the depletion mode. application to sexithiophene films and single crystals. *Eur Phys J-Appl Phys.*, 1(3):361, 1998.

[19] M.E. Hajlaoui, F Garnier, L. Hassine, F. Kouki, and H. Bouchriha. Growth conditions effects on morphology and transport properties of an oligothiophene semiconductor. *Synth. Met.*, 129(3):215, 2002.

[20] C Vaterlein, B Ziegler, and W et al. Gebauer. Nonlinear-optical absorption in separate-confinement multi-quantum-well structures due to spatial band bending. *J. Appl. Phys.*, 76(2):133, 1994.

[21] M. Wu and E.M. Conwell. Transport in alpha-sexithiophene films. *Chem. Phys. Lett.*, 266(3-4):363, 1997.

[22] S. Hotta and K. Waragai. Crystal-structures of oligothiophenes and their relevance to charge-transport. *Adv. Mater.*, 5:896, 1993.

[23] S. Hotta and K. Waragai. Alkyl-substituted oligothiophenes - crystallographic and spectroscopic studies of neutral and doped forms. *J. Mater. Chem.*, 1:835, 1991.

[24] Y. Matsuura, Y. Oshima, Y. Misaki, and et al. Synthesis and properties of oligothiophene cation radical salts. *Synth. Met.*, 82:155, 1996.

[25] H. E. Katz, A.J. Lovinger, and J.G. Laquindanum. alpha,omega-dihexylquaterthiophene: A second thin film single-crystal organic semiconductor. *Chem. Mater.*, 10:457, 1998.

[26] G. W. Gray and J. W. G. Goodby. *Smectic Liquid Crystals*. Leonard Hill, 1984.

[27] K. R. Amundson, H. E. Katz, and A. J. Lovinger. Phase behavior of alpha,omega-dihexyl-alpha-quaterthiophene and ordering on a textured substrate. *Thin Solid Films*, 426:140–149, 2003.

[28] M. Moret, M. Campione, A. Borghesi, L. Miozzo, A. Sassella, S. Trabattoni, B. Lotz, and A. J. Thierry. Structural characterisation of single crystals and thin films of alpha,omega-dihexylquaterthiophene. *J. Mater. Chem.*, 15:2444, 2005.

[29] A. Facchetti, Y. Deng, A. Wang, Y Koide, H. Sirringhaus, T.J. Marks, and R.H. Friend. Tuning the semiconducting properties of sexithiophene by alpha,omega-substitution - alpha,omega-diperfluorohexylsexithiophene: The first n-type sexithiophene for thin-film transistors. *Angew. Chem.*, 39:4547, 2000.

[30] A. Facchetti, M. Mushrush, H.E. Katz, and T.J. Marks. n-type building blocks for organic electronics: A homologous family of fluorocarbon-substituted thiophene oligomers with high carrier mobility. *Adv. Mater.*, 15:33, 2003.

[31] A. Facchetti, M. Mushrush, M.H. Yoon, G.R. Hutchison, A. Ratner, and T.J. Marks. Building blocks for n-type molecular and polymeric electronics. perfluoroalkyl-versus alkyl-functionalized oligothiophenes (nt; n=2-6). systematics of thin film microstructure, semiconductor performance, and modeling of majority charge injection in field-effect transistors. *J. Am. Chem. Soc.*, 126:13859, 2004.

[32] P. R. L Malenfant and al. N-type organic thin-film transistor with high field-effect mobility based on a n,n'-dialkyl-3,4,9,10-perylene tetracarboxylic diimide derivative. *Appl. Phys. Lett.*, 80:2517–2519, 2002.

[33] R.J Chesterfield and al. Variable temperature film and contact resistance measurements on operating n-channel organic thin film transistor. *J. Appl. Phys.*, 95:6396–6405, 2004.

[34] R.J Chesterfield and al. Organic thin film transistors based on n-alkyl perylene bisimides: Charge transport kinetics as a function of gate voltage and temperature.

[35] S Tatemichi, M Ichikawa, T Koyama, and Y Taniguchi. High mobility n-type thin-film transistors based on n,n '-ditridecyl perylene diimide with thermal treatments. *Appl. Phys. Lett.*, 89:112108, 2006.

[36] C. Rolin, K. Vasseur, S. Schols, M. Jouk, G. Duhoux, R. Mller, J. Genoe, and P. Heremans. High mobility electron-conducting thin-film transistors by organic vapor phase deposition. *Appl. Phys. Lett.*, 2008.

[37] A.K. Pandey, S. Dabos-Seignon, and J-M. Nunzi. Pentacene: Ptcdi-c13h27 molecular blends efficiently harvest light for solar cell applications. *Appl. Phys. Lett.*, 2006.

[38] S.A. Vanslyke, C.W. Tang, and L.C. Roberts. Electroluminescent Device with Organic Luminescent Medium *AU.S. Patent 4,720,432A*, 1998.

[39] D.Z. Garbuzov, V. Bulovic, P.E. Burrows, and S.R. Forrest. Photoluminescence efficiency and absorption of aluminum-tris-quinolate (alq3) thin films. *Chem. Phys. Lett.*, 249:433–437, 1996.

[40] C.W. Tang and S.A. Vanslyke. Organic electroluminescent diodes. *Appl. Phys. Lett*, 51:913–915, 1987.

[41] J.D. Anderson, E.M. McDonald, P.A. Lee, M.L. Anderson, E.L. Ritchie, H.K. Hall, T. Hopkins, E.A. Mash, J. Wang, A. Padias, S. Thayumanavan, S Barlow, S.R. Marder, G.E. Jabbour, S. Shaheen, B. Kippelen, N. Peyghambarian, R.M. Wightman, and N. R. Armstrong. Electrochemistry and organic light-emitting materials and devices electrogenerated chemiluminescence processes of the components of aluminum quinolate-triarylamine, and related organic light-emitting diodes. *J. Am. Chem. Soc.*, 120:9646–9655, 1998.

[42] K.A. Higginson, X. Zhang, and F Papadimitrakopoulos. Thermal and morphological effects on the hydrolytic stability of aluminum tris(8-hydroxyquinoline) (alq3). *Chem. Mater.*, 10:1017–1020, 1998.

[43] M Brinkmann, G Gadret, M Muccini, C Taliani, N Masciocchi, and A Sironi. Correlation between molecular packing and optical properties in different crystalline polymorphs and amorphous thin films of mer-tris(8-hydroxyquinoline)aluminum(iii). *J. Am. Chem. Soc.*, 122:5147–5157, 2000.

[44] R.G. Kepler, P.M. Beeson, S.J. Jacobs, R.A. Anderson, M.B. Sinclair, V.S. Valencia, and P.A. Cahill. Electron and hole mobility in tris(8-hydroxyquinolinolato-n1,o8) aluminum. *Appl. Phys. Lett.*, 66:3618–3620, 1995.

[45] GM. Sugimoto, M Anzai, K Sakanoue, and S. Sakaki. Modulating fluorescence of 8-quinolinolato compounds by functional groups: a theoretical study. *Appl. Phys. Lett.*, 79:2348–2350, 2001.

[46] M Sugimoto, S Sakaki, K Sakanoue, and M.D. Newton. Theory of emission state of tris-8- quinolinolato.aluminum and its related compounds. *J. Appl. Phys.*, 90:6092–6097, 2001.

[47] Horgan and M. Anthony. Composite Layered Imaging Member for Electrophotography. *U.S.Patent 4047948*, 1977.

[48] C. Adachi, K. Nagai, and N. Tamoto. Molecular design of hole transport materials for obtaining high durability in organic electroluminescent diodes. *Appl. Phys. Lett*, 66:2679–2681, 1995.

[49] F.G. Webster and W.C. McColgin. U.S. Patent 3,852,683, 1974.

[50] S. Toffanin, R. Capelli, T-Y. Hwu, K-T. Wong, T. Plotzing, M. Forst, and M. Muccini. Molecular host-guest energy-transfer system with an ultralow amplified spontaneous emission threshold employing an ambipolar semiconducting host matrix. *J. Phys. Chem. B*, 114(1):120–127, 2010.

[51] A. Mills and A. Lepre. Controlling the response characteristics of luminescent porphyrin plastic film sensors for oxygen. *Anal. Chem.*, 69:4653–4659, 1997.

[52] G. Ponterini, N. Serpone, M.A. Bergkamp, and T.L. Netzel. Comparison of radiationless decay processes in osmium and platinum porphyrins. *J. Am. Chem. Soc.*, 105:4639–4645, 1983.

[53] D.B. Papkovski. New oxygen sensors and their applications to biosensing. *Sensors Actuators B*, 29:213–218, 1995.

[54] H.Y. Liu, S.C. Switalski, B.K. Coltrain, and P.B. Merkel. Oxygen permeability of sol-gel coatings. *Appl. Spectrosc.*, 46:1266–1272, 1992.

[55] M.A. Baldo, D.F. OBrien, Y You, A. Shoustikov, S. Sibley, M.E. Thompson, and S.R. Forrest. Highly efficient phosphorescent emission from organic electroluminescent devices. *Nature*, 395:151–154, 1998.

[56] K.A. King, P.J. Spellane, and R.J. Watts. Excited-state properties of a triply ortho-metalated iridium(iii) complex. *J. Am. Chem. Soc.*, 107:1431–1432, 1985.

[57] K Dedeian, P.I. Djurovich, F.O. Garces, G. Carlson, and R.J. Watts. A new synthetic route to the preparation of a series of strong photoreducing agents: fac tris-ortho-metalated complexes of iridium (iii) with substituted 2-phenylpyridines. *Inorg. Chem.*, 30:1685–1687, 1991.

Chapter 6

Single-layer and Bi-layer OFETs/OLETs

In recent years it has become clear that the chemical structure of the organic semiconductor is not the only factor that determines whether an organic FET exhibits predominantly p-channel or n-channel behaviour. Processing and characterization conditions, device architecture, and choice of electrodes are important as well. It is thus not appropriate to speak of p-type or n-type materials, but one should rather refer to p-channel or n-channel transistors. A key discovery was the identification of the crucial role of the gate dielectric and the identification of electron trapping mechanisms in devices based on SiO_2 gate dielectrics [1]. This subsequently led to the general observation of n-channel and ambipolar characteristics in a broad range of organic semiconductor FETs based on trap-free gate dielectrics [2].

In an ideal ambipolar transistor with just one semiconducting layer, the ambipolar regime is characterized by a hole and an electron accumulation layer next to the respective electrode that meet at some point within the transistor channel. There, oppositely charged carriers recombine. In electroluminescent materials, this leads to light generation within the channel. The length of each channel and thus position

of the recombination zone depend on the applied gate and source-drain voltage and mobility ratio. The behaviour of an ambipolar field-effect transistor in the ambipolar regime of a transfer characteristic can roughly be imagined as that of a saturated hole and electron field-effect transistors in series [3].

One of the reasons of the emerging interest in realizing ambipolar OFETs is that they seem predestined for light emission since they can provide an effective pn-junction within the transistor channel and thus radiative recombination of holes and electrons [4].

In the multi-component approach, OLETs can be obtained superposing two layers of unipolar materials in bilayer structure [5] or can be fabricated by simultaneous co-evaporation of two unipolar materials realising a bulk heterojunction [6].

In the case of bilayer structures, a balanced ratio between hole and electron current density should guarantee the maximization of electroluminescence emission. However the physical separation between p-transport and n-transport material confines holes and electrons in the respective unipolar layers almost preventing exciton formation and light emission.

In some cases another approach of bi-layer has been attempted. Indeed, some research groups utilized a structure comprising a light emitting material superimposed on a transporting material (small molecule or polymer) in order to increase the light emission efficiency, at the expenses of charge transport.

In this chapter we will focus the attention on the electronic and morphological properties of single layer OFETs fabricated with the organic semiconductor materials, reported in chapter 5. Then, with the best choice of transport materials in terms of morphological and energetic compatibility, bilayer vertical heterojunction devices will be fabricated and their opto-electronic characteristics will be studied [7]. Since the intrinsic complexity of organic-based device architecture and the different processes

taking place in the device active region (charge transport, energy/charge transfer, exciton formation, light emission), in-depth understanding of the electronic interfacial phenomena, before implement the most promising materials in a more complex tri-layer structure, it is of the most importance doing a systematic study of the materials in bi-layer devices.

In these by-layer devices, the first layer thickness will be minimized as much as possible so that, when place in the tri-layer structure [8, 9], the accumulation region will be as close as possible, yet physically separated, to the central recombination layer, still maintaining good transport properties. Moreover, the eventual presence of electro-luminescence, correlated to possible charge diffusion and recombination between the layers, has been checked.

6.1 Single Layer OFETs

The aim of this section, as reported previously, is to discover the best transport materials to be implemented in a multilayer structure. the substrate used is, in every device, a glass 1.1 mm thick with a patterned ITO used as gate contact and a layer of 450 nm of PMMA used as dielectric layer. This platform substrate, instead of the often used Si^{++}/SiO_2, has the advantage to be almost completely transparent to visible light, thereby allowing one to obtain an efficient light extraction in more complex field-effect structures like organic light-emitting transistors (OLETs).

Each device was prepared with the same deposition conditions of organic layers (evaporation rate of 0.1Å$/s$ and a thickness of 15 nm). All the devices had the drain-source electrodes made with 50 nm of gold.

The use of gold electrodes for all devices, could seem not the best choice due to gold high workfunction that could obstacle electrons injection in n-type OFETs. In reality, during devices fabrication we experienced that the best results were obtained

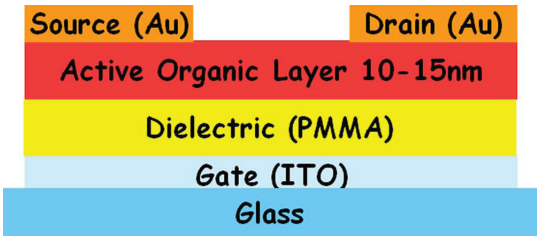

Figure 6.1: Schematic structure of the single-layer OFET.

with gold [10]. Indeed, it appears to be the most non-interacting, most stable and thus most controllable metal during deposition, compared to other low work-function metals in which side effect of deposition lead to a worse injection.

All devices, were grown at room temperature (RT) or, in some cases, at higher temperature in order to find the best deposition conditions of active layers. The device structure can be seen in Fig.6.1.

6.1.1 P13 OFET

As it can be seen from Fig.6.2, in the saturation curve measured, the two nearly overlapping lines are for forward and backward scanning of the Gate-Source voltage while V_{ds} is kept constant. This indicates the near absence of hysteresis and consequently low charge trapping in the dielectric layer. The charge mobility value associated to the measurement is $\mu^n = 0.17\ cm^2/Vs$, while the threshold voltage is $V_{th}^n = 15\ V$.

Another defining parameter to assess the performance of an OFET is the on/off switch ratio. In this case, the switching rate of 10^5 matches the highest values reported for thin film organic transistor based on P13. The AFM image (see Fig.6.2b) shows a very smooth surface of about 2 nm of RMS.

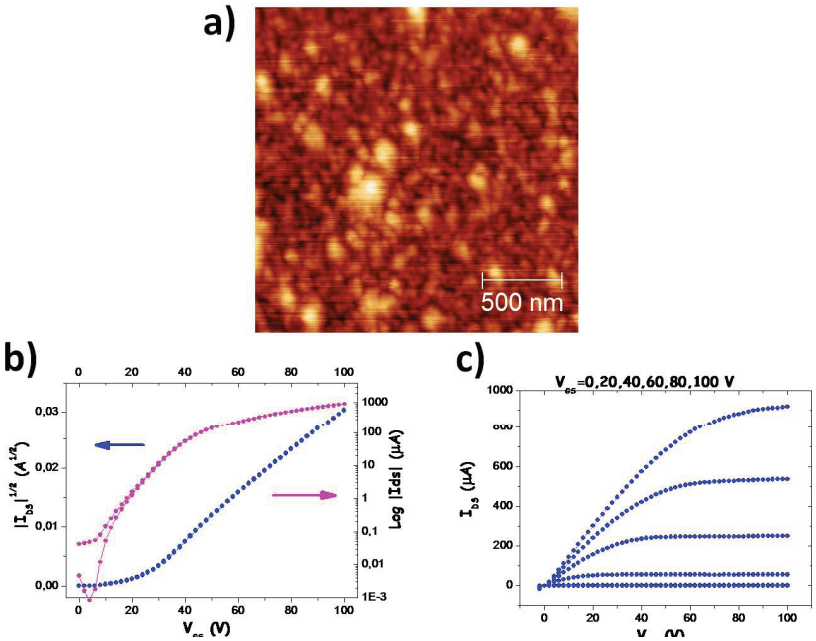

Figure 6.2: a) AFM image of the P13 surface on glass/ITO/PMMA substrate. b) Blue dots: Square Root of the *Locus Curve* - Purple Dots: *Transfer Curve* in saturation regime (V_{ds} kept constant at 100V), represented in logarithm scale. c) Multiple Output IV curve.

6.1.2 DHF4T OFET

When DHF4T is grown on the ITO/PMMA surface it shows morphological features quite different with respect its alkyl-substituted counterpart, DH4T. Holding the substrate at room temperature DHF4T molecules on a PMMA surface tend to form 2D islands with ragged grain boundaries which then coalesce completely in the first monolayer (Fig.6.3a). As the thickness of the film is increased, columnar 3D growth takes place with very high oblate protrusions (Fig.6.3b). Nonetheless, electrical performances of DHF4T-based thin-film transistors are very interesting since the field-effect current is very high, the electron mobility is around $0.5\ cm^2/Vs$ and the hysteresis in the electrical characteristics is almost negligible (Fig.6.3). on/off ratio is $\sim 10^3$. Indeed, as it is well known [11], the field-effect charge carrier transport is spatially restricted to the first nanometers from the dielectric/organic semiconductor

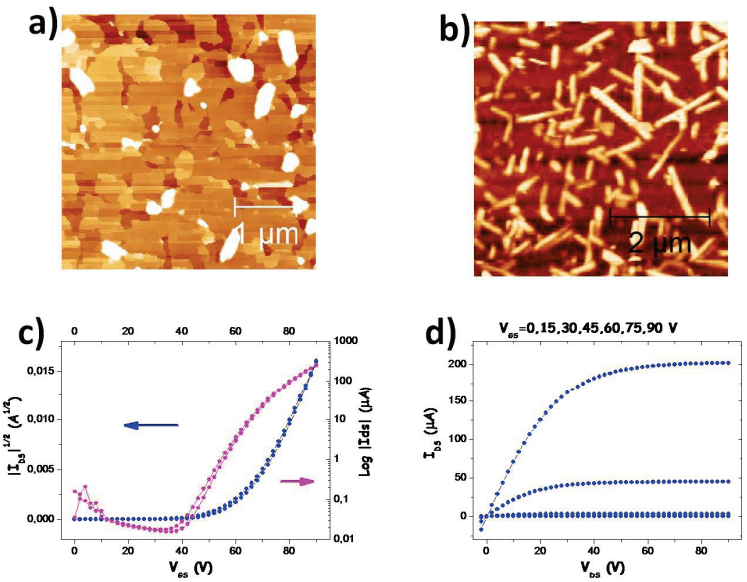

Figure 6.3: a) AFM image of DHF4T first monolayers. b)AFM image of DHF4T 15 nm-thick film. c)Blue curve: square root of locus curve. Purple curve: transfer curve in logarithmic scale with $V_{ds} = 90\ V$; e) I-V output curves at different V_{gs} values.

interface so that only a good in-plane connectivity in the first monolayer is sufficient for guaranteeing charge carrier transport.

The quite high voltage threshold $V_{th}^{n} = 64\ V$ shown by these device electrical characteristics can be correlated to the possible inefficient electron injection from gold source electrode due to the lack of smoothness and sharpness of metal/organic semiconductor interface.

6.1.3 DM4T OFET

DM4T molecule, whose structure has been shown in Fig.5.4, is a T4 alkyl derivative with the shortest chain (methyl groups) attached at the same positions. Single-layer OFET characteristics, on glass/ITO/PMMA substrates, are reported in Fig.6.4 for deposition at RT, while in Fig.6.5 are reported the curves for deposition with substrate at $90°$C. At RT, the electrical characteristic of the devices fabricated are $\mu^{p} = 0,036$

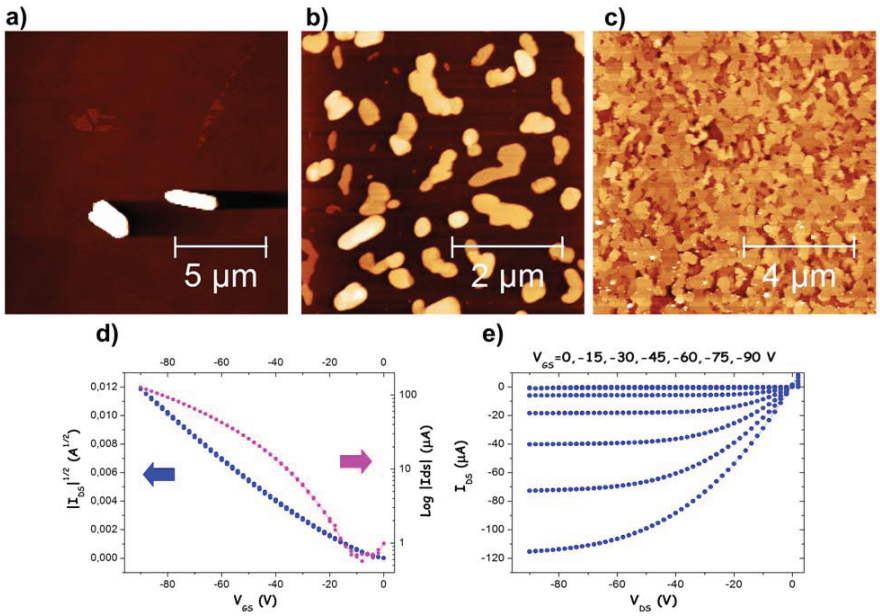

Figure 6.4: DM4T grown on ITO/PMMA substrate with T_{sub} =RT. AFM topographical images: a) 1 nm thick layer; b) 3 nm thick layer; c) 10 nm thick layer; d) Blue curve: square root of locus curve. Purple curve: transfer curve in logarithmic scale with $V_{ds} = -90\ V$; e) I-V output curves at different V_{gs} values.

cm^2/Vs and $V_{th}^p = -18\ V$ with an On/Off current ratio of 10^2.

The AFM pictures at 1 and 3nm of thickness (Fig.6.4a,b), show a tendency to organize in a crystal blade shaped form, according to the geometrical regularity of the structures.

The surface of the thicker sample (Fig.6.4c), shows apparently a disordered structures with an incomplete coverage of the underneath layers. OFET curves and AFM images at $90°$C of substrate temperature are shown in Fig.6.5. From the electrical point of view single-layer DM4T OFETs at $90°$ has a mobility μ^p of $8 \cdot 10^{-3}\ cm^2/Vs$ with a V_{th}^p of -26V. The On/Off current ratio was 10^2. With respect to the case at RT, at $90°$C there is a small hysteresis effect between the forward and backward curves, mobility decreased considerably and threshold voltage increased. The AFM images show a different scenario with respect to the RT case. In this case, indeed, the 3D crystal like aggregations are smaller than at RT and, when thickness increase (see

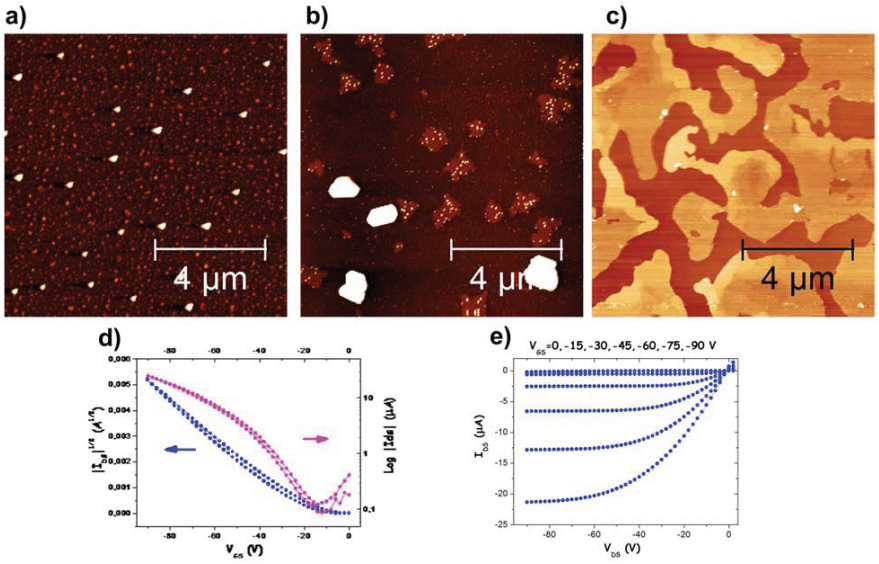

Figure 6.5: DM4T grown on ITO/PMMA substrate with $T_{sub} = 90°C$. AFM topographical images: a) 1 nm thick layer; b) 3 nm thick layer; c) 10 nm thick layer; d) Blue curve: square root of locus curve. Purple curve: transfer curve in logarithmic scale with $V_{ds} = -90\ V$; e) I-V output curves at different V_{gs} values.

Fig.6.5c) the films seems more uniform than the previous case.

An X-Ray Diffraction (XRD) analysis of the two samples (see section 9.1.1) confirmed the presence of a lower crystal order for DM4T grown at $90°C$ with respect to RT, in agreement with the electrical results.

6.1.4 DB4T OFET

DB4T is a molecule characterized by a medium length chain (n-butyl groups) attached at α,ω position of 4T conjugated core. In Fig.6.6 and 6.7 are reported the electrical curves and AFM images of the single-layer DB4T OFETs made at RT or at $90°C$, respectively. The electrical characterization of the OFETs at different temperatures is: $\mu^p = 6 \cdot 10^{-3}\ cm^2/Vs$ with $V_{th}^p = -20\ V$ and On/Off ratio of 10^4 for the RT OFET and $\mu^p = 0.01\ cm^2/Vs$ with $V_{th}^p = -28\ V$ and On/Off ratio of 10^2 for the $90°C$ OFET.

DB4T OFETs mobilities are quite similar in the two cases. Data show also an increase

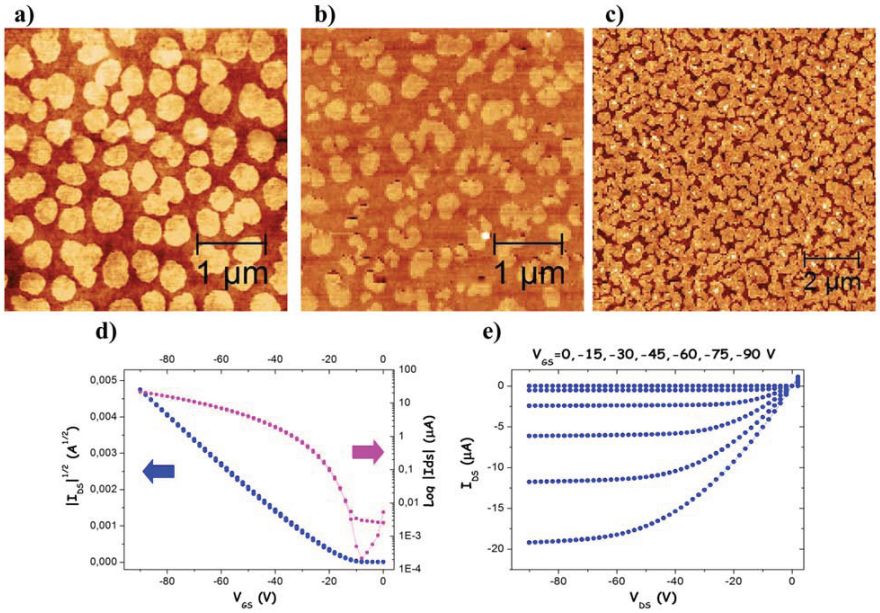

Figure 6.6: DB4T grown on ITO/PMMA substrate with T_{sub} =RT. AFM topographical images: a) 1 nm thick layer; b) 3 nm thick layer; c) 10 nm thick layer; d) Blue curve: square root of locus curve. Purple curve: transfer curve in logarithmic scale with $V_{ds} = -90\ V$; e) I-V output curves at different V_{gs} values.

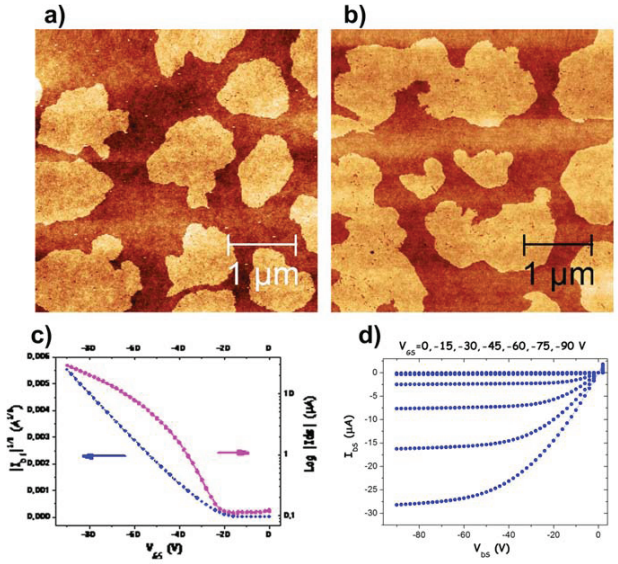

Figure 6.7: DB4T grown on ITO/PMMA substrate with T_{sub} = 90°C. AFM topographical images: a) 1 nm thick layer; b) 10 nm thick layer; c) Blue curve: square root of locus curve. Purple curve: transfer curve in logarithmic scale with $V_{ds} = -90\ V$; d) I-V output curves at different V_{gs} values.

in V_{th} from RT to $90°$C, that could be explained mainly considering that new traps are formed at the dielectric surface due to the substrate heating during deposition (see 9.1.1). The On/Off ratio is two order of magnitude lower in $90°$C case with respect to RT case.

AFM analysis of the DB4T surface at different thicknesses, show a very flat film morphology with tendency of growing bi-dimensionally in a layer-by-layer structure. This kind of morphology is typical of DH4T (see 6.1.5), thus one might expect at least a comparable electrical behaviour between the two materials, instead DB4T has a very low μ compared to its dihexyl counterpart.

XRD analysis, showed that DB4T contrarily to DH4T, has no detectable cyrstal structure (see 9.1.1).

6.1.5 DH4T OFET

In Fig.6.8 are shown the typical I-V curves for OFETs made with DH4T films deposited on substrates kept at RT, as well as the morphologies of the early growth stages for thickness values of 1, 3 and 10 nm.

Both the locus and transfer curves (see Fig.6.8.d-e) present nearly no hysteresis between the forward and backward branches. μ^p, calculated from the locus curve, is $0.09\ cm^2/Vs$, V_{th}^p is $25\ V$ and on/off ratio is about 10^5.

From the AFM images of the early growth stages (see Fig.6.8.a-c) result a longer range ordered organic structure at the dielectric interface. Indeed, at 1 nm of nominal thickness, the film growth is bi dimensional (2D), with islands almost isotropic in shape. As the film thickness is increased to 3 and 10 nm, the islands coalesce while the growth remains bi-dimensional.

At $90°$C μ^p and V_{th}^p calculated from the I-V curves (see Fig.6.9d) are, respectively, $0.083\ cm^2/Vs$ and $30\ V$ with a on/off ratio of 10^6. These data show that, for DH4T on glass/ITO/PMMA, μ^p does not noticeably vary with increasing T_{sub}. As

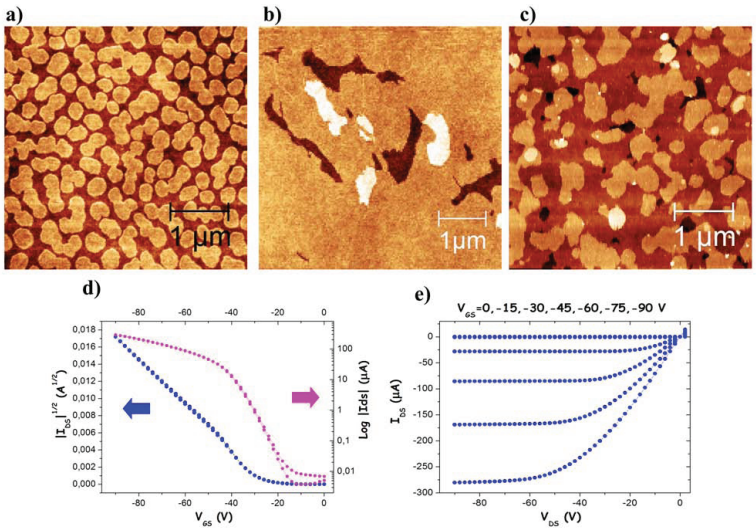

Figure 6.8: DH4T grown on ITO/PMMA substrates with $T_{sub} = RT$. AFM topographical images: a) 1 nm thick layer; b) 3 nm thick layer; c) 10 nm thick layer; d) Blue curve: square root of locus curve. Purple curve: transfer curve in logarithmic scale, with V_{ds} = -90V; e) I-V output curves at different V_{gs} values.

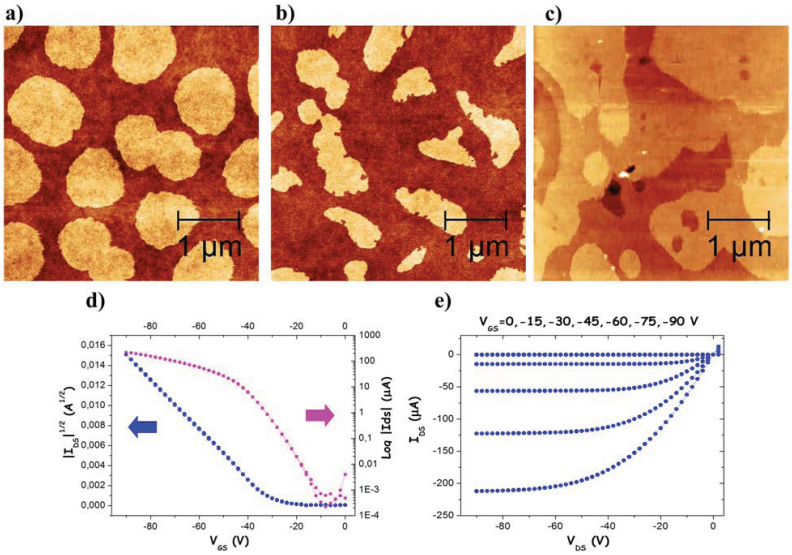

Figure 6.9: DH4T grown on ITO/PMMA substrate with T_{sub} = 90°C. AFM topographical images: a) 1 nm thick layer; b) 3 nm thick layer; c) 10 nm thick layer; d) Blue curve: square root of locus curve. Purple curve: transfer curve in logarithmic scale with V_{ds}=-90V; e) I-V output curves at different V_{gs} values.

the highest μ^p can be obtained when there is the right balance between the grain size and film connectivity, this independence on T_{sub} is probably due to the fact that DH4T on PMMA at RT presents already the most favourable microstructure. This can be confirmed by means of the AFM images taken at $90°$C (see Fig.6.9a-c): the morphology is almost identical to RT, excluding the average grain size that is larger, as expected.

A comparison between the V_{th}^p values at RT and at $90°$C shows a tendency to increase with increasing T_{sub}. This effect, found also in DM4T and DB4T, might be explained considering the mechanical mobility at $90°$C of the most external branches of the PMMA polymer units at the surface. This might induce the creation of superficial traps leading to higher V_{th} values. In fact, since a deviation of the surface T_g of a polymeric film from the bulk value has been reported [12, 13], we expect also for PMMA films a lower T_g in a few nm region close to the air interface with respect to the bulk. It has been shown by Kim et al. that, for pentacene on PMMA, this effect leads to a strong decrease in μ and a decrease of the average grain size, already at a deposition temperature of $70°$C. Since it has been heated the substrate at $90°$C, it is enough to induce the mechanical mobility of the most external branches of the polymer film and, although in DM4T, DB4T and DH4T a noticeable difference in the grain size and μ has not been observed, the same effect might be the cause of the higher V_{th}.

6.1.6 Final Remarks

Using the transport materials, we have fabricated single-layer OFET devices, in order to study their electrical properties and morphologies in thin-film on transparent glass/ITO/PMMA substrates, used for fabricating OLETs. The main target of these preliminary studies was to find the best selection of materials to be implemented in multilayer OLETs.

The main electrical parameters obtained by the devices characterization are reported in table 6.10.

From the electrical point of view the choice of candidates is determined mainly by

		Mobility (cm^2/Vs)	V_{th} (V)	On/Off ratio
n-type	**P13**	0,17	15	10^5
	DHF4T	0,5	64	10^3
p-type	**DM4T**	0,036	-18	10^2
	DB4T	0,01	-28	10^2
	DH4T	0,09	-25	10^5

Figure 6.10: Summary table of the electrical values of the single-layer OFETs studied.

materials mobility and threshold voltages.

However, in order to define if a material is a good candidate to be used in a multi-layer OLET, also the thin-film morphologies must be considered. Indeed a 3D morphology could prevent the OLET from working properly, since the bad coverage of the upper layers of the stack.

Given this premise, looking at the electrical data and at the AFM morphologies of the materials, it has been possible to determine DH4T as the best material for p-type transport and P13, DHF4T as the best ones for n-type transport.

The decision to consider DHF4T as a material to be implemented in an OLET, although it has a 3D growth modality and an high V_{th} on glass/ITO/PMMA substrates, is based on the following considerations:

1. DHF4T has a very high mobility.

2. In a multilayer OLET, charge injection, and thus V_{th}, are not dependent only by the single material properties, but is a consequence of the interaction between

the active layers.

3. DHF4T at few nanometers of thickness present a rather good layer-by-layer 2D morphology with a ragged grain formation, thus limiting DHF4T thickness could prevent morphology incompatibility.

4. DHF4T OFETs curves have almost no hysteresis.

Lastly but most important, DHF4T has a good HOMO-LUMO energy levels compatibility with many organic recombination systems, thanks to its high band gap (this aspect will be reported in detail in the next sections).

6.2 Bi-Layer OFETs/OLETs

6.2.1 Glass/ITO(GATE)/PMMA/DHF4T-DH4T/Gold(D-S) OFETs

As part of this preliminary study, we realized the bi-layer OFET reported in Fig.6.11a, formed by a superposition of 7 nm thick DHF4T film and 15 nm thick DH4T film. We focused on the p-type and n-type charge accumulation capability and on the ambipolar performance of the DHF4T/DH4T bi-layer OFET.

In Fig.6.11b and 6.11c, the electrical characteristics of the device are reported: the output and transfer electrical curves show an almost ideal ambipolar behaviour with a balanced hole and electron transport and almost no hysteresis, index of absence of trapping states at the DH4T/DHF4T and DHF4T/PMMA interfaces.

The typical V-shaped" current transfer curve, whose minimum is located in the middle bias and that indicates the maximum of ambipolarity, shows a very good balance between electron and hole densities.

The calculated n-type and p-type mobility values are, respectively, $\mu^n = 0.01\ cm^2/Vs$ and $\mu^p = 0.01\ cm^2/Vs$. The corresponding gate threshold values are $V_{th}^n = 40\ V$

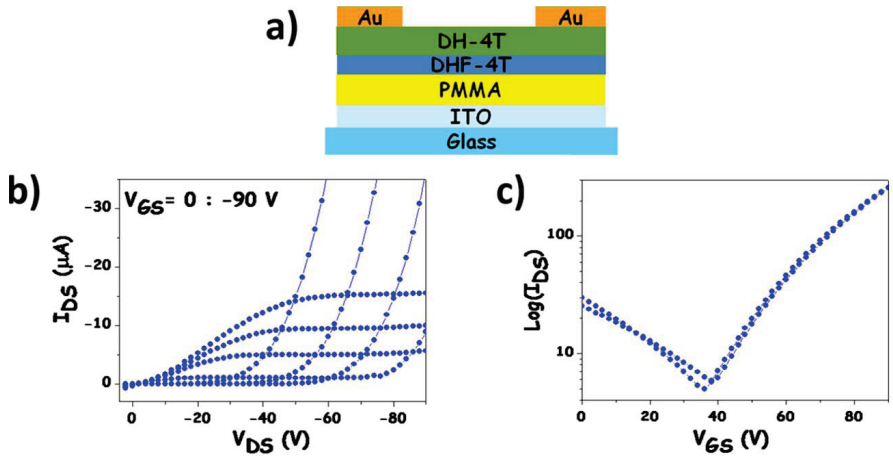

Figure 6.11: 2D scheme of the bi-layer vertical heterojunction made on DHF4T-DH4T structure (a). Output electrical characteristics measured by operating the device in p-type mode. V_{gs} values are 0, -15, -30, -45, -60, -75 and -90 (b). Transfer electrical characteristics measured in saturation regime ($V_{ds} = 90\ V$). The two curves, almost overlapping, represent the forward and backward sweeps (c).

and $V_{th}^{p} = -40\ V$. These results show a very efficient ambipolar organic field-effect transistor with performance at the state of the art among bi-layer OFETs [5, 14–16]. No light emission has been collected from the bi-layer device in agreement with the electronic properties of the materials.

6.2.2 Glass/ITO(GATE)/PMMA/DH4T-DHF4T/Gold(D-S) OFETs

Changing the order the organic layers respect to the previous structure lead to a completely different device behaviour.

In this case we have deposited 7 nm of DH4T and then a 15 nm thick film of DHF4T, then we deposited gold on top of the structure. The device structure and electrical characteristics of the device are shown in Fig.6.12. Contrarily to what happened in the previous OFET, in this device there is a strongly unbalanced charge transport. Indeed, holes flowing through the lower layer of DH4T dominates with respect to

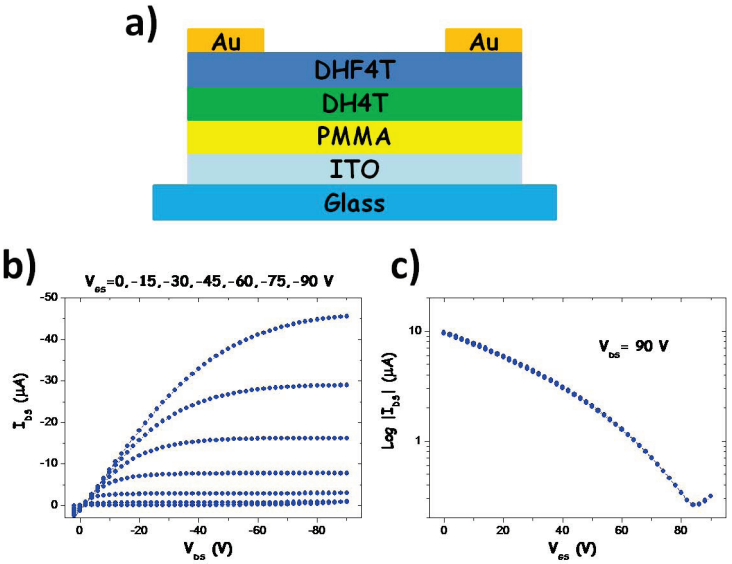

Figure 6.12: 2D scheme of a bi-layer vertical heterojunction made on DH4T-DHF4T structure (a). Output electrical characteristics measured by operating the device in p-type mode. V_{gs} values are 0, -15, -30, -45, -60, -75 and -90 (b). Transfer electrical characteristics measured in saturation regime ($V_{ds} = 90\ V$)(c).

the electrons current of the upper layer of DHF4T that is more than two order of magnitude lower. Mobility and threshold voltages are: $\mu^p = 5 \cdot 10^{-2}\ cm^2/Vs$, with $V_{th}^p = -13\ V$ for p-type and $\mu^n = 1 \cdot 10^{-3}\ cm^2/Vs$, with $V_{th}^n = 48\ V$ for n-type transport.

The current unbalance is clearly visible in the electrical curves (Figs.6.12b,c). In particular from Fig.6.12c, contrarily to the previous case, the "V-shaped" curve is almost not present due to the high threshold and low mobility of the n-type region. This big difference between the two typologies of OFETs, likely relies on the fact that, in the DHF4T/DH4T device (see 6.2.1), the interaction between DHF4T on PMMA, DH4T on DHF4T and the good charge injection of the gold in direct contact with DH4T, lead to an overall balance of the two charge carriers. On other hands in the device composed by DH4T/DHF4T, there is a poor electron injection between the top DHF4T layer and gold contacts. The reason of this behaviour is to be found in

the high work-function of the metal and, then, in a bad DHF4T/gold interface. The last phenomenon occurs, since the minimum DHF4T thickness to have a conductive top layer is about 15 nm and, at that thicknesses, the semiconductor presents a rough 3D morphology that obstacles the formation of a good interface with metal.
Like in the previous device structure, also in this one, no electro-luminescence was detected.

6.2.3 Glass/ITO(GATE)/PMMA/DH4T-P13/Gold(D-S) OFETs

This device was fabricated with the same thicknesses of the previous ones. The first layer of 7 nm of DH4T was deposited on PMMA layer, then a 15 nm of P13 was superimposed on DH4T. Finally 50 nm of drain-source gold electrodes were deposited on top of the stack.
The I-V output characteristic and the transfer characteristic along with the device structure are reported in Fig. 6.13. As it can be seen from the electrical curves, this device structure exhibits the most-balanced ambipolarity with mobilities of $\mu^n = 5.4 \cdot 10^2\ cm^2/Vs$ and $\mu^p = 1 \cdot 10^2\ cm^2/Vs$. μ^p did varied slightly with respect to the single-layer devices, while μ^n decreased by one order of magnitude despite the fact that P13 growth was carried out under optimized conditions.
This effect is likely to be due to differences in growth modality of P13 on DH4T surface with respect to PMMA, in both chemical composition and morphology. The p-type and n-type threshold voltages were $V_{th}^p = -28\ V$ and $V_{th}^n = 59\ V$, respectively. The I-V output characteristic (Fig.6.13b) shows clearly the ambipolar nature of the device, in which after the typical current plateau due to electron saturation, when $V_{ds} > (V_{gs} - V_{th}^p)$ the overall current start to increase again thanks to the hole injection.

The good ambipolar balance between charge carriers of the device can be seen

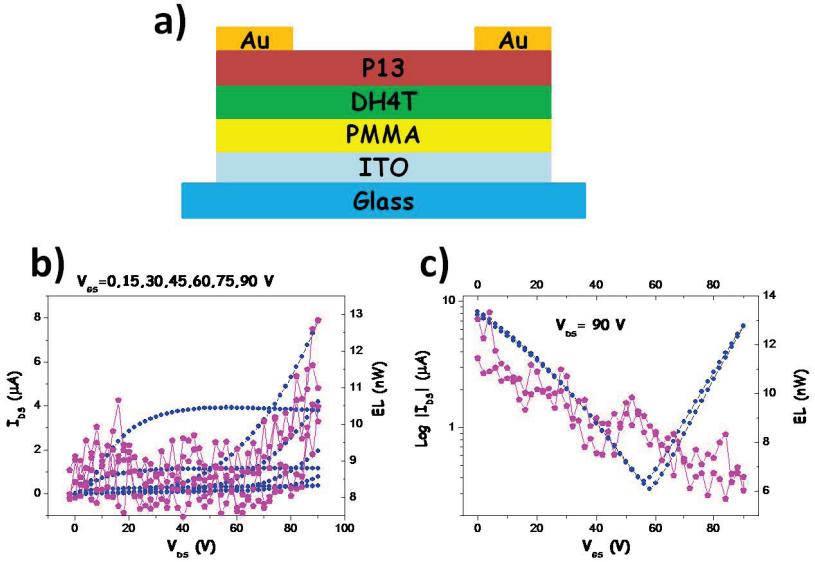

Figure 6.13: 2D scheme of a bi-layer vertical heterojunction made on DH4T-P13 structure (a). Output electrical characteristics measured by operating the device in n-type mode. V_{gs} values are 0, 15, 30, 45, 60, 75 and 90 (b). Transfer electrical characteristics measured in saturation regime ($V_{ds} = 90\ V$) in logarithm scale(c). In both curves blue dots represent the drain-source current (left scale), while the purple dots represent the EL extracted from the device during operation (right scale).

looking at the transfer characteristic (Fig.6.13c). In this curve is present a very balanced V-shaped curve, index of ambipolarity. The two branches representing the p-type and n-type regions have the same height. There is no hysteresis between the forward and backward plots of the curves, demonstrating the presence of almost no trap states at the DH4T/PMMA and P13/DH4T active interfaces.

In this configuration electro-luminescence (EL) emission has been also detected. Indeed, in both curves there is light emission that increases in correspondence of the p-type bias region. As explained in the previous chapter (see section 3.3.1), this EL behaviour happens always when the bias is related to charge transport of the layer directly in contact with the substrate. The emission is located under the drain electrode and it is due to the recombination of charges at DH4T/P13 interface due to

the very high vertical electric field.

Similar results were obtained on the same bi-layer structure on Si^{++}/SiO_2 substrate [5].

6.2.4 Glass/ITO(GATE)/PMMA/DH4T-Alq3:DCM/Gold(D-S) OFETs

Another approach to fabricate an OLET, is to superimpose a host matrix transporting layer doped with an emitting guest dye, whose energy levels enable Förster energy transfer, on an opposite charge transport organic semiconductor.

Of course, in this case, the main aim is to improve light emission efficiency despite of the upper layer charge transport and of the overall balanced ambipolarity of the OLET.

Here we report of a device whose structure is shown in Fig.6.14a, along with its electrical characteristics. The device was fabricated depositing a 7 nm of DH4T on PMMA, then depositing a co-evaporation of 20 nm of Alq3 doped with DCM at 3% wt on DH4T and finally, depositing 50 nm of gold drain-source electrodes on top of all.

In this structure, then, DH4T operates as hole transport layer, Alq3 operates as recombination host matrix as well as electron transport layer (since its electron transport properties) and DCM acts as guest dye, doped inside Alq3, for improving light emission.

Surprisingly, contrarily to what expected, the electrical behaviour shows no electron transport al all. Both, in the I-V output curve and in the transfer curve, there is no presence of n-type regions, but just a p-type charge transport with a mobility of $\mu^p = 0.1 cm^2/Vs$ and $V_{th}^p = -22\ V$. Moreover, no electro-luminescence has been detected in the device.

These results, put in evidence how the strategy of using a bi-layer structure, in which

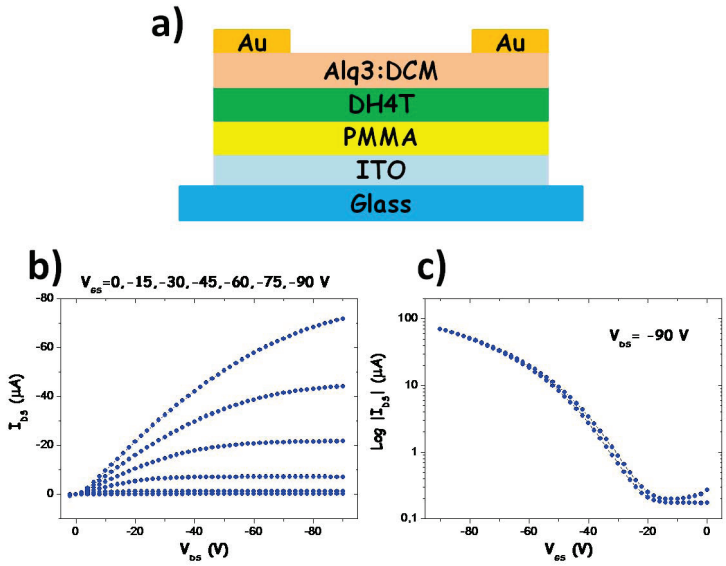

Figure 6.14: 2D scheme of a bi-layer vertical heterojunction made on DH4T-Alq3:DCM structure (a). Output electrical characteristics measured by operating the device in p-type mode. V_{gs} values are 0, -15, -30, -45, -60, -75 and -90 (b). Transfer electrical characteristics measured in saturation regime ($V_{ds} = -90\ V$) in logarithm scale(c).

one of the two charge carriers are blended with a dye, is not always the best choice for improving the electroluminescence. Indeed, the lack of one charge carrier, often leads to a very low electroluminescence efficiency of the device or, like in this case, to a total absence of light emission.

6.3 Conclusions

Through this preliminary studies in which we analysed the operation of single-layer and bi-layer vertical heterojunction OFETs/OLETs, we focused the attention on the importance of having transport materials with an optimal coupling. Indeed, a good electrical transport characteristic of the semiconductor is not enough to fulfil the requirements for fabricating a bi-layer. The highest compatibility between the materials is a necessary condition for having good transport in a more complex structure like tri-layer OLETs.

For fabricating bi-layer devices, we considered some of the most promising struc-

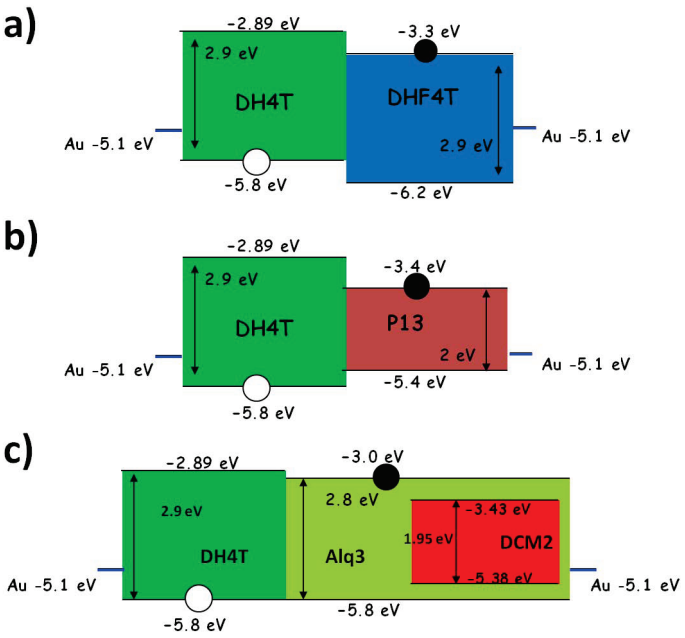

Figure 6.15: a) Energy level scheme of DH4T-DHF4T system. b) Energy level scheme of DH4T-P13 system. c) Energy level scheme of DH4T-Alq3:DCM system. In this scheme the DCM is inside Alq3 since it is a dopant material of an host:guest system.

tures with the materials presented in the previous chapter. The devices fabricated with DHF4T-DH4T, DH4T-DHF4T and DH4T-P13 showed a very good ambipolar behaviour, with very balanced n-type and p-type transport and almost no hysteresis. Moreover, in DH4T-P13 bi-layer device electroluminescence has been detected under the electrode, opening-up the possibility of obtaining a more efficient OLET, when inserted in the tri-layer structure.

In order to choose the best materials for a tri-layer structure, it is also important to consider the energy levels compatibility. In this case, the best match is found in the DHF4T-DH4T combination, since both of them have an high band gap ($\sim 3eV$) that matches, energetically, the most of host:guest systems usually used as recombination and emission layers. For what concerns P13, from this point of view it is not the best

choice, since it has only $\sim 2eV$ of band gap and, with high band gap host matrices, charges, instead of recombining in the middle emission layer, could percolate inside P13 and, there, recombine non-radiatively (for details on the energetic levels of the bi-layer systems, see Fig.6.15).

Despite all the considerations done so far, having a good material compatibility in a bi-layer structure is not an exhaustive result for considering them as good candidates to be used in an high efficiency tri-layer working device, but this could be regarded as a first critical step to discriminate which materials configuration is most promising.

6.4 REFERENCES

[1] J. Zaumseil and H. Sirringhaus. Electron and ambipolar transport in organic field-effect transistors. *Chem. Rev.*, 107(4):1296, 2007.

[2] L. L. Chua, J. Zaumseil, J. F. Chang, E. C. W. Ou, P. K. H. Ho, H. Sirringhaus, and R. H. Friend. General observation of n-type field-effect behaviour in organic semiconductors. *Nature*, 434(7039):194–199, 2005.

[3] R. Schmechel, M. Ahles, and H. von Seggern. A pentacene ambipolar transistor: Experiment and theory. *J. Appl. Phys.*, 98:084511, 2005.

[4] A. Dodabalapur, H. E. Katz, and L. Torsi. Molecular orbital energy level engineering in organic translators. *Adv. Mater.*, 8:853, 1996.

[5] F. Dinelli, R. Capelli, M. A. Loi, M. Murgia, M. Muccini, A. Facchetti, and T. J. Marks. Ambipolar organic light-emitting transistors employing heterojunctions of n-type and p-type materials as the active layer. *Adv. Mater.*, 18(33):1416, 2006.

[6] C. Rost, S. Karg, W. Riess, M. A. Loi, M. Murgia, and M. Muccini. Light-emitting ambipolar organic heterostructure field-effect transistor. *Appl. Phys. Lett.*, 85:1613, 2004.

[7] G. Generali, R. Capelli, S. Toffanin, A. Facchetti, and M. Muccini. Ambipolar field-effect transistor based on α,ω-dihexylquaterthiophene and α, ω-diperfluoroquaterthiophene vertical heterojunction. *Microelectron. Reliab.*, 50(9-11):1861–1865, 2010.

[8] R. Capelli, S. Toffanin, G. Generali, H. Usta, A. Facchetti, and M. Muccini. Organic light-emitting transistors with an efficiency that outperforms the equivalent light-emitting diodes. *Nat. Mater.*, 9:496–503, 2010.

[9] G. Generali, F. Dinelli, R. Capelli, S. Toffanin, , and M. Muccini. Influence of the substrate platform on the opto-electronic properties of multi-layer organic light-emitting field-effect transistors. *J. Phys. D: Appl. Phys.*, 2011. In press.

[10] G.R. Dholakia, M. Meyyappan, A. Facchetti, and T. J. Marks. Monolayer to multilayer nanostructural growth transition in n-type oligothiophenes on au(111) and implications for organic field-effect transistor performance. *Nano Lett.*, 6(11):2447–2455, 2006.

[11] F. Dinelli, M. Murgia, P. Levy, M Cavallini, F. Biscarini, and D de Leeuw. Spatially correlated charge transport in organic thin film transistors. *Phys. Rev. Lett.*, 92:6802, 2004.

[12] C. Kim, A. Facchetti, and T.J. Marks. Polymer gate dielectric surface viscoelasticity modulates pentacene transistor performance. *Science*, 318:76, 2007.

[13] Z.and Forrest J. A. Qi, D.and Fakhraai. Substrate and chain size dependence of near surface dynamics of glassy polymers. *Phys. Rev. Lett.*, 101:096101, 2008.

[14] H. Yan, T. Kagata, and H. Okuzaki. Ambipolar pentacene/c60-based field-effect transistors with high hole and electron mobilities in ambient atmosphere. *Appl. Phys. Lett.*, 94:0233051–53, 2009.

[15] R. Ye, M. Baba, K. Ohta, K. Suzuki, and K. Mori. Fabrication of ambipolar organic heterojunction transistors with various sexithiophene alkyl-substituted derivatives. *Jpn. J. Appl. Phys.*, 48:04C168104C1683, 2009.

[16] J-F. Li, W-L. Chang, G-P. Ou, and F-J. Zhang. Air-stable ambipolar organic field effect transistors with heterojunction of pentacene and n,n0-bis(4-trifluoromethylbenzyl) perylene-3,4,9,10- tetracarboxylic diimide. *Chinese Phys. B*, 1807:3002–3006, 2009.

Chapter 7

Tri-layer Vertical Heterojunction Ambipolar OLETs

In order to exploit completely the scientific and technological potentiality of OLET devices it is necessary to achieve the maximum of electroluminescence efficiency in the correspondence of the maximum of charge current density.

In this thesis is reported a new approach in realizing ambipolar OLETs based on a device architecture that can guarantee higher and well-balanced current density for both electrons and holes and the separation of the region of maximum charge accumulation from the region of exciton formation and light emission, thus preventing charge-exciton quenching. The concept of this kind of new device is based on a tri-layer vertical heterojunction of active materials in a bottom gate/top contact OFET configuration in which two layers (the bottom and the top ones) are devoted to the electrons and holes transport (n- and p-transport layers) [1–3] while the middle layer is for exciton formation and light emission (recombination layer). This layer is engineered as a molecular host-guest system with an efficient Förster energy transfer.

Hereafter the working principles of the tri-layer heterojunction based OLETs are described in more details [4]. The first organic thin-film in contact with the device

dielectric layer is devoted to the unipolar field-effect transport. The second layer, deposited onto it, is the recombination layer which presents high emission quantum efficiency and OLED-like vertical bulk mobility value. The third layer is devoted to unipolar p-type charge transport (complementary to that of the first layer).

In this configuration, in the first and top layers a planar field-effect transport of opposite charges takes place, generating the ambipolar electrical characteristics of the device.

The vertical field created by the two opposite charge distributions in the field-effect accumulation regions enable a portion of the electrons and holes currents to percolate into the recombination layer. The bulk conducting properties of the recombination layer guarantee that either both or one of the charge carriers can migrate (through hopping or diffusion) in that layer until the condition for excitons formation are energetically favourable. Indeed in the structure presented, the recombination layer is engineered so that exciton formation may take place by an energy transfer process in the host-guest system [5].

In the vertical tri-layer heterojunction approach, each layer must be optimized according to its own function. From the charge transport (p-type or n-type) to the energy transfer and charge recombination.

In particular, functional interfaces play the predominant role in determining the performance of vertical tri-layer heterojunction [6]. Since OFETs are planar devices, only the first few nanometers of the transport layers from the gate dielectric layer are fundamental for having a completely formed conduction channel and, thus, achieving good charge transport [7], it is clear then, that the interfaces between the dielectric and the bottom transport layer and between the recombination and the top transport layer are crucial for guaranteeing ambipolar field-effect electrical characteristics (even if the top layer is not in direct contact with the dielectric layer).

Moreover, interfaces between the bottom transport and the recombination layer and between the recombination and the top transport layer should provide the favourable conditions for charges percolation in the recombination layer.

Another important issue that must be taken into account, for fabricating a tri-layer OLET, is the overall energetic level scheme of the system. Indeed, the HOMO and LUMO levels of the recombination layer should be favourably aligned with those of the transport layers in order to allow exciton formation in it. Indeed, to enable the vertical charge diffusion process, at the basis of the OLET electroluminescence mechanism, energetic compatibility between the materials forming the heterostructure is required. The lowest unoccupied molecular orbital (LUMO) of the n-type transport layer should be equal or higher than the LUMO of the host matrix of the central layer, while the highest occupied molecular orbital (HOMO) of the p-type transport layer should be equal or lower than the host matrix HOMO level, to favour hole percolation into it.

In this chapter we will report the results of some tri-layer OLETs, fabricated with the organic semiconductors introduced before on glass/ITO(150nm)/PMMA (450nm) transparent substrates.

7.1 DHF4T-Alq3:DCM(3%)-DH4T: The Highest EQE ever Reported for an OLET

To date, only the exciton-metal interaction has been successfully addressed in OLETs based on ambipolar single layers [8–13]. Under proper bias conditions, the spatial location of the light-emitting area is far from the metal electrodes preventing exciton-metal quenching. However, in these single layer devices the charge carrier accumulation and the exciton formation zones largely coincide, leading to severe exciton-charge quenching. Indeed, even in the most impressive demonstration to date, the external

quantum efficiency (EQE), that represent the ratio between the number of photons emitted from the device to the number of electrons that flows in the device channel, does not exceed 0.5-0.6% [14]. Consistently, single layer unipolar OLETs, in which only one type of charge carrier is effectively transported across the channel, reached remarkable results in terms of brightness [15, 16], but their EQE is only 0.2%, mainly because excitons are subjected to both metal and charge quenching, and electrode induced photon losses [15].

A horizontal pn-heterojunction has also been implemented in the channel of the OLET, which confines the light emission area in a pre-defined position far from the contacts, however, does not avoid exciton-charge quenching [17]. A bi-layer approach has been used to target OLET devices with either an improved device brightness, or a higher and more balanced charge mobility. In the first case a highly efficient luminescent layer is superimposed over a unipolar conducting layer [18], while in the second case p-type and n-type transport films are directly in contact with each other [3]. In both cases the bi-layer structure does not offer any control of the exciton quenching and photon losses as the light emission area is in contact with the minority carrier injecting electrode. Excitons interact with accumulated charges and the metal electrode, while photons are absorbed by the contacts. **In this chapter, we report the first tri-layer heterostructure approach for OLETs, which operates as contactless OLED devices, enabling simultaneous control of electrode induced photon losses, exciton-metal and exciton-charge interactions. OLET devices with EQE of 5% are reported, which largely exceeds the one of the best OLED based on the same emitting layer and optimized transport layers (2,2%) [19].** The tri-layer heterostructure OLETs used in this study is reported in Fig.7.1a.

The active region consists of the superposition of three organic layers. The first, in contact with the PMMA dielectric, and the third layers are field-effect electron

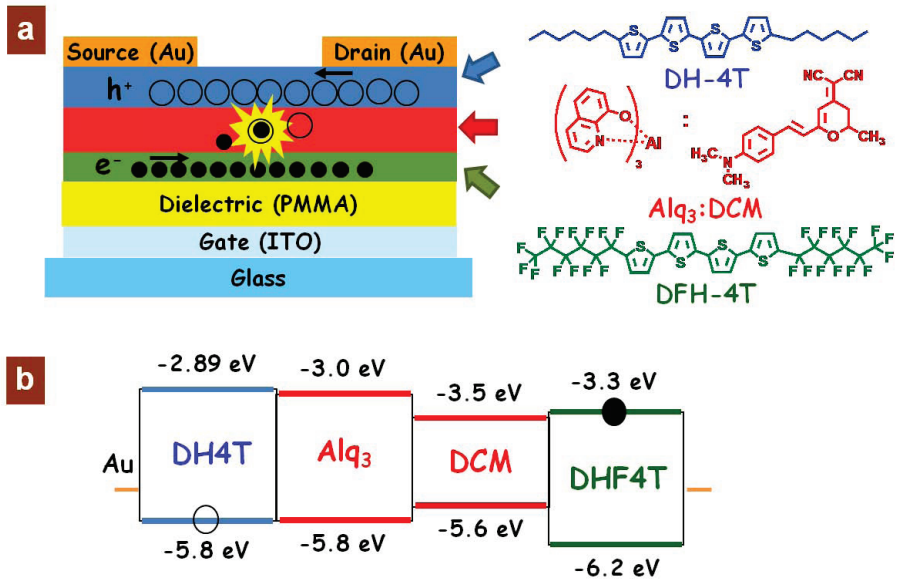

Figure 7.1: Tri-layer OLET device structure and active materials forming the heterostructure. a) Schematic representation of the tri-layer OLET device with the chemical structure of each material composing the device active region. The field-effect charge transport and the light generation processes are also sketched. b) Energy level diagram of the tri-layer heterostructure. The energy values of the HOMO and LUMO levels of each molecular material are indicated together with the Fermi level of the gold contacts.

transporting (n-type, 7 nm) and hole-transporting (p-type, 15 nm) semiconductors, respectively, whereas the middle layer is a light emitting host-guest matrix (40 nm). The device structure is completed by the deposition of the gold (source and drain, 50 nm) contacts.

We identified the α,ω-dihexyl-quaterthiophenes (DH4T) and perfluorohexyl (DHF4T) chains as the hole and the electron transporting films, respectively [20]. To realize the central light-formation layer an Alq3:DCM host-guest blend was used.

Fig.7.1 also reports the chemical structure and the electrochemically-derived energy level diagram of the organic heterostructure, clearly showing the energetic compatibility of these materials.

The tri-layer OLETs were fabricated with the Alq3:(3%)DCM light-emitting layer

sandwiched between the charge-transporting DHF4T and DH4T films. In this case, these devices have been fabricated with an interdigitated geometry for the drain-source gold contacts with a channel length of 150 μm and a channel width of 20 cm. Fig.7.2 shows an optical image of a lit device as well as a zoom of the OLET channel with the light generated within it.

In Fig.7.2c the OLET photoluminescence (PL) and electroluminescence (EL) spectra

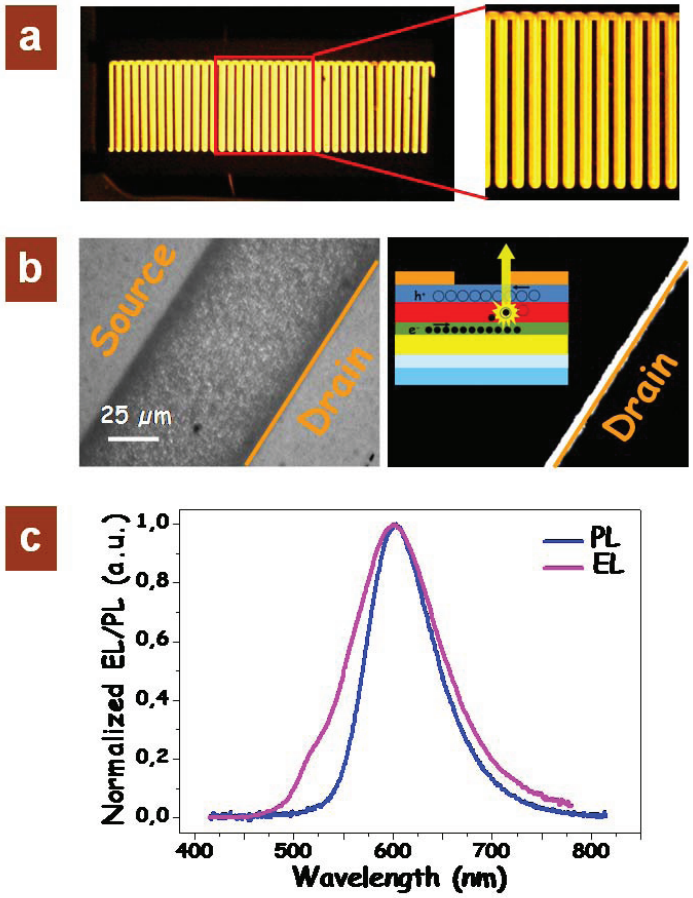

Figure 7.2: Optical micrographs of the lit tri-layer OLET and emission spectra. a) Optical micrograph of the interdigitated tri-layer heterostructure OLET biased with $V_{ds} = V_{gs} = +90V$. Channel length and channel width are 150 μm and 20 cm, respectively. b) Optical micrograph of the OLET channel when no bias is applied to the device, and when the applied bias is $V_{ds} = V_{gs} = +90V$. The schematic representation of the tri-layer heterostructure OLET showing the expected location of the light-generation area is reported in the inset. c) Comparison between the EL and PL spectra of the tri-layer heterostructure OLET.

are compared. The central emission peak is positioned at 600 nm in both cases and corresponds to the DCM emission. In the electroluminescence spectrum a shoulder appears at about 530 nm, which can be attributed to the residual Alq3 emission [21]. Emission features from DHF4T and DH4T are not detected in neither the PL nor the EL spectrum confirming that the central Alq3:DCM layer is the sole responsible of the light generation in the tri-layer heterostructure OLET.

7.1.1 Optoelectronic Characteristics and Heterostructure Morphology

The opto-electronic characteristics of the tri-layer OLET are reported in Fig.7.3. The curves shown in Fig.7.3a and 7.3b were obtained by operating the device within the unipolar regime ($|V_{ds}| = |V_{gs}|$) and correspond to the field-effect transport of only electrons and holes, respectively. Thus, Fig.7.3a shows the charge transport taking place in the DHF4T layer, while Fig.7.3b shows the charge transport occurring in the DH4T film. Light emission is collected in correspondence of the electron transport (Fig.7.3a).

When charge carriers recombine at the drain electrode through one, or more, upper layers, a diode-like mechanism gives rise to light emission [3, 18]. This process is characterized by a linear correlation between the EL and current intensity, clearly observable in Fig.7.3a, and by the spatial localization of the emission region at the drain electrode region. A large difference between the hole and the electron currents is observed in this OFET structure. While the electron mobilities are comparable to those of the single layer DHF4T OFETs ($\mu^n = 0.5 cm^2/Vs$, $V_{th}^n = +34V$, the hole mobilities are severely degraded with respect to the DH4T OFETs ($\mu^p = 5 \cdot 10^{-5} cm^2/Vs$, $V_{th}^p = -40V$). Thus, the insertion of the third Alq3:DCM layer between the DHF4T and the DH4T films strongly affects the transport properties of the top DH4T layer. AFM images carried out on each layer of the heterostructure (Figs.7.3e, 7.3f and

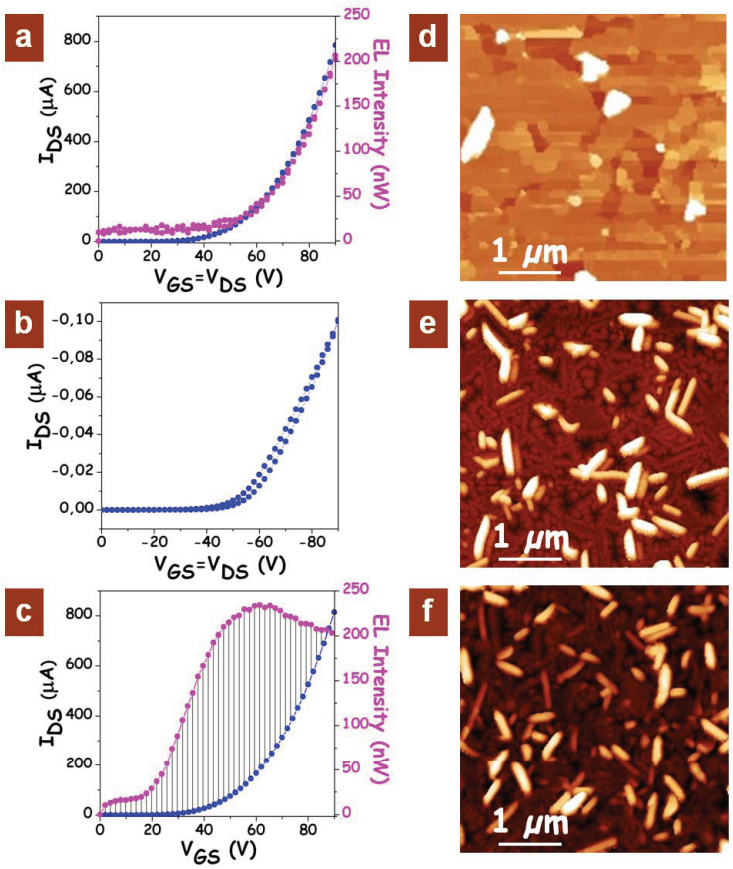

Figure 7.3: Optoelectronic characteristics of the tri-layer OLET and topographical images of the individual layers forming the heterostructure. Locus electrical curves (blue) of the OLET in n-polarization (a) and in p-polarization (b). During the n-polarization also the electroluminescence (EL) output power (purple) is collected. In the transfer characteristic curves (c), the source-drain current (I_{ds}) is measured keeping the drain-source potential constant at 90 V, while sweeping the gate-source potential from 0 to 90 V. d) AFM image of a 7 nm-thick DHF4T film grown on glass/ITO/PMMA substrate. e) AFM image of a 40 nm-thick film of Alq3:DCM 3% blend grown on top of the DHF4T thin-film reported in (d). f) AFM image of a 15 nm-thick DH4T film grown on top of the Alq3:DCM 3% film reported in (e). For ease of comparison the same z-axis colour scale is used for both images (e) and (f).

7.3g) accounts for the degraded hole transport in these OLETs.

Fig.7.3e shows that DHF4T films vapor-deposited on the PMMA surface form 2D islands which then coalesce completely in the first monolayer. An incipient 3D growth with the formation of thick elongated needles is also present in the 7 nm-thick film. Fig.7.3f shows the morphology of a 40 nm-thick Alq3:DCM film grown on the previous DHF4T layer. The surface of this layer is composed by 3D globular aggregates with 100-300 nm diameters. Clearly the surface roughness and the presence of voids and protuberances partially prevent the layer-by-layer growth of the 20 nm-thick DH4T film on the optical layer (Fig.7.3f).

The DH4T film topology mirrors that of the underneath Alq3:DCM layer, resulting in an inhomogeneous and poorly connected film that limits transport efficiency [22]. When the device bias conditions allow the simultaneous charge injection from both the source and drain electrodes ($|V_{gs}| < |V_{ds}|$) the OLET is in the ambipolar operation regime and representative transfer curves are reported in figs.7.3c (linear scale) and 7.5a (logaritmic scale). The strong unbalanced transport in the DHF4T/Alq3:DCM/DH4T heterostructures, makes the V shape, characteristic of ambipolar transistors operated in transfer mode, recognizable only in the logarithmic plot of Fig.7.5a.

Consequently, the ambipolar (Fig.7.3c) and unipolar (Fig.7.3a) electrical transfer curves are very similar. However, despite the current similarity, the comparison between Figs.7.3a and 7.3c clearly shows that a novel mechanism of EL generation is taking place in these OLETs when operated in the ambipolar regime. The shaded area in Fig.7.3c highlights the EL originated by the ambipolar current.

The optical micrographs of the device channel (Fig.7.4) show the position of the light emission region with respect to the edge of the drain electrode as a function of the applied voltages. The first frame (Fig.7.4a) is the reference optical image of the

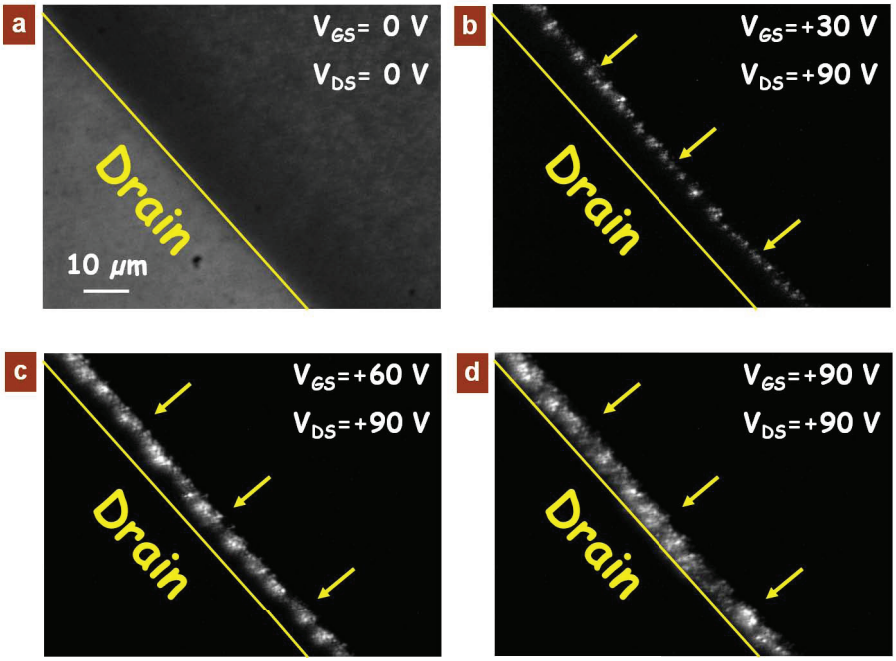

Figure 7.4: Imaging of the light emission area within the OLET device channel. Optical micrographs of the emission zone within the device channel of the tri-layer heterostructure OLET during a transfer scan at $V_{ds} = +90V$ and $V_{gs} = +30V$ (b), $60V$ (c) and $90V$ (d). For reference an optical micrograph of the device channel without bias is reported in (a) to highlight the position of the drain electrode edge that is marked with a yellow line. Three arrows in b), c) and d) indicate the initial position of the recombination and emission zone.

device channel, where the drain electrode edge is clearly recognizable and marked by a yellow line. It can be observed in Fig.7.4b that in the ambipolar operation mode the narrow light emission stripe is located far from the drain electrodes, at a distance of $\sim 8\mu$m. By increasing the gate voltage, the emitting region broadens and shifts towards the drain electrode.

Fig.7.4 therefore confirms that the ambipolar light formation process takes place well inside the channel far from the electrodes thus preventing photon losses at the injecting electrodes and the exciton-metal quenching. Moreover, since in the tri-layer structure the light emitting layer is physically separated from the charge flows, exciton-charge quenching is also simultaneously prevented. The light generation process is

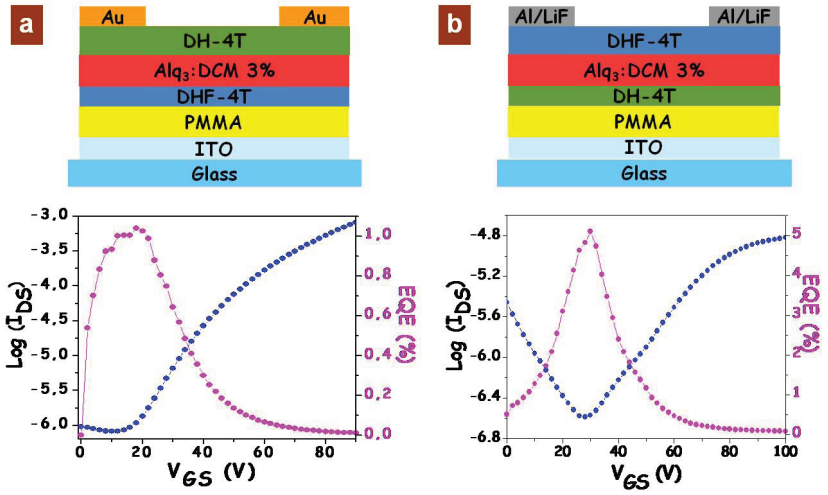

Figure 7.5: External quantum efficiency as a function of the applied gate voltage (purple) for the two tri-layer heterostructure OLET configurations. In (a) the bottom layer and the top layer are thin-films of DHF4T and DH4T respectively while in (b) the layer configuration is reversed. The transfer curves with the drain-source current (I_{ds}) plotted in logarithmic scale are also reported (blue). I_{ds} is measured keeping the drain-source potential constant at 90 V, while sweeping the gate-source potential from 0 to 90 V.

based on the charge percolation of electrons and holes moving from the respective transport layers to the Alq3:DCM layer, where excitons are formed. The transverse electric field generated by electron and hole accumulation in the DHF4T and DH4T films, respectively, promotes the charge percolation. The nature of the force driving the charge recombination, which is correlated to the electron-hole annihilation capability of the central recombination film, leads to a self-regulated equilibrium between the amount of charges located in the transport layers and those entering the optical layer.

It is known that in ambipolar OLETs, where the recombination occurs well within the channel, all injected electrons and holes must recombine since the charges cannot move through several micrometer of an accumulation layer of opposite charge without recombining [23]. In the tri-layer OLET this holds true for the charges entering the recombination layer. It is expected that exciton-charge quenching is prevented in

the tri-layer OLET because:

1. there is no overlap of the opposite charge accumulation layers;
2. the recombination layer has a thickness of 40 nm, which decreases the spatial density of excitons and charges;
3. excitons do not interact with trapped charges eventually localized at the dielectric interface that are likely to be luminescence quenching sites [14].

A quantitative analysis of the optical properties of the tri-layer OLET without considering any exciton-charge quenching shows that the OLET light outcoupling efficiency is $\sim 27\%$, which is 30% higher than that of the typical OLED structure ($\sim 20\%$). This finding is in agreement with the avoidance of losses at the metal cathode. Any sizeable exciton-charge quenching in the tri-layer OLET would result in outcoupling efficiencies exceeding 30%, which is unlikely because of the losses at the ITO/PMMA structure. Therefore, the tri-layer OLET does not show any sizable exciton-charge quenching.

The active part of the device can be regarded as a contactless OLED where exciton-charge quenching is intrinsically prevented. Despite the degraded mobility of the hole minority carriers, the maximum external quantum efficiency (EQE, Fig.7.5a) of ambipolar OLETs in this tri-layer configuration is higher than 1% and is greater than the maximum EQE estimated for an ideal single layer OLET [14]. Note that in determining the EQE of the tri-layer OLET we did not introduce any corrections related to the device geometry, but calculated the efficiency directly as the ratio between the total emitted photons and the flowing charges (OLET drain current), thereby avoiding any risks of overestimating the EQE.

In order to verify whether improved interfacial characteristics would increase the ef-

ficiency, we fabricated a tri-layer OLET by reversing the order of the two charge transport layers (DH4T-Alq3:DCM3%-DHF4T). Indeed the flat morphology of the DH4T layer might be favourable for the realization of a smoother top interface in the heterostructure [1]. The top electrodes were made of LiF/Al to favour electron injection into the LUMO level of DHF4T. By implementing the DH4T thin-film (7 nm) as first layer in contact with the PMMA and the DHF4T thin-film (25 nm) as top layer, a maximum EQE exceeding 5% and a symmetric EQE profile peaking at the position of maximum ambipolarity (Fig.7.5b) is obtained. The impressive improvement of the EQE obtained by controlling the interfaces in the heterostructure demonstrates the potential of our approach. We note that the current density is decreased by one order of magnitude with respect to the previous case due to an absolute value of the threshold voltage higher than 50 V for both types of charges in the reverse device configuration.

However, this data demonstrate that the achievement of balanced ambipolar transport in devices with current densities similar to those observed in the first tri-layer OLET, would enable OLET devices with simultaneous high efficiency and brightness.

7.2 Alternative Tri-Layer OLET Structures

Given the versatility of the tri-layer vertical heterojunction, different strategies can be adopt for improving the overall device performances. Since each single layer is aimed to a specific function, it is possible to implement different materials which preserve the same functional properties but show molecular packing in thin-films more suitable for a multilayer structure. In this section we will explore the operation of new tri-layer OLET and we will discuss about their opto-electronic properties.

7.2.1 DH4T-Alq3:DCM2(3%)-P13 OLETs

A sketch of the OLET based on a tri-layer heterojunction implementing new material combination is reported in Fig.7.6a.

In this case, instead of doping Alq3 with DCM, we used 4-dicyanomethylene-2-

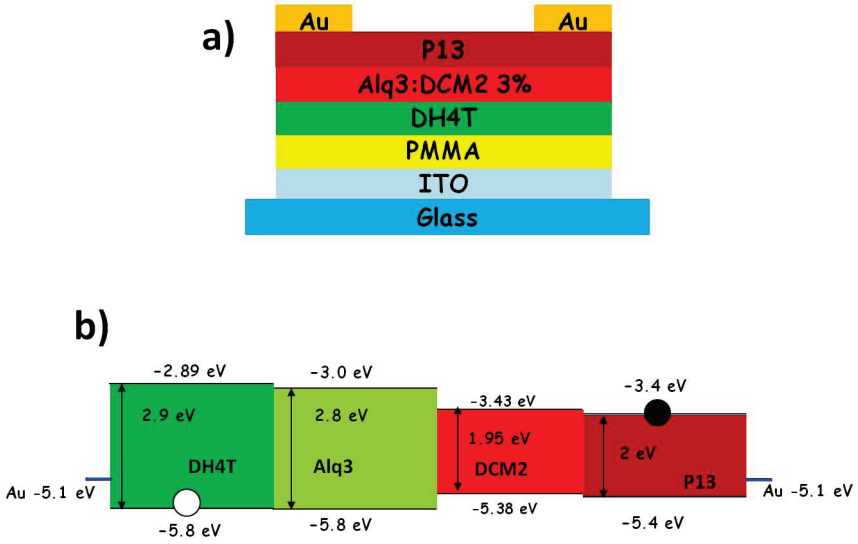

Figure 7.6: a) Scheme of the OLET based on a tri-layer heterojunction. b) Energy diagram of the tri-layer heterojunction system.

methyl-6-(2-(2,3,6,7-tetra-hydro-1H,5H-benzo)[ij]quinolizin-8-yl)-4H-pyran (DCM2) since it shows negligible absorbance at the emission wavelength and slight lower Amplified Spontaneous Emission (ASE) threshold [24] with respect to DCM, even if it is less thermal stable.

In the recombination layer the percentage in weight of DCM2 molecules (guest material) with respect to Alq3 (host material) is 3% for guaranteeing an efficient Förster energy transfer to take place. The thickness of the recombination layer is 40 nm.

If we consider the energy diagram of the tri-layer heterojunction (Fig.7.6c) the radiative recombination of holes and electrons in the Alq3:DCM2 layer is likely to happen through a mechanism similar to what reported in the previous paragraph. In particular we suppose that holes after being trapped in Alq3 in the proximity of the interface

with DH4T can generate a local electric field able to attract the electrons inside the recombination layer. If the electric field is intense enough electrons can be transferred directly from P13 to Alq3 LUMO overcoming the potential barrier. Since Alq3 is an n-type material, electrons can diffuse inside the matrix towards holes trapped in Alq3 in the proximity of the interface with DH4T. Then excitons can be formed in Alq3 molecules and then be non-radiatively transferred to DCM2 dye molecules.

It is also fundamental to perform morphological and electronic characterization on the active materials of the single-layer devices in order to be able to correlate the opto-electronic performances of the final tri-layer vertical heterojunction device with the modification of the molecular organization within every single layer due to the interaction with the others. morphological and electronic data of the materials single layer OFETs as well as in bi-layer OFETs is shown in chapter 5 and 6, respectively.

Given the very good ambipolar electronic results of the single layer and bi-layer device, it turns out that in tri-layer configuration the morphological behaviour of the recombination layer must be the key parameters to control for achieving high performances OLETs. Moreover, since in tri-layer heterojunction-based OLET electron transport is restricted inside the P13 layer to the first few nanometers at the interface with the recombination layer underneath, it is evident the correlation between the Alq3:DCM2/P13 interface morphology and the opto-electronic performances of the overall device.

The opto-electronic performances of the tri-layer heterojunction-based OLET are reported in Fig.7.7.

As it can be seen from the saturation transfer curves reported, the hole and electron mobilities ($\mu^p \sim 2 \cdot 10^{-1} cm^2/Vs$ and $\mu^n \sim 2 \cdot 10^{-2} cm^2/Vs$) are well-balanced and comparable to the values of the corresponding single layer devices.

Nevertheless we have to notice that even if we have increased light emission in abso-

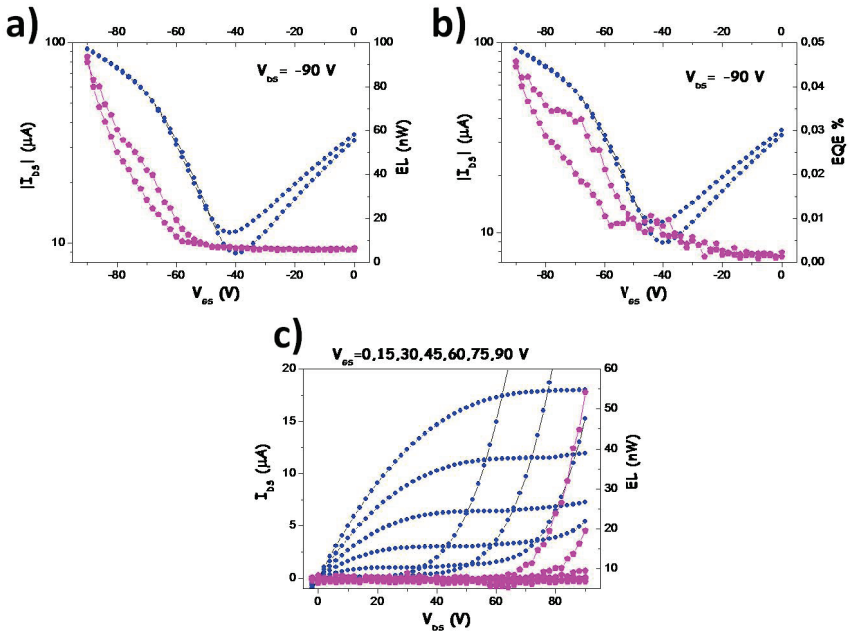

Figure 7.7: Saturation transfer curve for p-type polarization (blue dots) with electro-luminescence intensity (purple dots) (a) and with EQE of electro-luminescence (purple dots) (b). Output I-V curve for p-type polarization (blue dots) with electro-luminescence intensity (purple dots).

lute value with respect to the bi-layer approach, still the most part of EL is located in correspondence of the unipolar transport region. This means that, when the current densities are maxima for both carriers (in the ambipolar gate voltage region), the light emission is not maximized. This is a clear evidence of the fact that the recombination layer is not working properly (this aspect is also demostrated by the poor EQE yield of 0.05% shown in Fig.7.7b, purple dots).

7.2.2 α-NPD:DCM based Tri-layer OLETs

In order to find the best materials combination for improving tri-layer OLET efficiency, we explored the use of a different matrix for the host-guest system to be used as recombination layer.

In this section, we report the results obtained using α-NPD as host matrix. We

measured the opto-electronic characteristics of three different device configurations. Initially we considered a tri-layer with DH4T as first transport layer, DHF4T as third layer and the system α-NPD:DCM 3% wt. doped as recombination layer. The device structure and the opto-electronic results are shown in Figs.7.8 and 7.9, respectively.

Like for previous devices fabricated with DCM, also in this configuration the opti-

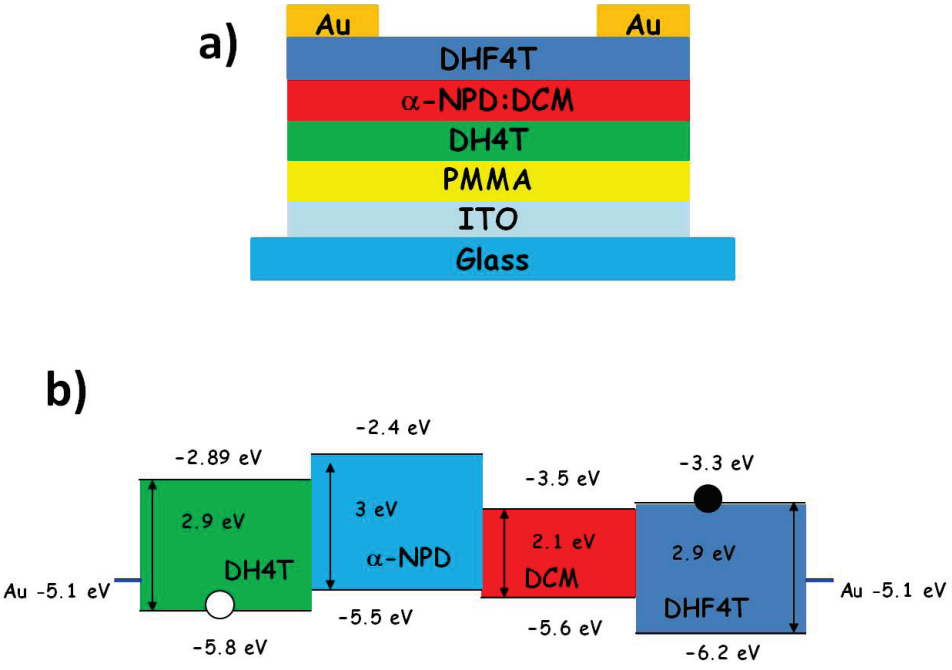

Figure 7.8: a) Scheme of the α-NPD based tri-layer heterojunction OLET. b) Energy diagram of the tri-layer heterojunction system.

mized doping of α-NPD, with DCM, was 3%. This amount of doping has been found to be the best for having the most efficient Förster energy transfer effect inside the system.

Looking at the energy-levels diagram of Fig.7.8b the exciton formation mechanism and thus light emission, is similar to the previously reported one except that in this case, since α-NPD is a poor hole transporting material, the hypothesis for exciton formation is that electron are being trapped in the proximity of the α-NPD/DHF4T interface and that, the local negative electric field generated, attracts the holes that

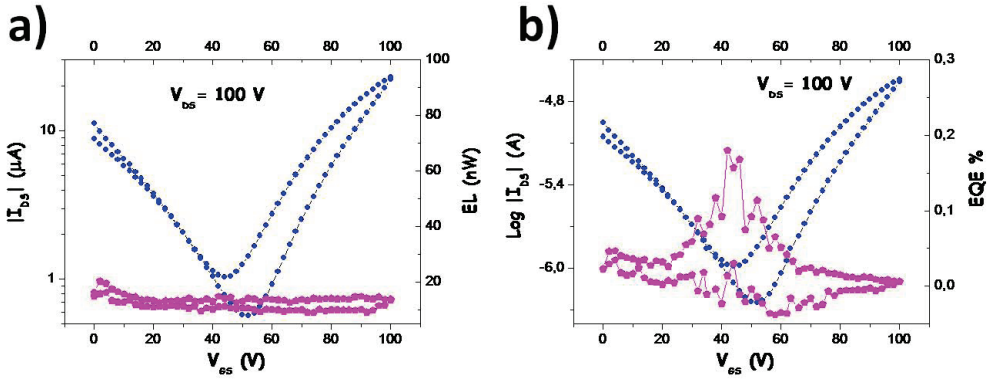

Figure 7.9: Saturation transfer curve for n-type polarization (blue dots) with electro-luminescence intensity (purple dots) (a) and with EQE of electro-luminescence (purple dots) (b). Both electrical curves are represented in logarithm scale.

can diffuse inside α-NPD from DH4T. Then excitons can form inside the matrix and transferred through energy transfer to the dye. Electrical curves show a very good ambipolar behaviour, represented by a very well defined and balanced V-shaped curve (see Fig.7.9). Mobilities are $\mu^p = 1 \cdot 10^{-3} cm^2/Vs$ and $\mu^n \sim 2 \cdot 10^{-2} cm^2/Vs$ and threshold voltages are $V_{th}^p = -53V$ and $V_{th}^n = 50V$. Surprisingly, the purple curves, show no presence of light emitted from the device. This effect can be likely due to the quite low currents that flow into the channel (n- and p-type) as consequence of the high threshold voltages for both charge carriers. These low currents are unable to determine a perceivable light emission outside the device. Since, as explained before, the key parameter for a working tri-layer OLET is a good morphology at the interfaces between the recombination layer and the upper transport layer, we fabricated also an inverse OLET, made with DHF4T as first layer and DH4T as last layer.

In this case the results obtained were completely different from the previous case and are reported, along the device structure, in Fig.7.10 and 7.11, respectively. The opto-electronic data obtained for p-type are: $\mu^p = 1.3 \cdot 10^{-4} cm^2/Vs$ and $V_{th}^p = -20V$, while for n-type: $\mu^n = 0.33 cm^2/Vs$ and $V_{th}^n = 38V$. These results, show an un-

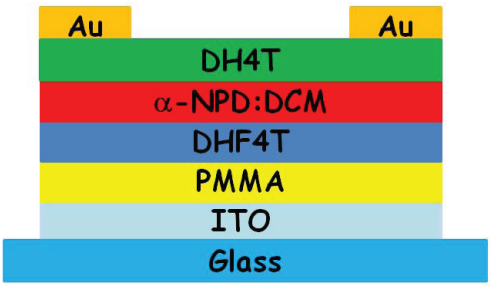

Figure 7.10: a) Scheme of the "inverse configuration" α-NPD based tri-layer heterojunction OLET.

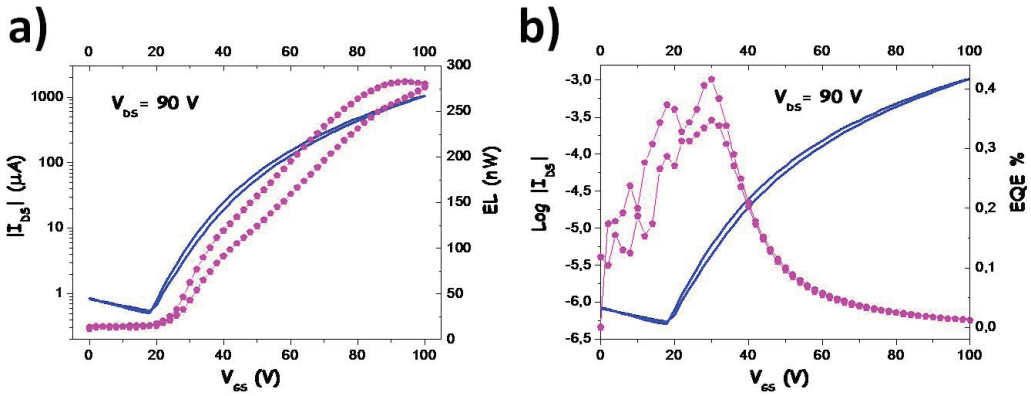

Figure 7.11: Saturation transfer curve for n-type polarization (blue dots) with electro-luminescence intensity (purple dots) (a) and with EQE of electro-luminescence (purple dots) (b). Both electrical curves are represented in logarithm scale.

balanced transport, due likely to a lack of uniformity of the upper DH4T layer that lead to a degraded hole mobility, compared to the high mobility of the DHF4T in direct contact with PMMA. Nevertheless in this configuration, light emission has been measured both in ambipolar and unipolar regions.

The main difference between the tri-layer vertical heterojunction configurations we presented here and the previous one is that the recombination layer is grown on surface with different chemical-physical and morphological features.

As we described in Chapter 5, linear end-substituted oligothiophenes such as DH4T

and DHF4T tend to pack in polycrystalline thin-film according the herringbone structure with molecule long axis oriented normal to the surface so that thin-film surface energy is generally dominated by the chemical nature of the substituents.

In our specific case, since the alkyl chains in DH4T behave as weakly electron-donating groups while the fluroalkyl chains in DHF4T behave as electron-withdrawing groups, DH4T thin-film surface is much less polar than DHF4T one. Thus, either the high hydrophobicity or the smoothness of the DH4T layer surface could, likely, be responsible, in the first device configuration, for a different growth modality of α-NPD:DCM layer, since the recombination layer growth conditions are invariant in the two vertical tri-layer heterojunction. Of course, this fact, affected also the DHF4T growth on α-NPD layer, leading to a lower current flowing into the device and thus a poor charge diffusion in the middle layer. On the contrary, in the second case, most likely due to a different interaction between the more polar DHF4T molecule and α-NPD, the overall current is higher and, although more unbalanced, it lead to a detectable light emission.

From these results, we can deduce that in some cases a good smoothness and the energetic compatibility of the first layer with respect to the recombination one, does not guarantee the good operation of the OLET device. Most likely other kinds of interactions (i.e.electrostatic), that must be investigated, occur at the interfaces.

7.2.3 α-NPD:IrMDQ(acac) based Tri-layer OLET

The last device configuration fabricated using α-NPD as matrix, was done doping it with the IrMDQ(acac) dye.

The main difference between the use of DCM (or DCM2) and IrMDQ(acac), as doping dye, is that in the first case the light was obtained by radiative decay only of singlet excitons, while in this case it is possible to harvest both singlet and triplet excitons.

Since the ratio between triplet and singlet population is 3:1, is straightforward that using a triplet emitter, could enable OLETs with even higher EQE and brightness. The scheme of the device and the opto-electronic results of the device are reported in Figs.7.12 and 7.13, respectively.

The recombination layer optimal doping ratio was determined to be 10% wt of

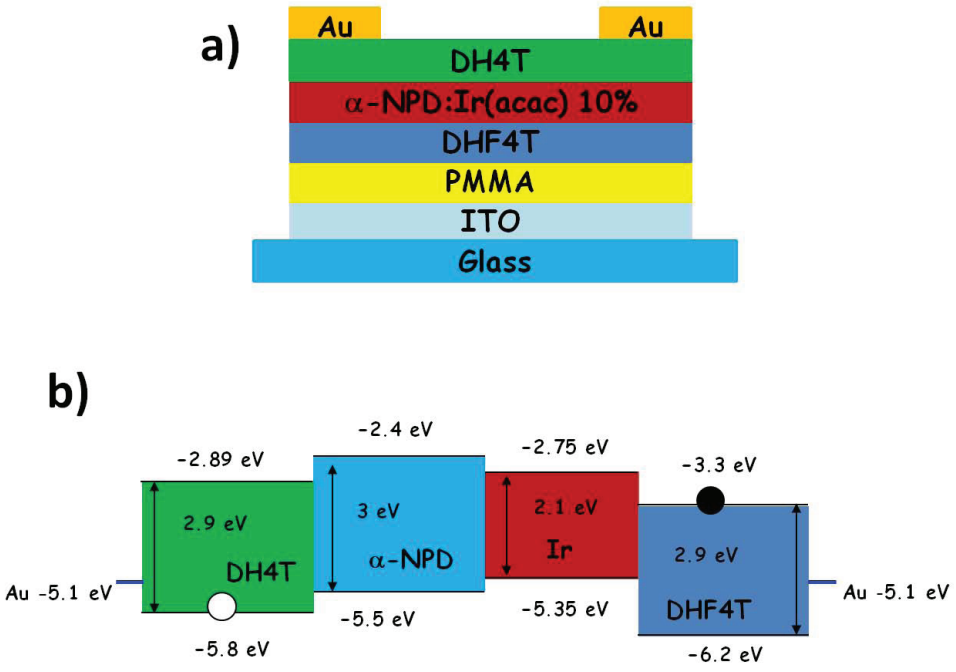

Figure 7.12: a) Scheme of the α-NPD based tri-layer heterojunction OLET. b) Energy diagram of the tri-layer heterojunction system.

IrMDQ(acac). The electronic results determined by the device characterization were: for p-type: $\mu^p = 1.5 \cdot 10^{-4} cm^2/Vs$ and $V_{th}^p = -20V$, while for n-type: $\mu^n = 0.35 cm^2/Vs$ and $V_{th}^n = 36V$. This results are in line with the device previously reported with the same transport layers configuration. The light emission curve (together with EQE curve) shows a slightly higher light intensity in ambipolar region, with respect to the same device with DCM dye. Of note is a pronounced bend of EL curve near the n-type unipolar region (see right side of purple curve of Fig.7.13b), that indicates the presence of exciton quenching under the electrode with respect to

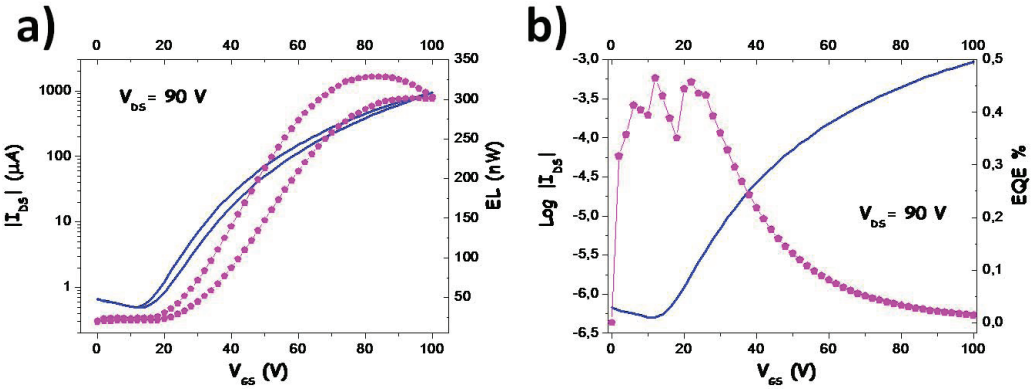

Figure 7.13: Saturation transfer curve for n-type polarization (blue dots) with electro-luminescence intensity (purple dots) (a) and with EQE of electro-luminescence (purple dots) (b). Both electrical curves are represented in logarithm scale.

light emitted in the channel. The maximum of EQE is comparable to the device with DCM, thus the initial hypothesis of enabling higher efficiency devices, using a triplet emitter has to be reconsidered. It might be that, like in the previous case, there are interface effects or bad interactions between the materials that hinder the enhanced light emission of the dye.

7.2.4 Alq3:PtOEP based Tri-layer OLETs

In order to have a deeper understanding of the working performances of a tri-layer OLET with a triplet emitter, we decided to use another triplet dye, the PtOEP, described in the previous chapter (see chap.5). In this case as matrix, we used again Alq3, that showed the best results with DCM and is also energetically compatible with this dye.

The best device configuration was the one with DH4T as first layer and a doping amount of PtOEP inside Alq3 of 8% wt. The device scheme, together with the energy levels diagram of the system, is reported in Fig.7.14.

The opto-electronic characteristics of the device are reported in Fig.7.15. The

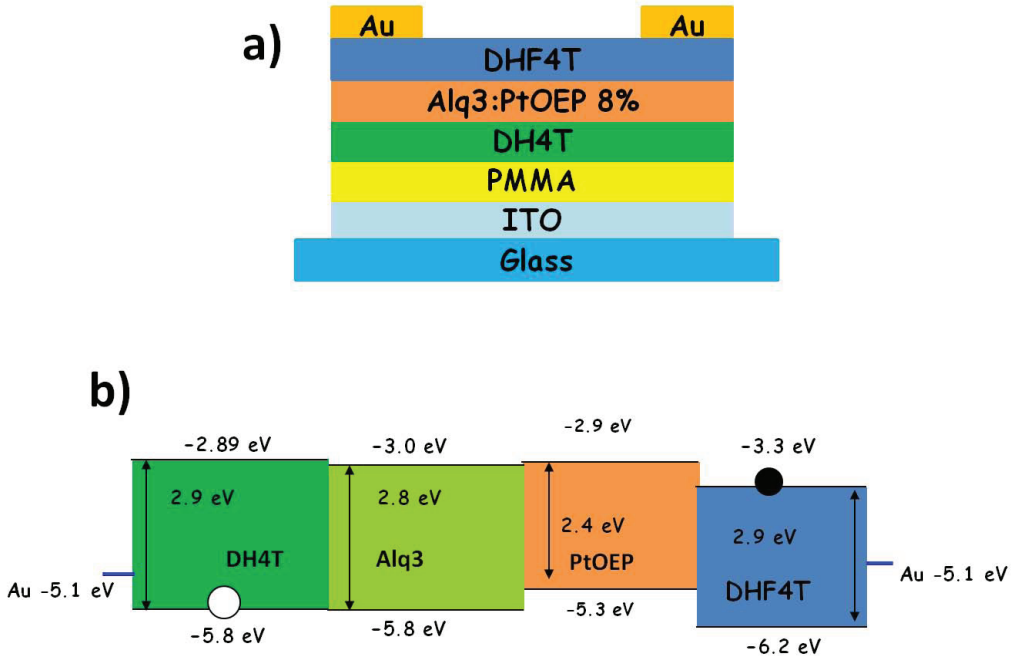

Figure 7.14: a) Scheme of the tri-layer heterojunction OLET with Alq3:PtOEP 8% wt. as recombination layer. b) Energy diagram of the tri-layer heterojunction system.

key parameters of the OLET, extrapolated from the curves, were the following: $\mu^p = 0.1 cm^2/Vs$ and $V_{th}^p = -57V$, while for n-type: $\mu^n = 6{\cdot}10^{-3} cm^2/Vs$ and $V_{th}^n = 40V$.

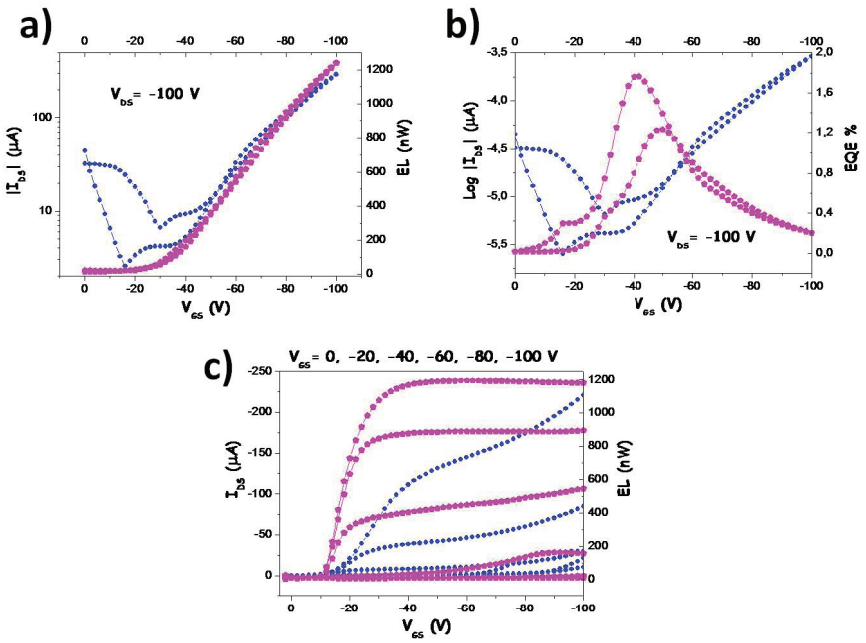

Figure 7.15: Saturation transfer curve for p-type polarization (blue dots) with electro-luminescence intensity (purple dots) (a) and with EQE of electro-luminescence (purple dots) (b). Both electrical curves are represented in logarithm scale. c) Multiple p-type I-V output curve at different gate bias voltages.

The transfer opto-electronic curves in logarithm scale (see Figs.7.15a,b), show a quite unbalanced V-shaped curve with a some bends and an increased hysteresis, between the forward and backward curves, near the maximum of ambipolarity of the device. The hysteresis in that region can be considered as the index of the presence of percolation of charges from the transport layers to the recombination one. Looking at the electroluminescence intensity value (Fig.7.15a purple dots), it is possible to see a very high increase with respect to the best result obtained so far in the first reported device with Alq3:DCM. Since the structure is the same except for the dopant, this demonstrates that using a triplet emitter is the right way to enable higher light emission from OLETs. Also the EQE value is very high (1.8%), but still not higher of the tri-layer with Alq3:DCM.

The measured EL spectra, is the same as the photoluminescence spectra of PtOEP,

without any presence of Alq3 emission, thus demonstrating a complete energy transfer of the host:guest system. In Fig.7.16 are shown the measured EL spectra of the tri-layer (Fig.7.16a) and an image of the illuminated channel of a working device (Fig.7.16b).

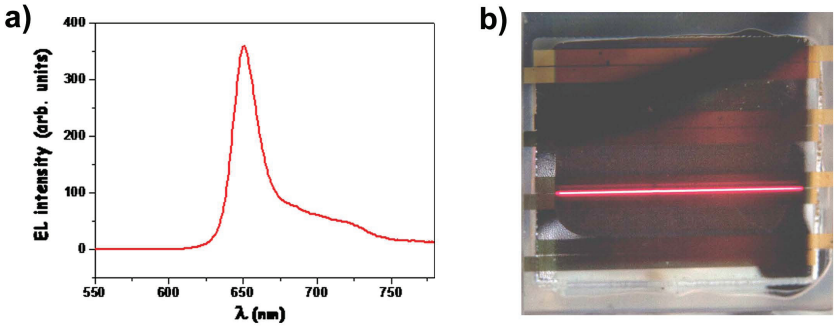

Figure 7.16: a) Electro-luminescence spectra of the Alq3:PtOEP tri-layer OLET. b) picture of the light emission of a working OLET with Alq3:PtOEP.

7.3 Conclusions

In order to understand deeply the working properties of the tri-layer OLET and to improve its light emission efficiency and brightness, other studies must be done.

For example, a systematic study of the EL spectra of the devices is mandatory for discerning which, between the energy diagram of the system and the morphology of the interfaces, have the most influence in light formation mechanism in tri-layer heterojunction devices.

The proper choice of materials, starting from the substrate/gate/dielectric platform and ending with the organics and drain-source contacts, is also of the most importance. Indeed at this stage the main focus is to improve further the performances of the tri-layer heterojunction either by selecting and implementing new materials that facilitate exciton formation or by carefully controlling the molecular packing of the different layers and this can be done only by means of a profound comprehension of

the physics of the OLET.

7.4 REFERENCES

[1] G. Generali, R. Capelli, S. Toffanin, A. Facchetti, and M. Muccini. Ambipolar field-effect transistor based on α,ω-dihexylquaterthiophene and α, ω-diperfluoroquaterthiophene vertical heterojunction. *Microelectron. Reliab.*, 50(9-11):1861–1865, 2010.

[2] R. Capelli, F. Dinelli, M. A. Loi, M. Murgia, R. Zamboni, and M. Muccini. Ambipolar organic light-emitting transistors employing heterojunctions of n-type and p-type materials as the active layer. *J. Phys-Condens. Mat.*, 18(33):S2127–S2138, 2006.

[3] F. Dinelli, R. Capelli, M.A. Loi, M. Murgia, M. Muccini, A. Facchetti, and T.J. Marks. High-mobility ambipolar transport in organic light-emitting transistors. *Adv. Mater.*, 18(11):1416, 2006.

[4] R. Capelli, S. Toffanin, G. Generali, H. Usta, A. Facchetti, and M. Muccini. Organic light-emitting transistors with an efficiency that outperforms the equivalent light-emitting diodes. *Nat. Mater.*, 9:496–503, 2010.

[5] S. Toffanin, R. Capelli, T-Y. Hwu, K-T. Wong, T. Plotzing, M. Forst, and M. Muccini. Molecular host-guest energy-transfer system with an ultralow amplified spontaneous emission threshold employing an ambipolar semiconducting host matrix. *J. Phys. Chem. B*, 114(1):120–127, 2010.

[6] G. Generali, F. Dinelli, R. Capelli, S. Toffanin, , and M. Muccini. Influence of the substrate platform on the opto-electronic properties of multi-layer organic light-emitting field-effect transistors. *J. Phys. D: Appl. Phys.*, 2011. In press.

[7] C.R. Newman, C.D. Fisbie, D.A. Da Silva Filho, J.L. Bredas, P.C. Ewbank, and K.R. Mann. Introduction to organic thin film transistors and design of n-channel organic semiconductors. *Chem. Mater.*, 16:4436, 2004.

[8] J. S. Swensen, C. Soci, and A. J. Heeger. Light emission from an ambipolar semiconducting polymer field-effect transistor. *Appl. Phys. Lett.*, 87:253511, 2005.

[9] J. Zaumseil, R. H. Friend, and H. Sirringhaus. Spatial control of the recombination zone in an ambipolar light-emitting organic transistor. *Nature Mater.*, 5:69–74, 2006.

[10] J. Zaumseil, C. L. Donley, J-S. Kim, R. H. Friend, and H. Sirringhaus. Efficient top-gate, ambipolar, light-emitting field-effect transistors based on a green-light-emitting polyfluorene. *Adv. Mater.*, 18:2708–2712, 2006.

[11] S. Z. Bisri, T. Takenobu, Y. Yomogida, H. Shimotani, T. Yamao, S. Hotta, and Y. Iwasa. High mobility and luminescent efficiency in organic single-crystal light-emitting transistors. *Adv. Funct. Mater.*, 19(11):1728–1735, 2009.

[12] Y. Wang, R. Kumashiro, R. Nouchi, N. Komatsu, and K. Tanigaki. Influence of interface modifications on carrier mobilities in rubrene single crystal ambipolar field-effect transistors. *J. Appl. Phys.*, 105:124912, 2009.

[13] M. Schidleja, C. Melzer, and H. Seggern. Electroluminescence from a pentacene based ambipolar organic field-effect transistor. *Appl. Phys. Lett.*, 94:123307, 2009.

[14] J. Zaumseil, C.R. McNeill, M. Bird, D.L. Smith, P.P. Ruden, M. Roberts, M.J. McKiernan, R.H. Friend, and H. Sirringhaus. Quantum efficiency of ambipolar light-emitting polymer field-effect transistors. *J. Appl. Phys.*, 103(6):064517, 2008.

[15] T-H. Ke, R. Gehlhaar, C-H. Chen, J-T Lin, C-C. Wu, and C. Adachi. High efficiency blue light emitting unipolar transistor incorporating multifunctional electrodes. *Appl. Phys. Lett.*, 94:1533071–1533073, 2009.

[16] E. B. Namdas, J.S. Swensen, P. Ledochowitsch, J.D. Yuen, D. Moses, and A.J. Heeger. Gate-controlled light emitting diodes. *Adv. Mater.*, 20(7):1321–1324, 2008.

[17] N. Suganuma, N. Shimoji, Y. Oku, and K. Matsushige. Novel organic light-emitting transistors with pn-heteroboundary carrier recombination sites fabricated by lift-off patterning of organic semiconductor thin-films. *J. Mater. Res.*, 22:2982–2986, 2007.

[18] E. B. Namdas, P Ledochowitsch, J.D. Yuen, D Moses, and A.J. Heeger. High performance light emitting transistors. *Appl. Phys. Lett.*, 92:183304, 2008.

[19] T. Matsushima and C Adachi. Extremely low voltage light-emitting diodes with p-doped alpha-sexithiophene hole transport and n-doped phenyldipyrenylphosphine oxide electron transport layers. *Appl. Phys. Lett.*, 89:253506, 2006.

[20] A. Facchetti, M. Mushrush, M-H. Yoon, G. R. Hutchison, M. A. Ratner, and T. J. Marks. Building blocks for n-type molecular and polymeric electronics. perfluoroalkyl- versus alkyl-functionalized oligothiophenes (nt; n=2-6). systematics of thin film microstructure, semiconductor performance, and modeling of majority charge injection in field-effect transistors. *J. Am. Chem. Soc.*, 126:13859–13874, 2004.

[21] J. C. Pinto, G.L. Whiting, S. Khodabakhsh, L. Torre, A.B. Rodriguez, R.M. Dalgliesh, A.M. Higgins, J.W. Andreasen, M.M. Nielsen, M. Geoghegan, W.T.S. Huck, and H. Sirringhaus. Organic thin film transistors with polymer brush gate dielectrics synthesized by atom transfer radical polymerization. *Adv. Funct. Mater.*, 18:36–43, 2008.

[22] J Ackermann, C. Videlot, P. Dumas, A. El Kassmi, R. Guglielmetti, and V. Safarov. Control of growth and charge transport properties of quaterthiophene thin films via hexyl chain substitutions. *Org. Electr.*, 5:213–222, 2004.

[23] J. Zaumseil, R.H. Friend, and H. Sirrighaus. Spatial control of the recombination zone in an ambipolar light-emitting organic transistor. *Nature Mater.*, 5:69–74, 2006.

[24] V.G. Kozlov, V Bulovic, P.E. Burrows, M. Baldo, V.B. Khalfin, G. Parthasarathy, S.R. Forrest, Y. You, and M.E. Thompson. Study of lasing action based on forster energy transfer in optically pumped organic semiconductor thin films. *J. Appl. Phys*, 48(8):4096, 1998.

Chapter 8

Future Perspectives and Open Issues

The present thesis, aimed at studying different classes of π-conjugated organic materials that present functional properties suitable for the realization of optoelectronic devices and their implementation in an OFET or OLET structure. With the most promising materials, OLET devices have been fabricated with a new architecture, **the trilayer vertical heterojunction structure**, in order to study its opto-electronic characteristics and to find the best materials combination for achieving the best device performances.

For the materials selection, we focused our attention on the two specific properties that are deeply correlated to the molecular arrangement in the thin films and hetero-structures: charge transport and light emission. Indeed, the description of the solid state electronic properties of organic materials necessitates of taking into account the nature of intermolecular interactions which depends, among others, on the molecular arrangement in the solid state. In the technologically appealing thin films, the molecular arrangement is extremely sensitive to the deposition procedures and to the nature of the substrate. Thus, of great interest is the understanding, at the micro- and nano-scale, of the molecular architecture and morphological fea-

tures which favour charge transport and/or energy transfer, in order to enhance performances of optoelectronic devices based on thin films. Whereas it has been demonstrated that the molecular properties can be tuned by chemical tailoring, morphology and supramolecular arrangement are generally more difficult to control, and this appears to be one of the next challenges in the field of organic π-conjugated materials. When organic materials are implemented as active layers in device realization, interfaces formed by different materials are intrinsically important. Organic based devices are composed by many different interfaces and OFETs in particular are considered truly interface devices. The comprehension of the physics behind each interface is a crucial point to design new materials for device applications or to improve the performances of the existing ones. The possibility of combining different functionalities in a single device is of great relevance for the further development of organic electronics in integrated components and circuitry. Organic light-emitting transistors (OLETs) have been demonstrated to be able to combine in a single device the electrical switching functionality of a field-effect transistor and the capability of light generation. With respect to light-emitting diodes, OLETs present some characteristics which overcome key physical and technical drawbacks in the realization of nano-scale integrated electro-optical devices. In particular, these characteristics include: control over the position of the emission zone, emission far away from injecting metal electrodes, high current densities, low charge concentration within the emission zone, and perfectly balanced hole and electron currents.

The final chapter of the thesis reports on a new vertical tri-layer heterojunction approach, on a transparent substrate platform, for realizing efficient organic light-emitting transistor. The specificity of the presented tri-layer based OLET is the intrinsic separation of the charge transport region from the exciton formation region thus preventing completely the exciton-carrier quenching.

In this new structure, each layer is devoted to a single functionality within the device and can be optimized by controlling the growth of the different organic/organic, organic/metal and organic/dielectric interfaces. In the heterostructure we propose, the first layer and third layers are optimized for field-effect charge (electrons and holes) transport. The second layer is formed by a host-guest matrix with high optical performance. The optimization of charge transport and light emission properties allowed the realization of a tri-layer heterojunction presenting balanced electron and hole mobility, high charge carrier density in correspondence of the maximum electroluminescence emission and intense light generation.

A possible exploitation of this technology derives from the fact that the tri-layer heterojunction structure can be considered as an attractive platform for realizing micro-scale integrated multifunctional devices. Indeed not only the high charge current density achievable in OFET and low charge-exciton interaction in tri-layer configuration, but also the easily implementation of a resonant cavity in a planar geometry, make the trilayer OLET device reported an appealing structure for realizing electrically-pumped laser.

Another possible future application of this kind of structure will be in the field of disposable bio-sensing devices. For example, it is possible to develop a device for monitoring cardiovascular health.

To date Microfluidic (or Lab-on-a-Chip) devices have not been well suited to point-of-care applications. Although the chips themselves are cheap and small, they must generally be used in conjunction with bulky optical light-sources and detectors. The lack of an integrated, versatile detection scheme is a major obstacle to the deployment of portable diagnostic devices. It has been demonstrated that integration of organic diodes and photodetectors is a viable route to meet this need. The idea is to develop a radically new generation of devices, in which organic photonic field-effect

transistors are used for both light generation and detection. The use of OLETs in place of diodes would have four principle benefits. Firstly they can be pre-fabricated on the substrate (the microfluidic chip), ensuring optimal registration between the organic photonic components and the underlying fluidic architecture. Secondly the devices can be completed by depositing a single layer of organic semiconductor followed by the gate dielectric/electrode, thus avoiding the need for too much complex structures and of ITO electrodes. Thirdly in-plane light generation by the transistors, which is directly generated at the interface with the microfluidic chip surface, provides improved optical coupling into wave-guiding structures, leading to significant performance gains. Fourthly current-multiplying auxiliary transistors can also be included thereby enabling immediate amplification of the signal at the point-of-generation. In combination these factors offer a compelling solution to the challenge of point-of-care detection that will offer unprecedented sensitivity and superior reliability at a markedly reduced cost.

Lastly, the capability of the OLET semiconductor platform to enable voltage-dependent microscaled localized light-emission could enable the development of a novel approach for high-spatial-resolution optical control of functional neuronal circuitry in living mammalian system.

By interfacing the device with neuronal cells retroviral-injected with light sensitive ion-channels or loaded with neurotransmitters caged molecules, the device could act as photo-stimulator with high spatial resolution of few micrometers.

In response to the photo-stimulation, light sensitive ion channels enable entry of Na+ ions in the cell, resulting in neuronal depolarization and possibly action potential. When action potential occurs, a displacement current is generated at the junction between the device dielectric and the probed cell due to charge accumulation at that interface. The formed electric field, will attracts charges inside the

OLET semiconductors, thus activating the conduction channel. If the drain-source contacts are at a different potential, a current (I_{ds}) is generated. Thus, I_{ds} current variation induced by cell or neuronal photo-induced electrical activity enables real time monitoring of the cell electrical activity.
In case of cell response to specific excitation wavelengths, the OLET platform allows the direct light stimulation of the cell thereby avoiding molecular probe loading. For examples photoreceptors retinal cells like cone cells endogenously express specific light sensitive channels that are selectively activated by light of specific wavelengths. The same approach that avoids genetic modification or probe loading could be used in different mammalian cells.

The innovative approach of the trilayer OLET structure leaves open some "device-related" critical issues that must be considered and overcome in order to have a full exploitation of this technology. First of all the brightness.
Indeed, although OLETs has got some interesting features concerning light emission that make it appealing (very narrow spatial localization of light, high external quantum efficiency), its perceived overall brightness needs to be improved. The target that must be at least reached, in order to consider OLETs as a potential light-source for pixels in display technology, is $\sim 300cd/m^2$, and the way to achieve it is tightly connected to the development of new high efficiency emitting materials.
Another issue that is common for organic electronic devices and thus is affecting also OLETs, is the limited lifetime of the active materials when exposed to air and moisture.
Indeed, like for OLEDs, the organic materials used in OLETs are typically sensitive to the surrounding environment and tend to oxidize very quickly, thus in order to permit the existence of the devices outside the drybox, an important step in the fabrication process is required, the encapsulation of the active area. For this process to be done,

a transparent cap must be attached to the device by means of a UV epoxy glue that must guarantee a perfect insulation from the outside. In order to prevent further the moisture and oxygen to affect the device, it is also possible to insert an oxygen getter inside the cap.

Lastly, in order to achieve higher OLETs performances, the injection through metal/organic interfaces should be improved. Indeed, for inorganic semiconductors, our understanding of contacts with metals is based on the concept of the conventional Mott-Schottky model (M-S). For organic semiconductors based on small molecules, the experimental data remain, to a large extent, unclear and irreproducible because of the poor interface control. Narrow bandwidth of organic semiconductors and weak van der Waals molecule/molecule and molecule/metal coupling make the behaviour of metal/organic interfaces qualitatively different from that of their inorganic counterparts. According the M-S model, contacts are expected to be ohmic when the work function of the metal is close to the HOMO (LUMO) energy level of a p-type (n-type) organic semiconductor. If this condition is not met, then an energy barrier forms at that interface, leading poor charge injection. In practice, the contact resistance of a "good metal/organic interface" in terms of M-S model, is higher than expected. In real devices, indeed, there is another effect that occurs at the interfaces and that must be considered. Indeed, the interface exhibits an additional dipole barrier that shift the vacuum level upward by more than 1eV, hence increasing the barrier height. The issue of contact resistance in organic transistors imposes serious limitations on the downscaling of organic thin-film devices. Thus, reducing the contact resistance in OFETs is another challenging direction of future experimental work, which will open-up, besides the capability of downscaling the devices, also the possibility to decrease threshold voltages of OLETs hence, firstly, making them working at biases more compatible with standard driving circuits and, secondly, improving considerably

their lifetime, since deterioration of optoelectronic devices is, usually, also related to their operating voltages.

Chapter 9

Annex

9.1 Additional Fundamental Studies

In addition to the fabrication and characterization of single layer devices, we report here of other studies made in order to improve the understanding of the basic phenomena that are at the basis of devices working properties. Among these studies we present in the next section the two most representatives: An analysis of the film morphology as a function of the alkyl chain length in thiophene derivatives and a study of the modification effect of the dielectric properties by blending it with a photo-switching molecule.

9.1.1 OFETs Dependency from Thiophene Derivatives Alkyl Chain Length

To better understand the correlation between the alkyl chain length and the mobility μ in end-substituted alkyl quaterthiophene derivative, we analyzed the characteristics of the three materials considered (DM4T, DB4T, DH4T). A summary of the electrical properties for all the three materials investigated is shown in Table 9.1.

From a chemical point of view, it is well known that the alkyl chain has the effect to modify the solubility of thiophene molecules [1]. When these molecules are sublimed

		ITO/PMMA RT	ITO/PMMA 90°C
DM4T	μ (cm^2/vs)	0.036	0.008
	V_{th}	-18 V	-26 V
	$I_{on/off}$	10^2	10^2
DB4T	μ (cm^2/vs)	0.006	0.01
	V_{th}	-20 V	-28 V
	$I_{on/off}$	10^4	10^2
DH4T	μ (cm^2/vs)	0.091	0.083
	V_{th}	-25 V	-30 V
	$I_{on/off}$	10^5	10^6

Figure 9.1: Summary of OFET electrical parameters. For each material, charge mobility, threshold voltage and $I_{on/off}$ are reported for $T_{sub} = RT$ and 90°C.

in vacuum and deposited onto a substrate, the alkyl chains give a certain degree of freedom to the molecules, as they interact with the substrate surface. Depending on the alkyl chain length there might be a different arrangement of the molecules within the first layer in contact with the substrate. The alkyl chains partially separate the conjugated core of the molecules from the substrate surface thus preventing charge trapping at the dielectric/organic semiconductor interface. A comparison among the AFM morphologies of the first few monolayers of the various materials indicates that there is an increasing tendency to grow in a 2D layer-by-layer fashion with increasing the alkyl chain length. The early stages of growth of the shorter chain material, DM4T, show an aggregation with large 3D crystalline domain (Fig.6.4a). On the contrary, DB4T and DH4T have very similar growth modality with layered structure parallel to the dielectric surface (Fig.6.6a and 6.8a).

If we compare the OFETs parameters, it becomes clear that the 2D-growth does not correlate with improved electrical characteristics. Indeed the transport properties do not monotonously improve with increasing the alkyl chain length: DB4T, the interme-

diate length molecule, presents the lowest μ. In order to gain a deeper understanding of this behaviour, we have performed XRD analysis of the films on the ITO/PMMA substrate. The results of the XRD measurements are shown in Fig.9.2. DM4T and

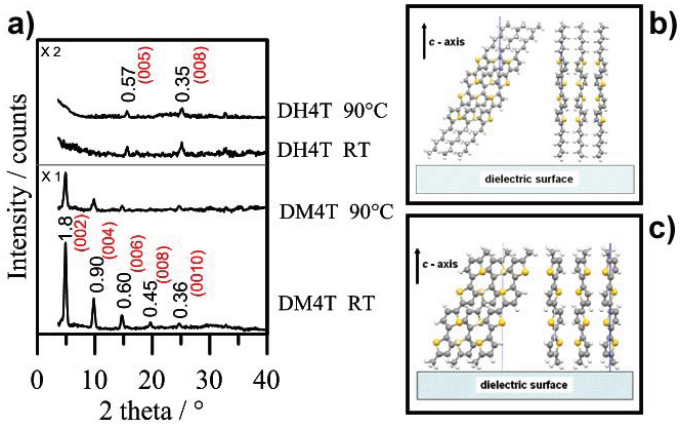

Figure 9.2: a) X-ray diffraction spectra, at 2θ angle, of DM4T and DH4T films grown on ITO/PMMA substrates with $T_{sub} = RT$ and 90°C. b-c) Crystal structures oriented with respect of substrate surface of DH4T and DM4T, respectively.

DH4T present all the reflection peaks typical of a well organized and crystalline material. A comparison with the structural data obtained from single crystals [2, 3] allows to index the reflections. In DM4T patterns, they are the even order of the 0 0 l periodicity and in DH4T patterns the two detected reflections are the 5^{th} and 7^{th} order of the same 0 0 l periodicity. The high peak intensity implies that in both the samples the a,b plane of the unit cell is coincident with the ITO/PMMA substrate. In this arrangement the molecules are oriented upright with respect to the substrate as sketched in Fig.9.2b and 9.2c.

Furthermore, a comparison between DM4T and DH4T indicates a tendency for both materials to reach a higher degree of film crystallinity at $T_{sub} = RT$ rather than at $T_{sub} = 90°$C. For DM4T this tendency is more evident and relevant, explaining why the substrate heating results in a drop of the μ value. For DH4T, contrarily to what is reported for films on Si/SiO_2 substrate [4], there is no evidence of a higher degree

of crystallinity for $T_{sub} = 90°$C with respect to RT. This result is compatible with the morphological analysis we carried out by AFM and strengthen the hypothesis that, on ITO/PMMA substrates, DH4T has an ordered structure at RT that does not strongly depend on T_{sub}.

Strikingly, for DB4T, the XRD analysis has evidenced no diffraction peak for both the RT and $90°$C samples. This is characteristic of films with no ordered structure. An explanation for this behaviour might be that, for a low number of carbon atoms in the alkyl chain, the C-C bond structure is not completely ordered, i.e. is not in all trans configuration. A similar phenomenon has been already reported for thiol SAMs, in which for alkyl chains shorter than 8 carbon atoms the structure is not ordered [5]. The lack of crystalline order explains also the difference in the electrical properties between DB4T and DH4T. Finally, we note that DB4T presents a slight increase in for films with $T_{sub} = 90°$C, whereas no diffraction peak is yet visible. It is in the end important to underline that data on the film morphology alone are not sufficient to predict the crystallinity of the domains. Similar morphologies can thus have large divergences in terms of field-effect electrical transport, like we have herein shown for DB4T and DH4T.

9.1.2 Modification of Dielectric Properties by blending PMMA with a Photo-Switching Molecule

All-optical or opto-electric molecular switches performing by virtue of a photochromic reaction have been of keen interest for last decades due to fast emerging applications of organic materials in electronics [6, 7]. The switch may be used as a logic or memory element in future optical computer chips and other circuits. One of the most challenging ideas has been the development of opto-electrical switches or photo-switchable transistors, where the current can be controlled by illumination. The use of photochromic bistable molecules may allow one to control the current by illumi-

nation with light that activate a reversible photochemical reaction. The light of a given wavelength triggers the reaction, hence changing the current, while an exposure of the device to radiation of a different wavelength results in a reverse reaction, resulting in the system return to its initial state. Suitably selected thermally stable photochromic molecules are able to remain in their metastable form for a sufficiently long time hence the current does not drop down after turning off the illumination. The performance of the switch is determined by the ratio of high-current (on) and low-current (off) states [8, 9].

In general the effect of photochromic materials, dissolved in an organic semiconductor matrix, is to reversibly modify the mobility of charge carriers due to formation and annihilation of charge carrier traps in the vicinity of highly polar molecules of the photochromic system.

In this study a novel system of organic FET with a photochromic material is put forward, by blending not the organic layer but the dielectric polymer with the photochromic molecule. In this case, if the insulating properties are maintained, it is possible to control the capacitance of the system by illuminating the substrate and thus changing the device characteristics.

One of the most frequently studied photochromic materials are spiropyrans, and among them $1'$,$3'$-dihydro-$1'$,$3'$,$3'$trimethyl-6-nitrospiro[2H-1-benzopyran-2,$2'$-(2H)-indole] (SP) (Fig.9.3).

Under UV illumination SP with dipole moment of 5.4 D transforms into metastable coloured photo-merocyanine (MR) with dipole moment about 11 D or even higher [10]. PMMA is a suitable dielectric material for OFETs: PMMA films are transparent for visible light and form good matrices for photochromic molecules allowing fast SP MR photochemical transformation. A solution of SP in PMMA was employed as the dielectric layer in the FETs under study.

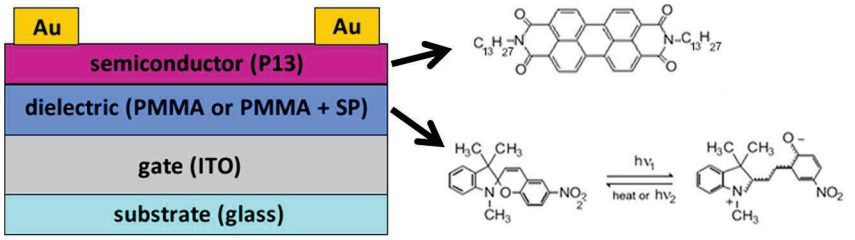

Figure 9.3: Schematic architecture of an OFET. The acronyms in the parentheses refer to the names of materials used in the OFET employed in the present study. The chemical formulae of the materials employed in the present study and the scheme of the SP MR photochromic reaction are shown on the right side of the figure

With these premises, a single-layer OFET was fabricated with P13 as active organic semiconductor layer and a blend of PMMA:SP as a dielectric-photochromic system (see device structure at Fig.9.3). I-V Output measurements are shown in Fig.9.4. After UV illumination, the source-drain current for (PMMA+SP)/P13 FETs

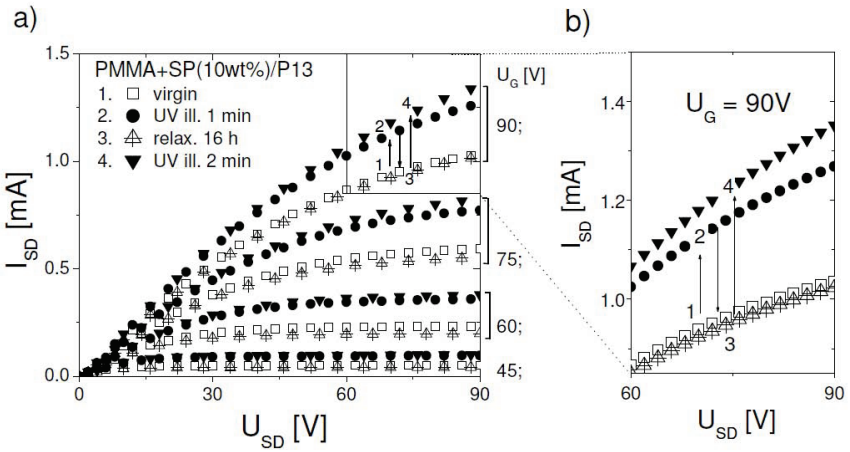

Figure 9.4: (a) Output current-voltage characteristics for (PMMA+SP)(10wt%)/P13 FET. The characteristics are plotted in the double-linear coordinates with V_{gs} displayed on the right margin. (b) Expanded section of (a) for $V_{gs} = 90V$ showing the switching cycle: (1)Virgin sample; (2) Sample irradiated with UV for 1 min; (3) Relaxed for 16 hours at ambient temperature; (4) Irradiated with UV for 2 min.

increased (Fig.9.4, curves 1 and 2), presumably due to the transition of SP to MR. Metastable MR can be re-converted into the stable SP form by illumination with visi-

ble light but it can also return to its initial form by thermal relaxation in the darkness. A family of the locus current-voltage characteristics measured in a (PMMA:SP)/P13 OFET is shown in Fig.9.5. The threshold voltage (V_{th}), for neat PMMA/P13 FETs

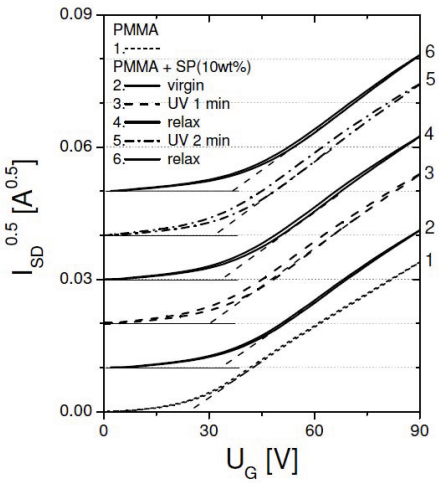

Figure 9.5: Locus current-voltage characteristics for PMMA/P13 (curve 1) and (PMMA+SP)(10wt%)/P13 FETs (curves 2-6).

was 22V. Addition of SP to PMMA in FETs increased V_{th} to 34V, the UV illumination (and the resulting conversion of SP into MR) shifted V_{th} to 29 V. The thermal relaxation (resulting in the reverse MR to SP reaction) restored the previous level of V_{th} (35V). The mobility of charge carriers in studied neat PMMA/P13 FETs was above 0.35cm^2/Vs, while addition of SP into PMMA increased the calculated value of μ to 0.4cm^2/Vs.

A negligibly small hysteresis is present on the transfer characteristics in the neat PMMA/P13 FETs. Addition of SP into PMMA slightly increased these hysteresis. UV illumination of (PMMA+SP) films resulted in an additional small broadening of the hysteresis between the forward and backward branches of the transfer curves.

The On/Off current ratio due to the photoswitching was found to be V_{gs} dependent, ranging between 1.3 times at the highest voltages to ∼2-3 times around V_{th}. To explain the behaviour observed, the effect of presence of dipolar photochromic

molecules was considered at the organic semiconductor/polymeric insulator interface and in the dielectric bulk.

The dominant mechanism seems to be associated with a change of the FET mobility resulting from changes in dielectric electric permittivity related to changes of the dipole moment during the photochromic cycle. These changes affect the source-drain current both indirectly, by changes in the FET mobility and directly, since, according to FET equations, the current is proportional to the capacitance of the dielectric layer.

9.2 REFERENCES

[1] F. Garnier, R. Hajlaoui, A. El Kassmi, G. Horowitz, L. Laigre, W. Porzio, M. Armanini, and F. Provasoli. *Chem. Mater.*, 10:3334, 1998.

[2] S. Hotta and K. Waragai. *Mater. Chem.*, 1:835, 1991.

[3] M. Moret, M. Campione, A. Borghesi, L. Miozzo, A. Sassella, S. Trabattoni, B. Lotz, and A. J. Thierry. *J. Mater. Chem.*, 15:2444, 2005.

[4] R.and Loi M. A.and Murgia M.and Muccini M.and Facchetti A.and Marks T. J. Dinelli, F.and Capelli. High-mobility ambipolar transport in organic light-emitting transistors. *Adv. Mater.*, 18:1416, 2006.

[5] Y. T. Tao. *J. Am. Chem. Soc.*, 115:4350, 1993.

[6] B.L. Feringa. *Molecular Switches*. Wiley-VCH, 2001.

[7] J.J. Bao, Z.and Locklin. *Organic Field Effect Transistors*. CRC Press: Boca Raton, 2006.

[8] H. Klauk. *Organic Electronics. Materials, Manufacturing and Applications*. Wiley-VCH, 2007.

[9] G Hadziioannou and G.G. Malliaras. *Semiconducting Polymers, 2nd Ed.* Wiley-VCH, 2007.

[10] W.and Ne-purek S.and Sworakowski J.and Zalesny R. Toman, P.and Bartkowiak. Quantum-chemical insight into the design of molecular optoelectrical switch. *Chem. Phys.*, 2005.